International Journal of
Molecular Sciences

MDPI

Review

Biomimetic Tumour Model Systems for Pancreatic Ductal Adenocarcinoma in Relation to Photodynamic Therapy

Olivia M. Smith [1], Nicole Lintern [1], Jiahao Tian [2], Bárbara M. Mesquita [3], Sabrina Oliveira [3], Veronika Vymetalkova [4], Jai Prakash [5], Andrew M. Smith [1,6], David G. Jayne [1,6], Michal Heger [2,7,*] and Yazan S. Khaled [1,6,*] on behalf of the Photodynamic Therapy Study Group

1 Leeds Institute of Medical Research, St. James's University Teaching Hospital, Leeds LS9 7TF, UK; olivia74@hotmail.co.uk (O.M.S.); nicolemaylintern@icloud.com (N.L.); andrewmalvernsmith@me.com (A.M.S.); d.g.jayne@leeds.ac.uk (D.G.J.)
2 Jiaxing Key Laboratory for Photonanomedicine and Experimental Therapeutics, Department of Pharmaceutics, College of Medicine, Jiaxing University, Jiaxing 314001, China; jiahaotian96@gmail.com
3 Department of Pharmaceutics, Utrecht Institute for Pharmaceutical Sciences, Utrecht University, 3584 CG Utrecht, The Netherlands; b.s.maiamesquita@uu.nl (B.M.M.); s.oliveira@uu.nl (S.O.)
4 Department of Molecular Biology of Cancer, Institute of Experimental Medicine of the Czech Academy of Sciences, 142 00 Prague, Czech Republic; veronika.vymetalkova@iem.cas.cz
5 Engineered Therapeutics Group, Department of Advanced Organ Bioengineering and Therapeutics, Technical Medical Centre, University of Twente, 7522 NB Enschede, The Netherlands; j.prakash@utwente.nl
6 School of Medicine, The University of Leeds, LS2 9JT Leeds, UK
7 Membrane Biochemistry and Biophysics, Department of Chemistry, Faculty of Science, Utrecht University, 3584 CS Utrecht, The Netherlands
* Correspondence: michal.heger@photonanomedicine.com (M.H.); y.khaled@leeds.ac.uk (Y.S.K.); Tel.: +86-15356737738 (M.H.); +44-1132433144 (Y.S.K.)

Abstract

Pancreatic ductal adenocarcinoma (PDAC) is the most common type of pancreatic cancer and is associated with poor prognosis. Despite years of research and improvements in chemotherapy regimens, the 5-year survival rate of PDAC remains dismal. Therapies for PDAC often face resistance owing in large part to an extensive desmoplastic stromal matrix. Modelling PDAC ex vivo to investigate novel therapeutics is challenging due to the complex tumour microenvironment and its heterogeneity in native tumours. Development of novel therapies is needed to improve PDAC survival rates, for which disease models that recapitulate the tumour biology are expected to bear utility. This review focuses on the existing preclinical models for human PDAC and discusses advancements in tissue remodelling to guide translational PDAC research. Further emphasis is placed on photodynamic therapy (PDT) due to the ability of this treatment modality to not only directly kill cancer cells by minimally invasive means, but also to perturb the tumour microenvironment and elicit a post-therapeutic anti-tumour immune response. Accordingly, more complex preclinical models that feature multiple biologically relevant PDAC components are needed to develop translatable PDT regimens in a preclinical setting.

Keywords: pancreas; cancer models; preclinical testing; chemotherapy; photodynamic therapy; in vitro analysis; cell viability assays; cell death; 2-D and 3-D cell culture; spheroids and organoids; patient-derived xenografts

Academic Editor: Samir Acherar

Received: 7 May 2025
Revised: 13 June 2025
Accepted: 17 June 2025
Published: 2 July 2025

Citation: Smith, O.M.; Lintern, N.; Tian, J.; Mesquita, B.M.; Oliveira, S.; Vymetalkova, V.; Prakash, J.; Smith, A.M.; Jayne, D.G.; Heger, M.; et al. Biomimetic Tumour Model Systems for Pancreatic Ductal Adenocarcinoma in Relation to Photodynamic Therapy. *Int. J. Mol. Sci.* **2025**, *26*, 6388. https://doi.org/10.3390/ijms26136388

1. Introduction

Pancreatic ductal adenocarcinoma (PDAC) remains one of the most lethal solid cancers, accounting for approximately 9600 annual deaths in the United Kingdom [1,2]. Complete

surgical resection remains the only curative option but is seldom achieved, with positive resection margins (R1) reported in up to 70% of cases [3–5]. With complete surgical resection, 5-year survival rates of ~40% are reported [6,7]. Approximately 70% of resected cases present with lymph node involvement, whilst distant metastases during surgical exploration are found in up to 25% of patients. Both are associated with a significantly decreased 5-year survival rate [8–10]. These statistics suggest that PDAC is a systemic disease and current therapeutics should focus on the unique biology of this cancer type.

Despite improvements in adjuvant and neoadjuvant chemotherapy regimens, chemotherapy approaches have had marginal benefits, with 5-year overall survival (OS) rates increasing from 6% to only 9% between 2014 and 2018 [11]. The observed chemoresistance is believed to be associated with inefficient drug penetration through the fibrotic stroma [12,13]. Therefore, there is a clinical need to create models representing the unique biological features of PDAC, and in particular the dense tumour microenvironment (TME) and its cellular and acellular constituents. These can be used to test novel chemotherapeutics [14] and immunotherapeutics [15] as well as experimental modalities such as photodynamic therapy (PDT) [16,17] to ultimately realise better therapeutic outcomes.

The PDAC TME is unique in that it comprises a thick desmoplastic stromal matrix composed of a variety of structural and cellular elements [17–19]. Among the most prominent are collagen, fibroblasts, and pancreatic stellate cells (PSCs) [20]. PDAC also bares a distinct immunosuppressive microenvironment owing to the presence of $CD4^+$ T cells, cancer associated fibroblasts (CAFs), tumour-associated macrophages (TAMs), and myeloid derived suppressor cells (MDSCs) [21]. An anti-tumour immune response would usually require $CD8^+$ effector T cells [22,23], though these are sparse in PDAC and usually deactivated [22]. Since the efficacy of PDAC immunotherapy relies on the existence of the patient's anti-tumour immunity, responses are often poor [24]. Therapeutic recalcitrance is further exacerbated by the relatively low density of intratumoural microcirculation and vascular narrowing due to desmoplastic tissue-induced compression [25], affecting the delivery of systemically administered therapeutics. Although the latter phenomenon is more difficult to circumvent, studies are focusing on the reversal of immunosuppression to increase the efficacy of anti-PDAC agents. Extensive genomic, proteomic, and molecular analyses have expanded our understanding of the heterogeneity of PDAC and disease progression [1,26,27]. However, modelling PDAC in a research setting remains challenging due to the biological heterogeneity—a key factor in the development of personalised and precision therapies—that is arduous to emulate.

The aim of this literature review is to summarise and critically appraise the state of the art regarding PDAC models, focusing on spheroids, hybrid culture models, organoids, scaffold-based models, assembloids, microfluidic models, and xenografts derived from cell lines, organoids, and patients. This information is presented as a backdrop to PDT research on PDAC inasmuch as PDT is directly cytotoxic to tumour cells whilst harnessing the ability to damage the TME and trigger an anti-tumour immune response—i.e., factors that otherwise dictate therapeutic recalcitrance.

2. Two-Dimensional and Three-Dimensional PDAC Models

The biology of various human PDAC cell lines has been extensively studied [28]. Two-dimensional (2-D) in vitro models, which comprise monolayers of cells in culture, play an important role in the development of anti-PDAC drugs and have added to our understanding of how PDAC cells develop, proliferate, invade, and respond to anti-cancer drugs [29–32]. These models have been instrumental in medical research and are low-cost, easy to create, and facilitate fast data curation [33]. Large quantities of cells can be grown, which also enables high-throughput screening [34].

Though these models have proven useful, they are associated with numerous limitations. Primarily, a 2-D model cannot faithfully represent the complex PDAC TME [33]. Extracellular protein expression, interactions between the extracellular matrix (ECM) components and cells, tumour heterogenicity, and the dense, fibrotic stroma that houses non-parenchymal cells are not truly represented [33,35]. Most PDAC cell lines are derived from rapidly growing PDAC tumours, so slower growing tumours are underrepresented [36]. Furthermore, Audero et al. [37] demonstrated the biological significance of acidic stress in the TME. Tumour acidification is a well-established phenomenon that results from tumour cells switching to anaerobic respiration as a result of hypoxia (Warburg effect). The authors demonstrated that exposure to acidic conditions selects PDAC cells with augmented migration and invasion abilities induced by epithelial–mesenchymal transition, potentiating their metastatic potential when re-exposed to a neutral pH. The rewiring occurs through transcriptomic changes that affect genes responsible for proliferation, migration, epithelial–mesenchymal transition, and invasion. Naturally, 2-D cell cultures are always kept at near-neutral pH, which obviates these acid-mediated processes that likely materialize in the more complex models (e.g., Figure 1).

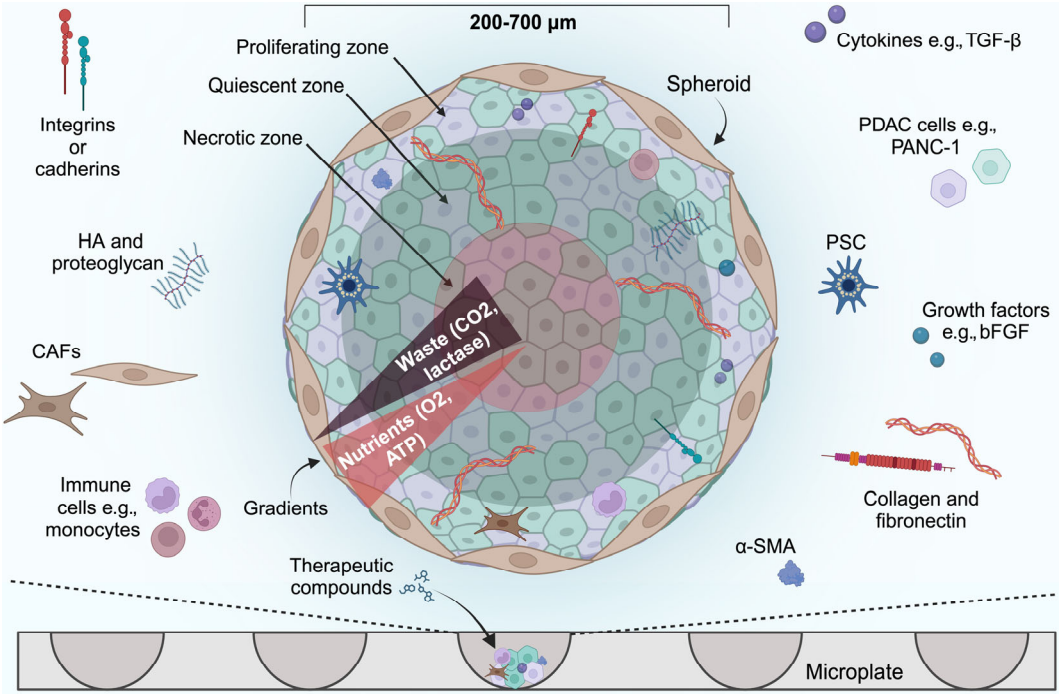

Figure 1. The pancreatic ductal adenocarcinoma (PDAC) stromal microenvironment can be replicated in vitro using 3-D spheroid structures. Spheroids can be formed using a low-adhesion microplate and consist of proliferating PDAC cells, quiescent cells, and a hypoxic core that is acidic due to lactate build-up. When co-cultured, additional cell types are introduced to better replicate the PDAC tumour microenvironment (TME). For example, cancer-associated fibroblasts (CAFs) can help to model the dense stroma by producing several of its constituents, such as the structural protein collagen, though such components can also be incorporated experimentally. Immune cells can also be used to help model the immunosuppressive features observed in PDAC. PDAC cells themselves express many of the extracellular matrix (ECM) proteins, including integrins and cadherins, which span the membrane and mediate adhesion to other PDAC cells and ECM components. Abbreviations: 3-D, 3-dimensional; α-SMA, alpha smooth muscle actin; ATP, adenosine triphosphate; bFGF, basic fibroblast growth factor; HA, hyaluronic acid; PSC, pancreatic stellate cell; TGF-β, transforming growth factor beta. Figure was made on Biorender.com.

Advancements in in vitro models of PDAC have led to three-dimensional (3-D) model types that better represent the PDAC TME [38], which is crucial for the proper appraisal of

anti-PDAC therapeutics [39]. Future studies should ideally utilise the following models to build more robust systems and increase the success rate of translational research.

2.1. Spheroid Models

Modelling the complex TME and 3-D structure of PDAC accurately has been challenging. Technological developments have allowed the creation of more advanced PDAC models from tumours using 3-D models that contain or are contained within artificial matrices. Spheroid models are clusters of cells within a 3-D structure. These models can be sourced from cell lines, tumour cells, or tumour tissues [40]. Cells are grown in a low-adhesion microplate to promote spheroid formation and must be cultured with growth factors and preferably ECM as well as components of the PDAC stroma, including CAFs [33,41]. Their 3-D organisation consists of cell–cell aggregation and proliferating heterogenous, necrotic, and quiescent cells within layers [42]. The methods available to culture spheroids have been reviewed elsewhere [43,44].

Proliferation-, metabolic-, and pH gradients can be represented by spheroid models [33,45]. This was shown in a study that investigated whether the mechanosensitive ion channel Piezo1 plays a role in transducing mechanical signals using PSC spheroids [46]. Acidification of the intracellular space inhibited Piezo1-mediated Ca^{2+} influx into PSCs in PDAC spheroids [46]. Ware et al. attempted to create a 3-D in vitro PDAC spheroid model to help increase our understanding of stroma development and tumour–stroma interactions [47]. Spheroid models made with PANC-1 cells and PSCs were structurally more compact and proliferated more than spheroids without PSCs. Researchers have also been able to model cell–ECM and cell–cell interactions present in PDAC using spheroids [48]. ECM components such as collagen I and III, smooth muscle actin (SMA), and fibronectin (a cell adhesion protein) have been successfully incorporated into PDAC spheroids and confirmed by immunohistochemistry [47]. Spheroids can also be used in high-throughput systems and for investigating the toxicity of novel PDAC drugs. Dufau et al. used Capan-2 pancreatic spheroids to evaluate spatio-temporal dynamics of chemotherapeutics. The authors compared the toxicity of gemcitabine alone and in combination with the checkpoint kinase-1 (CHK1) inhibitor 4-[[(3S)-1-azabicyclo[2.2.2]octan-3-yl]amino]-6-chloro-3-(1,3-dihydrobenzimidazol-2-ylidene)quinolin-2-one (CHIR-124) [49]. When gemcitabine was combined with CHIR-124, further cytotoxicity was induced in Capan-2 spheroids (~68% less ATP content was found, indicating lower cell viability) than with gemcitabine alone [49].

Many studies have suggested that spheroids are able to model drug resistance [40,50,51]. One study treated PANC-1, PSC, BXPC3, and Capan-1 pancreatic spheroids and corresponding 2-D models of these cell lines with a microtubule inhibitor, CB13, which inhibits cell division [40]. Significantly more chemoresistance occurred in the 3-D models than in the 2-D models following treatment. A decrease of ~59% in cell viability occurred in the 2-D models vs. 3% in 3-D models of the BXPC3 cell line [40]. It is believed that the chemoresistance exhibited by spheroids is due to the difficulty of chemotherapeutics in penetrating the multi-layered spheroid structure (Figure 1).

Limitations of Spheroid Models

The use of spheroids for PDAC modelling has several limitations. This model does not completely replicate the TME. For example, mono-culture spheroids do not model cellular diversity and cell–cell interactions and also lack the immune infiltrate which the PDAC tumour evades as well as the dense matrix and stroma [35,52,53]. Spheroids have low reproducibility, can be easily broken or removed during pipetting, and should be carefully handled [45]. Evidence also suggests that spheroids made using cell lines cannot accurately represent apicobasal polarity that plays an important role in cell migration [54,55]. As a result, spheroids are not ideal for modelling the physiological changes that occur in PDAC.

2.2. Co-Culture Models

Co-culture models for PDAC attempt to recapitulate the TME by incorporating multiple cell types, such as CAFs, immune cells, and endothelial cells. Around 90% of the volume of PDAC tumours are made up of supportive tissues as well as TME components [56]. The supportive tissues in PDAC tumours consist of pancreatic connective tissue, lymphatic vasculature, infiltrative immune cells, CAFs, and stroma [57–60]. The role of CAFs is to help regulate cytokines, growth factors, immune filtrate, and ECM deposition in the TME. These cells comprise a substantial proportion of the stroma and are the largest contributor to collagen, proteoglycan, and hyaluronan production [61,62]. CAFs are highly heterogeneous and exist within distinct subpopulations; each play a unique role in the pathogenesis of pancreatic cancer, so the incorporation of these different cell types into PDAC models is essential. A 2021 study developed a mouse model that mimicked the functional and histological characteristics of CAFs in PDAC [63]. The authors co-transplanted adipose-derived mesenchymal stem cells (which helped to generate CAFs) and the PDAC Capan-1 cell line into mice [63]. Global RNA sequencing, histological analysis, and single cell-based RNA sequencing showed that myofibroblast (myCAFs), inflammatory (iCAFs), and antigen presenting (apCAFs) CAF subtypes were represented in the model [63]. Accordingly, models of PDAC can be improved by co-culturing cancer cells with components such as stellate cells, fibroblasts, or other stromal cells [64–67] as shown in Figure 1.

Evidence suggests that co-culturing spheroids can represent a higher level of drug resistance due to the ability to model a dense PDAC stroma that drugs have difficulty penetrating [66]. One study used PANC-1 spheroids that were either mono-cultured or co-cultured with PSCs to compare gemcitabine resistance [66]. Cell viability was 5% greater in the co-cultured vs. mono-cultured spheroids [66]. Drug resistance was also greater in the co-cultures, though this was not significant. However, this study was limited to investigating one type of chemotherapeutic; the difference may be more apparent with other types of drugs. Another study compared the mechanical stiffness of PANC-1 monocultured spheroids and spheroids co-cultured with PSCs and transforming growth factor beta-1 (TGF-β1) [68]. PANC-1 co-cultured spheroids supplemented with TGF-β1 could model significantly more mechanical stiffness than the monocultures [68]. For example, the complex shear modulus (indicator of mechanical stiffness) increased by ~93% following 45 days of culture [68]. This may explain why co-cultured models are better for representing drug resistance in PDAC.

Evidence further suggests that co-culturing other 3-D models with CAFs can induce heterogeneity [57]. One study showed that organoids (another type of 3-D in vitro model) co-cultured with CAFs induced differential expression of SMA [55]. SMA plays an important role in PDAC progression and metastasis by suppressing E-cadherin, a tumour suppressor protein that prevents cell dissociation [69–71]. Öhlund et al. investigated whether subtypes of CAFs with distinct phenotypes exist in PDAC organoids co-cultured with PSCs, which are precursors of CAFs [72]. They found two CAF subpopulations; one, myCAFs, showed elevated expression of α-SMA and produced desmoplastic stroma. The other secreted interleukin 6 (IL-6) and other inflammatory mediators (iCAFs). This study shows that co-cultured models may be useful in helping to personalise treatment strategies by employing distinct cellular phenotypes in light of the fact that patients have different CAF subtype populations.

Co-culture models have been proficiently used for testing anti-PDAC drugs, drug delivery systems [73], and biomolecule-targeted interventions [74]. Kuninty et al. observed that microRNA (miR)-199a-3p and miR-214-3p were induced in 2-D cultures of patient-derived pancreatic CAFs and TGF-β-activated human PSCs, and that inhibition of miR-199a and miR-214 using hairpin inhibitors blocked TGFβ-induced differentiation markers

(collagen, α-SMA, platelet-derived growth factor β receptor), migration, and proliferation. Using a heterotypic spheroid model comprised of human PDAC (PANC-1) cells and human PSCs it was demonstrated that spheroid size was smaller when human PSCs were transfected with anti-miR-199a and anti-miR-214 compared to control anti-miR [32]. Anane-Adjei et al. investigated whether hyperbranched polymers would offer a suitable drug delivery system for PDAC [75]. They also assessed whether 2-D cell culture or MIA PaCa-2 spheroids co-cultured with bone marrow-derived mesenchymal stem cells (BM-MSCs) could better mimic the stromal tissue in PDAC since a small population of these cells can be observed in pancreatic tumours [75,76]. MSCs are adult stem cells that can differentiate into different cell types such as adipocytes (fat cells), osteocytes (bone cells), or chondrocytes (cartilage) [77]. Therefore, the authors compared the toxicity of conjugated hyperbranched N-(2-hydroxypropyl)methacrylamide (HPMA)-gemcitabine polymers and free gemcitabine in the mono-culture vs. co-culture spheroids. Higher cell viability was seen following treatment with 100 μM of free gemcitabine in the co-culture spheroids (~67%) compared to the mono-culture spheroids (~50%), demonstrating a higher level of drug resistance in the co-cultures [75]. However, no significant difference in drug resistance was seen between the co-culture and mono-culture spheroids when treated with HPMA polymers.

Limitations of Co-Culture Models

Co-culture models represent valiant efforts to maximally encapsulate the compositional features of the PDAC parenchyma and TME. Nevertheless, co-culture models often lack full tumour heterogeneity and the different genetic and epigenetic alterations in cells that comprise the PDAC in that most co-culture models include only a few selected cell types. Moreover, many co-culture models do not fully mimic the stiffness, composition, and mechanical properties of the actual tumour stroma [78]. While some co-culture models incorporate immune cells (e.g., macrophages or T cells), the models often lack the full repertoire of tumour-infiltrating lymphocytes, MDSCs, and dendritic cells. In that respect, an immune-suppressive environment of PDAC is difficult to recreate in vitro. PDAC tumours exhibit abnormal, hypoxic vasculature and corollary alterations in metabolism, which influences cancer progression and drug delivery. Most co-culture systems lack functional blood vessels, leading to unrealistic oxygen and nutrient gradients. Aside from the fact that many co-culture models fail to mimic the chemoresistance observed in vivo, drug diffusion in 3-D cultures rarely matches in vivo pharmacokinetics. Moreover, in vitro models do not fully replicate the metabolic interactions between cancer and stromal cells that include lactate recycling [79,80] and glutamine dependence [79,81]. The complexity of the system gives rise to additional technical challenges, such as those observed during long-term culture where co-culture systems degrade over time due to differences in cell proliferation rates. Cancer cells can outgrow other cell types with lower proliferation rates, leading to imbalances in the model. Finally, as with any model, variability in cell sources, passage numbers, and culture conditions leads to inconsistent results across studies. The lack of standardised protocols renders comparisons between different models difficult.

2.3. Organoid Models

Another type of 3-D in vitro models are organoids. These models are distinct from spheroids in that they are made using mechanically or enzymatically dissociated tumour samples as well as 2-D cell lines, whilst spheroids are only created from 2-D cell lines [45]. The organoid tissue is usually maintained in a Matrigel or collagen scaffold, in a growth factor-enriched medium that provides nutrients for tumour growth, or in suspension such as air-liquid interface culture (containing medium and collagen) [82]. The sources of these models include tumour cells, patient-derived resected tumour tissues, and embryonic,

adult, and pluripotent stem cells (stem cells that have been genetically reprogrammed into embryonic stem cells (ESCs) and are able to differentiate into any cell type) [33,83,84]. Using patient-derived resected tumour tissues to make organoids is particularly useful as it helps to reflect different CAF subtypes and specific characteristics in PDAC, including subclone epigenetic, phenotypic, and metabolic diversity. Their complex composition, as presented in Figure 2, consist of many cell lineages and helps to model the structure and function of PDAC. Self-assembled differentiated cells that are responsive to physical and chemical cues form part of the 3-D structure [85–87]. Laboratories experienced in generating organoids using surgically resected tumour tissue or endoscopic biopsies have had an organoid formation success rate of 75–95% [88].

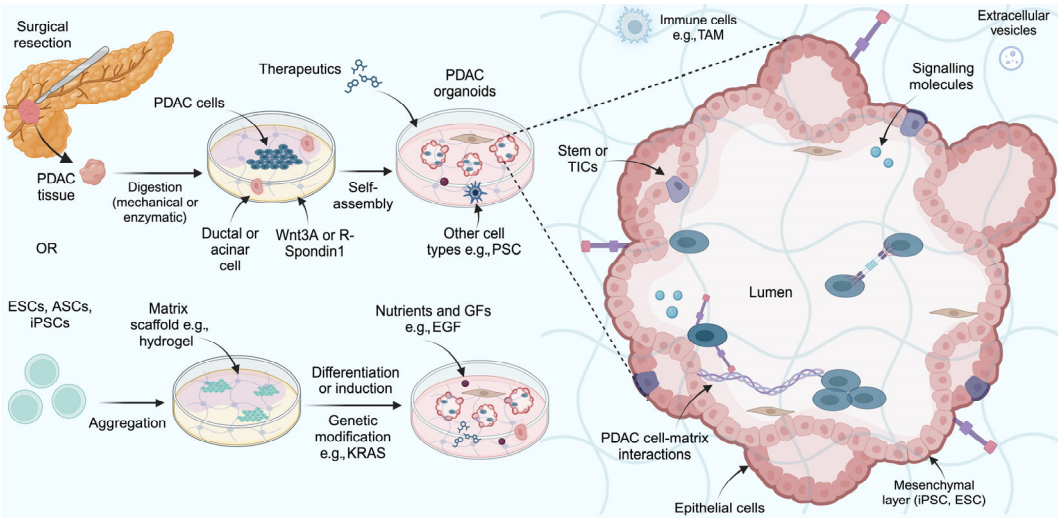

Figure 2. The structure and function of pancreatic ductal adenocarcinoma (PDAC) organoids. PDAC organoids are commonly derived from resected tumour samples or stem cells with the potential to form a structure that is able to recapitulate specific morphological and structural features of the malignancy. As organoids can be engineered to contain various PDAC tumour microenvironment (TME) components including fibroblasts, matrix proteins, and immune cells, they are able to replicate endogenous TME cell functions and heterogeneity. The optional use of naturally derived or synthetic polymers in culture can recreate the 3-D extracellular matrix (ECM) composition as the PDAC and epithelial (ductal or acinar) cells comprising the organoid interact with these components via receptor proteins such as integrins. Within the organoid, a large population of PDAC cells send and receive signals from the matrix and orchestrate both paracrine and autocrine signalling using a variety of signalling molecules, including the cytokine transforming growth factor beta (TGF-β). Abbreviations: 3-D, 3-dimensional; ASC, adult stem cell; EGF, epidermal growth factor; ESC, embryonic stem cell; GF, growth factor; iPSC, induced pluripotent stem cell; KRAS, Ki-ras2 Kirsten rat sarcoma viral oncogene homolog; PSC, pancreatic stellate cell; TAM, tumour-associated macrophage; TIC, tumour initiating cell. Figure was made on Biorender.com.

Organoid models have enabled intercellular and intracellular interactions, the cellular compartment, diversity, composition, and structure of PDAC to be modelled ex vivo [33,45,89]. They also have allowed many aspects of PDAC to be modelled without requiring an in vivo system, such as proteomic, histological, and genetic features and self-renewal [90]. Driehuis et al. demonstrated many comparable characteristics between 30 patient-derived organoid (PDO) lines from tumours in the pancreas and their corresponding primary tumours [91]. For example, a patient showing progressive disease under gemcitabine treatment had a corresponding PDO that was the most resistant to gemcitabine out of all of the organoids [91]. Three other patients with stable disease following gemcitabine treatment and their corresponding PDOs showed high or intermediate

sensitivity [91]. When sequenced, PDAC organoids exhibited many similarities to PDAC tumours. One study assessed whether any similarity could be observed between PDAC organoid models and human PDAC by sequencing miRNA profiles of extracellular vesicles (EVs), a promising diagnostic tool for PDAC [92]. Interestingly, the same set of miRNA EVs could be observed in both PDAC organoids and in blood plasma samples of PDAC patients. Organoids can also be passaged continuously for ongoing experimentation [93].

Organoid models usually consist of many different cell types. The cells occupy niches and therefore enable the modelling of the interactions and physiological characteristics observed in the native tumour [45]. Holokai et al. attempted to develop a clinically relevant PDAC organoid model that could be used to predict the efficacy of targeted therapeutics [94]. Their pancreatic organoids modelled the stromal and immune components seen in PDAC, including myCAFs and tumour-infiltrating lymphocytes. Depletion of arginase 1-expressing polymorphonuclear MDSCs, which block $CD8^+$ T cell anti-tumour immune responses rendered the organoids susceptible to anti-programmed death 1 receptor (PD-1)-programmed death ligand 1 (PD-L1)-induced death [94]. The data demonstrate that PDAC organoids are suitable for predicting the efficacy of targeted therapeutics.

Since the median time to create PDOs and pharmacotyping can be less than 2 months, depending on the tumour quantity and quality, one potential use for this model could be to assist a patient in their post-surgical recovery period to select adjuvant therapy [91,95]. Driehuis et al. attempted to describe a biobank of pancreatic PDOs characterised by methods such as DNA sequencing to show the importance of personalised medicine predicated on organoids. Different pancreatic organoid lines had distinct drug sensitivity profiles that could be sorted for 76 different anti-cancer agents (microtubule-targeting drugs, AURKA-targeting drugs, PIK3CA-targeting drugs, and TOP1-targeting drugs) [91]. PDAC organoid models could also be used to investigate disease physiology and the targeting of specific signalling pathways by novel therapeutics. For example, Krieger et al. recently tried to determine whether transcriptionally and histologically defined subpopulations, which had classical features in metastases, were associated with more aggressive clinical behaviour in PDAC [96]. They used PDAC organoids to identify classical subtypes of genes such as p081, which correlated to better chemotherapy response, including to gemcitabine.

Limitations of Organoid Models

Organoid models have several limitations. They can take longer to make and have higher costs than spheroid models, and pH gradients are unable to be modelled accurately [45,97]. In addition, PDOs derived from those receiving neoadjuvant therapy is dependent on viable tissue being present during resection [98]. Comparing data can also be challenging since Matrigel and collagen have interbatch differences in composition [35]. For example, Matrigel includes other components as well as collagen, including laminin, which promote the invasion phenotype in tumour cells [99,100].

2.4. Hydrogel Scaffold-Based Models

Hydrogel scaffold-based models comprise covalently bound hydrophilic polymers arranged in a 3-D network that retain a large amount of water [101,102]. The structure of the cells within the network influences cell function and responses to PDAC therapeutics [102]. Traditional hydrogel scaffold-based models can be made using gelatin methacrylate or Matrigel hydrogel.

Technological advancements have led to the development of hydrogel scaffold-based models that consist of a cellular network structure offering impressive biochemical, biocompatible, and biophysical tunability [102]. These models help promote 3-D cell proliferation, replicate the ECM, and allow for the diffusion of nutrients [102] (Figure 3). Recently, this

was illustrated in a study where hyaluronic acid- and gelatin-based hydrogels were used to create matrices for PDAC spheroids comprised of ASPC-1 cells and CAFs to model the PDAC TME [103,104]. Higher amounts of vascular endothelial growth factor receptor 2 (VEGFR2) were observed in stiffer hydrogels compared to softer hydrogels. This receptor mediates angiogenesis and subsequent progression of PDAC by allowing cells to obtain oxygen and nutrients from leaky blood vessels [103]. Other advantages of hydrogel scaffold-based models are that these models can represent both soft and elastic characteristics due to the presence of networks of hydrophilic polymers and the ability to swell in aqueous solution [105]. Curvello et al. assessed the ability of collagen-nanocellulose hydrogels to mimic the PDAC ECM [106]. When type I collagen fibrils and cellulose nanofibers were blended, the resulting hydrogel scaffold exhibited controllable stiffness and modelled the natural PDAC tissue.

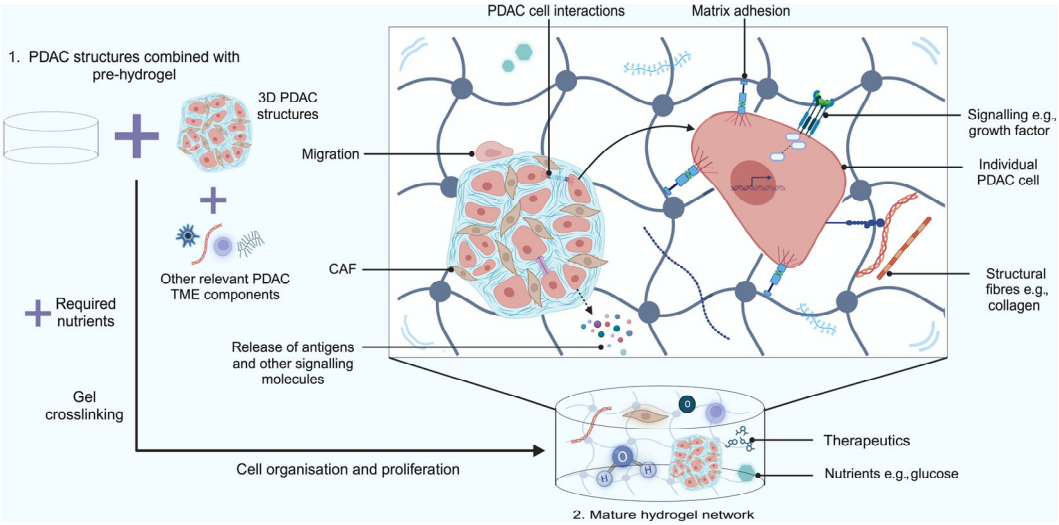

Figure 3. Three-dimensional hydrogel scaffold models of pancreatic ductal adenocarcinoma (PDAC). Various PDAC structures, including spheroids or organoids, can be inserted into hydrogel scaffolding, which comprises covalently bound hydrophilic polymers arranged in a 3-D network with water, oxygen, and nutrients. Both within and between the 3-D structures, PDAC cells biochemically and physically communicate via paracrine (signal secretion) or physical (junctions between neighbouring cells) mechanisms. Signals are received and internalised, which leads to gene transcription changes that reflect those observed in vivo. Similarly, PDAC cells interact with the scaffolding via adhesion proteins such as integrins as well as actin, which facilitates the conversion of mechanical forces from the matrix into biochemical signals that enter the PDAC cell nucleus. In many models, the stiffness of the matrix is tunable and facilitates the proliferation and migration of PDAC cells via focal adhesions to extracellular matrix (ECM) proteins. The matrix also enables the diffusion of soluble factors and signalling molecules. Abbreviations: CAF, cancer associated fibroblast; GF, growth factor; HA, hyaluronic acid; PSC, pancreatic stellate cell; TGF-β, transforming growth factor beta. Figure was made on Biorender.com.

Hydrogel scaffold-based models can be combined with other model types for PDAC. Spheroids can be cultured with hydrogels to model stronger cell–cell interactions and recreate the mechanical forces seen in vivo [107]. Ermis et al. created a hydrogel-based spheroid PDAC model comprising CAFs and ASPC-1 cells to more closely recapitulate the desmoplastic stroma [103]. They demonstrated very compact tissue formation with increased matrix stiffness compared to models without these cellular constituents [103].

Limitations of Hydrogel Scaffold-Based Models

The use of hydrogel scaffold-based models requires consideration. For one, the models lack spatial and temporal control, which leads to an uneven distribution and irregular seeding of cells [108,109]. The complex microvasculature seen in PDAC is absent in these models, resulting in a deficiency in nutrient and signalling molecule transport [108]. As a result, seeded cell viability and function are lost relatively quickly over time. This may limit the range of anti-PDAC drug toxicological investigations.

2.5. Assembloid Models

An assembloid model consists of multiple organoid types that self-organise into 3-D cell-based systems [110]. Assembloid models can be made with different tissues or cells, as shown in Figure 4. Formed using diverse cell lineages, the structures can facilitate the physiological changes seen in PDAC, enable cell–cell interactions, and demonstrate the effects of interventions on different organs.

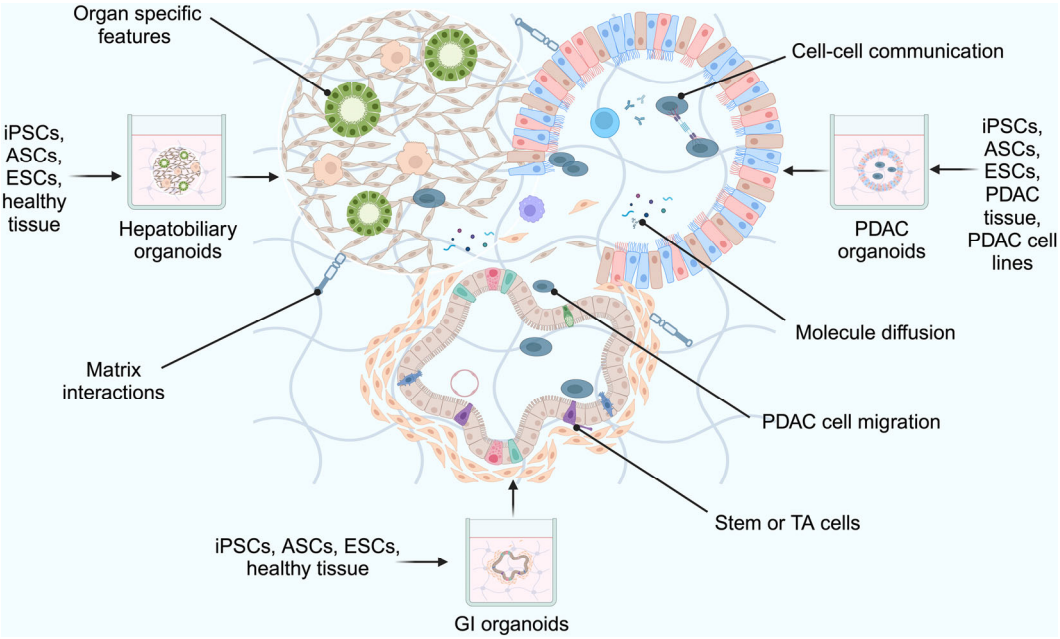

Figure 4. Exemplary 3-D assembloid model use for in vitro studies of pancreatic ductal adenocarcinoma (PDAC). Assembloid structures are most commonly formed by fusing multiple organoids that represent different organ systems. When cultured, additional relevant cell types can be included such as endothelial cells, which help form immature vasculature, and immune cells, which help replicate the immune tumour microenvironment in PDAC. These multi-region assembloids are unique in that they display a high level of connectivity and can demonstrate the interaction between organ-specific cell types. In particular, the movement of PDAC cells in between organoid types represents the process of metastasis to nearby organs. The diffusion of drugs, nutrients, oxygen, and metabolic waste can be modelled, as well as the interaction of the organoids with the incorporated extracellular matrix (ECM) components. Abbreviations: ASC, adult stem cell; ESC, embryonic stem cell; GI, gastrointestinal; iPSC, induced pluripotent stem cell; TA, transit amplifying. Figure was made on Biorender.com.

Choi et al. investigated the role of jagged-1 in PDAC cell plasticity since plasticity is poorly understood in organoids yet may influence drug efficacy [111]. Assembloids were made using peripheral blood mononuclear cells (PBMCs), endothelial cells, and CD44(−) cells isolated from PDAC organoids using fluorescent activated cell sorting (FACS). To investigate jagged-1 expression in pancreatic cancer compared to healthy pancreatic tissue, the authors analysed the Cancer Genome Atlas, the Pancreatic Adenocarcinoma dataset and the Genotype-Tissue Expression dataset [111]. Jagged-1 expression was significantly

increased in malignant tissue. They also analysed jagged-1 levels in the assembloids during differentiation, which revealed an increase in jagged-1(+)CD24(+)CD44(-)epithelial cell adhesion molecule (EpCAM)(+) cells in the assembloids. Though these models have demonstrated their potential in representing the various cellular and structural features observed in PDAC, this is a new technology and further studies and investigations will evolve this technique.

Limitations of Assembloid Models

While assembloids provide a more physiologically relevant system than the abovementioned, more traditional models, the assembloid models also come with several limitations. Because of their intricate nature, these models are plagued with complexity and standardisation issues. For example, assembloids require precise control over cellular composition, ratios, and spatial organisation, making these models technically demanding to generate. Differences in cell sources (e.g., patient-derived vs. cell line-derived) can lead to variability in reproducibility, especially in the face of lacking universal protocols. As was addressed for co-cultures, assembloids may experience loss of architecture over time and suffer from differential growth rates of individual cellular constituents, leading to loss of specific cell populations. Due to their 3-D nature and dense structure, insufficient oxygen and nutrient diffusion can lead to central necrosis, limiting viability. Moreover, desmoplastic stroma may not be fully recapitulated and immune cell–TME interactions are commonly incomplete (see also Section "Limitations of Co-Culture Models"). Assembloids require advanced culture conditions (e.g., hydrogels, bioreactors) and rely on expensive reagents (e.g., Matrigel, growth factors, specialised media) that limit high-throughput screening while increasing cost. The previously addressed issues related to vascularisation and consequential hurdles for drug permeability and pharmacokinetics (Section "Limitations of Co-Culture Models") also apply to assembloids. While patient-derived assembloids, which require fresh tissue samples that can be limited and pose ethical restraints, retain genetic heterogeneity, this also leads to variability in responses, complicating broad therapeutic predictions. Despite their complexity, these models do not fully replicate all in vivo conditions, as a result of which results may not always translate to the clinical setting.

2.6. Microfluidic Models

Microfluidic devices are miniaturised systems comprised of chambers and micro-scale fluidic circuits that mimic the PDAC TME by incorporating fluid flow, multiple cell types, and controlled biochemical gradients (Figure 5) [112]. The devices' conceptual framework was designed to overcome the limitations of earlier in vitro models of PDAC, including difficulties in modelling heterogeneity and biochemical gradients. PDAC spheroids can be cultured within the device, which facilitates the use of fewer cells and reagents due to its microscale dimension. This allows precise and quantitative measurements to be performed [112,113]. Microfluidic models are low-cost and easy to use since only small volumes of samples are needed [114]. Therefore, the model is suitable for high-throughput screening and labour-intensive work.

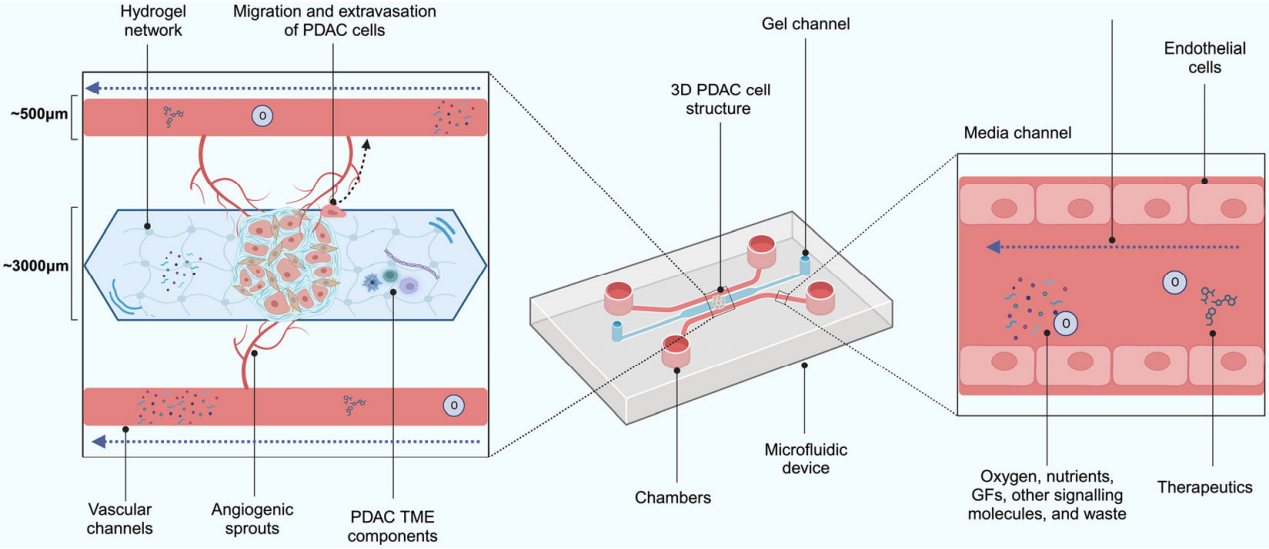

Figure 5. Microfluidic pancreatic ductal adenocarcinoma (PDAC) models. Three-dimensional (3-D) in vitro PDAC structures, including spheroids and organoids, can be cultured using microfluidic devices that contain miniature circuits with precise dimension. The circuit mimics the vasculature observed in the PDAC tumour microenvironment (TME), with the 'vessels' being lined with endothelial cells. Angiogenic sprouts can carry molecules to and from the PDAC cells and aid in the creation of gradients similar to those observed in vivo. The use of a co-cultured spheroid, which can include other cell types seen in the PDAC TME such as pancreatic stellate cells (PSCs), can help model the environment with even greater accuracy. Pharmaceutics can be injected into the microcircuit. One important use of such a technique is to investigate anti-tumour drug delivery through the PDAC stroma. In addition, the small scale of the device enables controlled drug flow to the PDAC structures, which facilitates the assessment of drug concentrations (e.g., efficacy and cytotoxicity) more precisely. The dotted arrows represent the flow direction of media. Abbreviations: GF, growth factor. Figure was made on Biorender.com.

Microfluidic models manufactured with human or murine cells embedded in 3-D ECM may also be used to feature in vivo behaviour such as the generation of shear stress during extravasation [112] and epithelial-mesenchymal transition and local invasion [115]. The geometry of blood vessels and the 3-D PDAC TME can also be demonstrated. One study investigated the effect of shear stress on the morphology and behaviour of human umbilical vein endothelial cells (HUVECs) using a microfluidic device [116]. Various levels of uniform wall shear stress were demonstrated using a novel microfluidic shear stress generator. Future studies could use microfluidic systems to control biophysical and biochemical conditions in the model more precisely [112]. In addition, multifluidic models can be adapted to form multi-organ-on-chip models. As this technology develops, it would be particularly useful in PDAC research since it can facilitate and monitor cross-communication between organs, thereby modelling systemic disease states in relation to PDAC. It is apparent that microfluidic models can be developed in numerous ways to create an advanced PDAC ex vivo model.

Microfluidic models would be useful for industrial work as well as large-scale PDAC therapeutic testing. In one study, a novel microfluidic model was manufactured using a cyclin olefin polymer chamber named HepaChip and cultured with PDAC PANC-1 spheroids [117]. This model was able to withstand higher doses of cisplatin when compared to other in vitro cultures.

Limitations of Microfluidics Models

Microfluidic devices require precise engineering and components (pumps, imaging systems, and precise fluid control) that makes design, fabrication, and assembly relatively complex and costly. Operating microfluidic systems requires specialised knowledge in microengineering and biofabrication, which in turn limits accessibility. Accessibility is further hampered by the fact that many PDAC-on-chip models are custom-built and not widely commercially available. Even small variations in chip fabrication can affect reproducibility, making cross-study comparisons challenging. Each chip must be carefully assembled and experiments often require continuous monitoring, making these models tedious. Consequently, microfluidic devices are generally low-throughput and difficult to use for large-scale drug screening, also owing to the possibility of only testing a few conditions at a time (unlike high-throughput spheroid or organoid systems). Drug testing is additionally complicated by a lacking liver metabolism and systemic pharmacokinetics infrastructure, limiting drug response accuracy. While microfluidics can model drug flow, the systems do not fully replicate the diffusion barriers seen in dense PDAC tumours whilst excessive or inadequate shear stress may alter drug effects in ways not seen in actual tumours.

Aside from these technical limitations there are also biological hurdles. First, current microfluidic models struggle to fully replicate ECM stiffness, composition, and cellular heterogeneity while long-term immune cell-tumour interactions are difficult to sustain in microfluidic systems despite the possibility to introduce immune cells. Although cancer, stromal, and endothelial cells can be incorporated, current models often lack certain key cell types, such as pericytes, MDSCs, and dendritic cells. Second, many microfluidic cultures cannot be maintained long-term due to nutrient depletion, fluid shear stress, or loss of cell viability and, unlike organoids or assembloids, these systems may fail to maintain proper 3-D tissue architecture over time. Third, current microfluidics models suffer from vascularisation and perfusion challenges. While some models incorporate artificial vasculature, true capillary networks with functional endothelial barriers are difficult to recreate. Emulating hypoxic PDAC conditions and interactions between PDAC cells and circulating immune cells or tumour-derived exosomes is hence arduous. As alluded to previously for other models, there is no universal protocol for PDAC microfluidic models, which can produce interstudy inconsistencies in these models too.

2.7. Xenograft Models

In a xenograft model, tissue or cells are transplanted into an animal (generally subcutaneously or orthotopically) to represent PDAC and emulate drug responsiveness more closely [118,119]. Different types of xenograft models include cell line-derived xenografts, organoid-based xenografts, and patient-derived tumour xenografts (PDX). The tissues or cells are usually implanted into an immunodeficient [120] or syngeneic mouse (where tumour cells are obtained from genetically identical animals) [121]. This avoids graft rejection by the host's immune system (Figure 6).

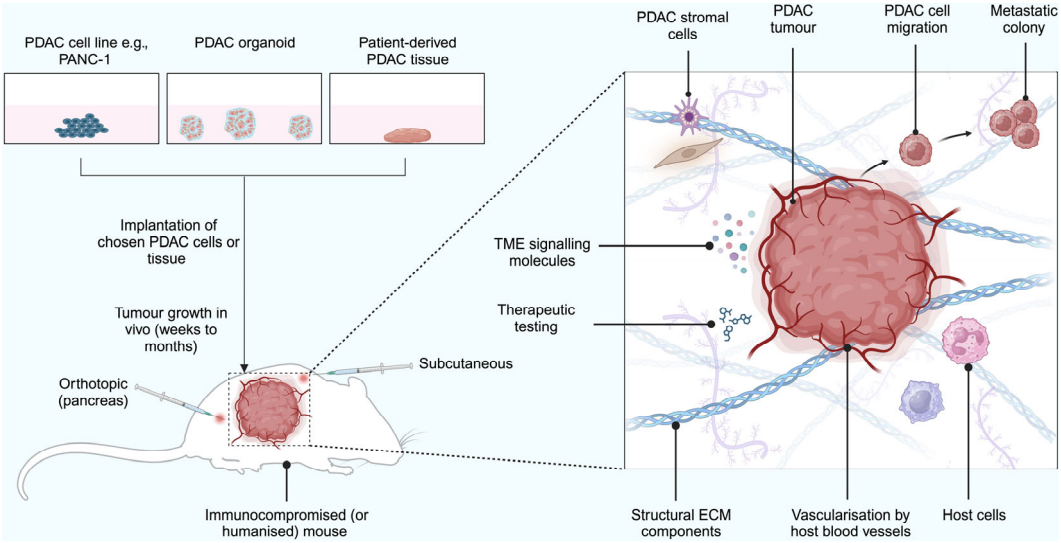

Figure 6. Pancreatic ductal adenocarcinoma (PDAC) xenograft models. Xenotransplantation involves the transfer of PDAC cell lines, PDAC organoids, or patient tissue into a recipient, usually an immunocompromised mouse. Though the establishment and growth of the cells in vivo is a long process (typically weeks), the developed tumour interacts with the graft and host tumour microenvironment (TME) components and displays a high similarity to PDAC disease progression in humans. The model is considered high fidelity owing to the vascularisation of the tumour by the host's blood vessels, which facilitate the delivery of various molecules, including any therapeutics, to the tumour. As well as the spatial structure of PDAC being represented, use of patient tissue can retain intratumour heterogeneity and tumour subtype. Abbreviations: ECM, extracellular matrix. Figure was made on Biorender.com.

2.7.1. Cell Line-Derived Tumour Xenograft Models

Cell line-derived xenograft models consist of human PDAC cell lines transplanted into immunocompromised mice [120]. These models improve the representation of the biology of PDAC and the responsiveness to drugs compared to the aforementioned models [36]. The models are practically more convenient than PDX models since no patient tissue samples are exacted. Cell line-derived xenograft models may be better alternatives to PDX models in instances where an improved in vivo model is desired but time is limited or patient access is restricted since no patient tissue needs to be obtained. Future studies could also incorporate the chicken embryo chorioallantoic membrane (CAM) model into the cell line-derived xenograft model line up since these are able to assist cell growth. Rovithi et al. cultured four primary PDAC cell lines (PDAC-1, PDAC-2, PDAC-3, and PDAC-4) on CAMs to generate low passage cell cultures and transduced the cell lines with lentivirus expressing firefly-luciferase (Fluc) [122]. By incorporating bioluminescence, the authors could measure tumour growth in situ. As cell numbers increased, Fluc activity increased.

Limitations of Xenograft Models

It has been reported that cell line-derived xenografts have predicted the therapeutic response in various cancers, including PDAC, inconsistently [123–125]. Bruns et al. created a pancreatic orthotopic xenograft model to investigate whether the anti-epidermal growth factor receptor (EGFR) antibody cetuximab inhibits PDAC growth and metastasis and whether gemcitabine exacerbates this effect [126]. The model was further used to examine therapeutics targeting EGFR as a potential treatment for PDAC. The authors observed that there was a reduction in tumour volume with cetuximab compared to the untreated control group. Moreover, the reduction in tumour volume was more profound when treatment was combined with gemcitabine (~94.7% decrease in tumour cells for 32 ng/mL gemcitabine

plus 2.5 µg/mL of cetuximab vs. a decrease of 10.5% in tumour cells without gemcitabine and only 2.5 µg/mL of cetuximab [126]). In contrast, it was found in a phase III clinical trial that patients who had advanced pancreatic cancer treated with gemcitabine and a placebo or gemcitabine with cetuximab experienced no benefit from treatment [127]. Other studies also further support the translational inconsistency between results seen with cell line-derived xenografts and clinical trials for various types of cancers [128,129]. One reason for the differences seen in drug responses may be due to the fact that cell line-derived xenograft models exhibit limited stromal infiltration, absent interactions with the adaptive immune system, and grow mainly as homogeneous masses of tumour cells [36]. However, issues with a lack of stromal infiltration in cell line-derived tumour xenograft models may be resolved by co-culturing these models with stromal components such as stellate cells, thereby modelling the thick desmoplastic stromal matrix in PDAC and drug resistance, albeit not overcoming inherent immune system defects.

2.7.2. Organoid-Based Xenograft Models

Organoid-based xenograft models (also referred to as patient-derived organoid xenografts) can be generated by transplanting PDAC tumour organoids into an immunocompromised mouse [82]. Organoid-based xenograft models represent tumour neoplastic cell heterogeneity and can emulate the different stages of PDAC disease progression [36], which may be due to the recovery of different stem cells during transplantation that reflect these varying stages [36].

Xenografts made using organoid models can recapitulate all stages of PDAC disease progression, making them distinct from other xenograft models. In addition, transplantation into a host is the only efficient way of incorporating blood vessels into organoids [130] that are also amenable to representative locoregional stressors such as vascular compression [131]. Interestingly, one study created a patient-derived PDAC organoid xenograft model that showed intraepithelial neoplasms progressing in an indolent or invasive way and associated these growth patterns with PDAC subtypes (classical or basal-like) [132]. Moreover, organoid-based xenografts help to recapitulate the large amounts of collagen seen in PDAC that is not represented in cell-based xenografts [133,134]. Recently, Tanaka et al. attempted to create a well-established preclinical model of PDAC to test new therapeutic targets [135]. They created a PDAC organoid-based xenograft model using the S2-013 cell line and performed pathological and immunohistochemical analysis to characterise this model. The model had similar tissue to that seen in PDAC patients, with abundant cancer stroma containing mature blood vessels and collagen [135]. As the vasculature and TME can be represented by this model, its use could be applied in the search for novel therapeutic targets in PDAC, including anti-angiogenics.

Another suitable use for organoid-based xenograft models would be to investigate personalised therapy for PDAC patients. Raimondi et al. attempted to investigate the feasibility of using patient-derived PDAC organoid xenograft models to screen for the response of oncolytic adenoviruses as personalised therapy [136]. They found that differences were seen in cytotoxicity with the oncolytic adenoviruses in different patient-derived PDAC organoid xenograft models, indicating the sensitivity to oncolytic adenoviruses seen in primary PDAC tumours [136]. The cell viability in an organoid derived from a PDAC patient following treatment with 1×10^4 pfu/well of the oncolytic adenovirus AduNuPARmE1A was ~27 ± 12% compared to ~83 ± 10% in an organoid derived from another PDAC patient [136].

Limitations of Organoid-Based Xenograft Models

Although organoid-based xenograft models fulfil an important role by bridging the gap between in vitro organoid cultures and traditional PDXs, the models do come with several limitations. Because of their complexity, these models require more resources that include immunodeficient mice, specialised facilities, and long-term maintenance, which drives up cost. Organoids take weeks to expand in culture and xenografts require weeks to months to develop into mature tumours, delaying experimental timelines. As a result, organoid-based xenograft models have low throughput, which makes these models impractical for large-scale drug screening. Logistical hurdles also come in the form of ethical concerns regarding animal experimentation and the use of immunodeficient mice in preclinical research. These are compounded by the possibility that organoid-based xenograft models may face challenges in regulatory approval for clinical drug validation, as they are not fully humanised. Mice process drugs differently from humans [137] and the xenografts therefore do not fully replicate human drug absorption, distribution, metabolism, excretion, and toxicity (ADMET), which may lead to differences in pharmacological profiles and limit direct clinical translation.

From a biological perspective, the murine host provides stromal components that are of non-human origin, which may not fully mimic human CAFs, ECM, and desmoplastic responses. Inasmuch as immunocompromised mice lack key components of adaptive immunity, which is critical in tumour control and eradication [138], no accurate studies on immune evasion and immunotherapy are possible. Furthermore, organoid-derived tumours may not fully recapitulate the dense fibrosis in PDACs, leading to altered drug penetration and response compared to human tumours. Organoids are typically expanded in vitro before implantation, which can lead to clonal selection and loss of intratumoural heterogeneity. Serial passaging of organoids before implantation may introduce genetic and epigenetic alterations [139,140] and certain subpopulations of stem-like or therapy-resistant cells may be lost during the organoid culture phase [141,142], making the xenograft model less representative of the original tumour. Another important biological factor that is often dismissed is local biochemical milieu. Most organoid-based xenograft models involve subcutaneous implantation, which may neither properly reflect the molecular landscape in the pancreas (e.g., abundance of digestive enzymes (trypsin, amylase, lipase) and hormones (insulin, glucagon)) nor accommodate natural tumour initiation and metastatic dissemination.

2.7.3. Patient-Derived Xenograft Model

PDXs are a type of xenograft model that use tumour tissue engraftment from patients transplanted into mice [143]. The direct sourcing of patient tumour tissue has allowed PDX models to improve in vivo modelling by representing the complex PDAC TME with higher accuracy. PDX models may also be employed to identify unique therapy sensitivities in precision medicine [144]. Recently, Magouliotis et al. attempted to investigate the suitability of PDAC PDX models for precision therapy [145]. The xenografts modelled the most and least aggressively differentiated population of the patient's PDAC tumours using immunohistochemistry [145]. This investigation confirmed that the models are suitable for the exploration of precision medicine for PDAC [145]. Evidence also suggests that these models may be most suitable for assaying the efficacy and efficiency of PDAC therapeutics [35]. Wu et al. utilised PDX PDAC models to test the feasibility of gemcitabine-based nanoparticles as a potential treatment for PDAC [146]. The nanoparticles could inhibit tumour progression and alleviate systemic toxicity. In a different study, Garcia et al. studied the anti-tumour efficacy of JQ1, a bromodomain protein inhibitor, in PDAC PDX models [147]. They found that JQ1 inhibited the growth of all the PDAC PDX models tested [147].

Limitations of Patient-Derived Xenograft Models

PDX models have issues associated with their use that echo organoid-based xenograft models. These models require high quantities of tissue and it can be difficult to resect enough tissue required for studies within a specific timescale. The models also usually require a high number of animals and take time to grow [35,148,149], providing a timeline that is often unrealistic [35] and costly [36]. These factors may contribute to the lower success rates of de novo PDX models compared to cell line-established models [35]. Another limitation of these models is their inability to accurately represent interactions with immune components in the TME due to the use of immunodeficient mice [150]. Therefore, this model cannot be used for immunotherapy research [151] unless the model employs humanised mice [152]. Passaging PDX models also results in clonal evolution, meaning that this model should only be used within three generations for therapeutic experiments [153]. Therefore, it may be difficult for large-scale serial passaging and expansion to be completed for the purpose of drug screening [36].

A summary of each different model type described in this review article is summarised in Table 1.

Table 1. Summary of PDAC models and their characteristics.

Model	Spheroid	Co-Cultured Spheroids	Microfluidic Spheroid Models	Hydrogel Scaffold-Based Models	Organoids	Assembloids	Organoid-Based Xenografts	Patient-Derived Xenografts	Cell Line-Derived Xenografts
Application	Investigating PDAC drug toxicity	Investigating PDAC drug toxicity	Industrial, large-scale PDAC drug testing	Testing PDAC drugs where loss of cell viability is not an issue	Investigating the physiology of PDAC	Investigating physiological changes in multiple organs	Investigating disease progression in PDAC	Investigating the efficacy of PDAC therapeutics (TME is well represented)	More convenient than PDXs, but do not fully represent the TME
Cost	Low	Moderate	Low	Moderate-high	Moderate	Moderate-high	Moderate-high	High	Moderate-high
Time	~3 to 5 days	~3 to 5 days	Within 7 days	~10 days	~4 days	≥7 days	1–2 months	Up to 6 months	1–2 months
Specimen	Cell lines	Cell lines	Cell lines	Cell lines	Tumour tissue, tumour cells, or stem cells	Tumour tissue, tumour cells, or stem cells	Tumour tissue, tumour cells, or stem cells and immunocompromised mice	Resected tumour tissue and immunocompromised mice	Cell lines and immunocompromised mice

2.8. Evolving Technologies for PDAC Mimicry

Though existing models of PDAC have improved substantially and can now replicate the TME quite accurately, they are complex to develop and maintain and translatability remains a major challenge. An alternative approach would be to adopt an in silico strategy. This often involves computational models that comprise databases, molecular modelling approaches, machine learning, data mining, and/or data analysis tools [154]. The use of in silico systems is associated with lower costs, better research ethics, and facilitates rapid data collection. As a result, utilisation of technology in this way will be particularly useful as it advances, particularly in the era of artificial and generative intelligence.

In silico models have many uses within research and may be particularly useful in the investigation of novel therapeutics for PDAC. Recently, one study used datasets available on the Gene Expression Omnibus database to investigate potential PDAC biomarker targets [155]. Based on their co-expression and protein–protein interaction networks, 79 gene candidates were enumerated. Five significant endoplasmic reticulum protein processing pathways involved in PDAC progression were found, including hsa04141 [155]. Having previously been associated with malignant behaviour, another study analysed transportome (membrane transporter and channel) expression changes in PDAC and their

correlation with functional and behavioural responses [156]. The authors filtered data from a DNA microarray Affymetrix GeneChip dataset using cut-off fold-change values of ≤ 2 or ≥ 2. Among several notable observations, some down-regulated genes, including calcium voltage-gated channel subunit alpha1 G, were linked to cell differentiation. These observational studies exemplify the use of in silico techniques for the investigation of PDAC biology and druggable targets. Follow-up confirmation in biological systems is always warranted after in silico analysis.

3. Application of Biomimetic PDAC Models in PDT Research

PDT is a relatively new approach that aims to overcome the recalcitrance to systemic therapy exhibited by many types of cancer, including PDAC [157]. PDT has been approved for the treatment of superficially located lesions and solid tumours [158,159] and is under investigation in clinical trials with respect to tumours in internal organs [160,161]. In the case of the latter cancer types, direct cytotoxic effects are conferred via the photo-excitation of a systemically administered photosensitiser (PS) and subsequent generation of reactive oxygen species [162] in the target tissue (Figure 7). The reactive transients chemically modify vital molecules (e.g., proteins [163,164], lipids [165], nucleic acids [166]), resulting in excessive and often irreparable damage that entails loss of membrane integrity [167], perturbation of cellular homeostasis [168], metabolic catastrophe [169], and eventually the manifestation of various modes of tumour cell death [170,171] and immunological cell death [172].

The application of PDT for PDAC is particularly relevant for several reasons. At mildly elevated levels, reactive oxygen species (ROS) are needed to steer tumour progression through cell transformation [173], proliferation [174], survival [175], angiogenesis [176], and metastasis [177,178]. As a protective measure, cancer cells upregulate anti-oxidant defence systems to maintain a sustainable level of redox homeostasis [179]. Hyperoxidative stress, as is caused by PDT (and other therapeutic modalities) [180,181], is a prelude to impending cell demise that can be offset by an anti-oxidant response to PDT [158,169,182]. These variables notwithstanding and as discussed in Section 3.3.3, PDT affects intratumoural redox states in a manner that is conducive to a positive treatment response beyond direct photochemical damage. PDT can destroy both the PDAC cells and surrounding desmoplastic tissue [17] whilst eliciting a post-therapeutic anti-tumour immune response [183] and inducing metabolic paralysis of parenchymal and non-parenchymal cells owing to vascular shutdown [184,185]. In addition to perturbing the tumour-promoting effects of PDAC stroma, including tumour–stroma interactions, PDT can enhance the response to chemotherapy [186] and immunotherapy [187]. Therefore, the use of models that faithfully represent and encompass the complex biology and biochemistry of PDAC are crucial in understanding and optimising PDT procedures.

To date, studies on PDT have incorporated a variety of preclinical PDAC models outlined above and detailed below.

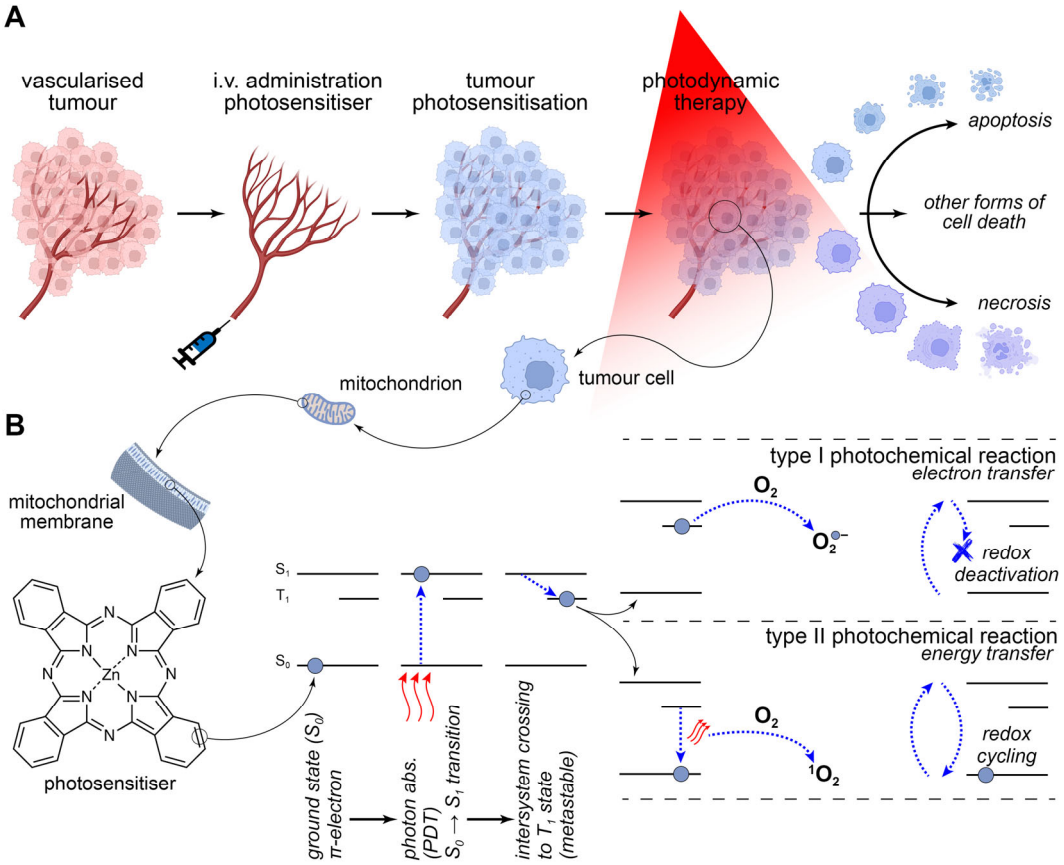

Figure 7. Mechanistic overview of photodynamic therapy (PDT). (**A**) PDT is used for the treatment of vascularised tumours inasmuch as intratumoural vascularisation is required to deliver intravenously administered photosensitiser (PS) molecules into the tumour and to ensure locoregional oxygenation. Tumour photosensitisation occurs once PS molecules have accumulated in the tumour, upon which the tumour is illuminated with light (i.e., PDT, typically at a wavelength of ≥630 nm) to activate the photosensitiser (**B**). This process culminates in mainly apoptosis and necrosis, but also other forms of cell death, that are chiefly responsible for post-therapeutic tumour removal. (**B**) Sequential zooming in from a tumour cell ((**A**), encircled) → mitochondrion → mitochondrial membrane → membrane-embedded PS → π-electron leads up to the visualisation of quantum chemical events during PDT. In the presented sequence of Jablonski diagrams, a ground state (S_0) electron is elevated to the first excited state (S_1) following the absorption of a photon (wavy red arrows) at (near-)resonant frequency. The excited state electron undergoes intersystem crossing from the S_1 state to a triplet state (T_1), from which one of two possible photochemical reactions takes place in the presence of a substrate—typically molecular oxygen (O_2). In case of type I photochemical reactions, the triplet state electron is transferred to O_2 to form superoxide anion ($O_2^{\bullet-}$) as primary reactive oxygen species (ROS). Since the PS loses an electron, the molecular structure of the PS changes and with it the spectral properties, which often results in an ipsochromic shift of the absorption band and a reduction in triplet state quantum yield at unaltered illumination wavelength (designated as redox deactivation). Alternatively, type II photochemical reactions are characterised by a $T_1 \rightarrow S_0$ transition of the electron with concurrent energy transfer to O_2. This leads to the formation of singlet oxygen ($^1O_2$), a highly cytotoxic ROS, with preservation of the redox cycle, meaning that the electron can repeat the photo-excitation and decay process ad infinitum as long as photons are absorbed and O_2 is present in the direct vicinity of the PS.

3.1. In Vivo PDAC Models Used in PDT Research

Mouse Models

Animal models of human PDAC are currently the most utilised for PDT-related research on PDAC as these models embody the sum of a PS's pharmacokinetics, pharmacodynamics, toxicology, and disposition (ADMET). Initial PDAC studies used chemically

induced xenograft models, though these were quickly replaced by cell line alternatives due to inefficiency [188,189]. The PDAC cells obtained via the chemical route were directly injected into the animal, usually orthotopically [190]. Whilst the obtained tumours retained some of the characteristics of PDAC, human cell lines (Table 2) are preferred in PDT studies nowadays as these better represent the clinically observed histopathological features [191]. The tumour xenografts also reflect the reaction of the PDAC TME to therapy, which include post-PDT anti-tumour responses [192,193]. Immunological responses are best studied in syngeneic xenograft models featuring orthotopic inoculation. Vascular infiltration into the xenografts not only provides the necessary conduits for PS delivery but allows studying the effects of intratumoural vascular shutdown following PDT [194], which gives rise to tumour hypoxia [195,196] and activation of specific survival pathways in residually viable tumour cells [158,182,197]. Survival signalling may have deleterious consequences on therapeutic outcome and can be combatted through adjuvant routes [158]. However, the PDAC stroma and its heterogeneity cannot be modelled precisely in homotypic cell-based xenografts as genetic and phenotypic features are restricted in immortalised cell lines [198].

To partly remediate this issue, a mixture of tumour and stromal cells can be incorporated into the inoculation bolus to produce heterotypic xenografts. One study co-implanted MIA PaCa-2 and human pancreatic cancer-associated fibroblast (pCAF) cells into mice. PDT plus vitamin D3 receptor activation in fibroblasts led to a reduction in tumourigenic signalling [199]. Another study using the same approach confirmed that a high degree of desmoplasia can be achieved in PDAC + pCAF xenografts [200]. PDT-treated pCAF-replete PDAC tumours exhibited substantial tumour necrosis and a 1.5-fold reduction in collagen density. PDT-induced collagen destruction was associated with better progression-free and overall survival [201], attesting to the importance of PDAC stroma disruption in treatment efficacy.

Although the hybrid approach enables the study of PDT effects on particular aspects of the stroma, the model cannot fully represent actual disease heterogeneity when single-source cell lines are used. As alluded to before, PDAC tumours bear different stromal subtypes with variations in collagen content, immune cell subsets, endothelial cells, and CAF populations [202]. Ideally this variation is reflected in the model as it is associated with different therapeutic responses, including to PDT [203,204].

3.2. Ex Vivo PDAC Models Used in PDT Research

PDX Models

PDX or organoid-based xenograft models entail patient-derived tissues comprising native stromal components and cell types and therefore properly resolve the structural and cellular heterogeneity dilemma pertaining to the PDAC TME. To date, PDXs have not been employed in PDT/PDAC research. Nevertheless, science can to an extent be borrowed from other cancer types, such as a recent study that used a bladder cancer PDX model to investigate a novel type of chemo-PDT [205]. Histological analysis revealed that the histopathological features of the parental tumour, including cell and tissue structures, were retained in the PDX after transplantation into mice. The uptake and distribution of the nanoformulated PS as well as the tumour response to PDT were characterised and included changes in the level of proteins related to apoptosis, DNA damage, and cytoskeletal aggregation. These findings are particularly useful given that PDX responses are believed to be correlated to the responses observed in patients during clinical treatment [206].

Next-generation PDAC models that fully recapitulate the TME are still under development. PDX models could incorporate patient-derived tumour cells as well as adjacent normal tissues cultured together with patient-derived stem cells [207], which may in part dictate the tumour's susceptibility to treatment [208]. PDAC PDX models developed in

this way would better reflect the complex histological and genetic attributes of the comprehensive tumour milieu. PDXs would further serve as a tool to model PDAC progression, which is pertinent in that PDAC responds to therapy according to the stage of development and molecular landscape [203]. In addition, though PDT clinical trials have focused on locally advanced PDAC, studying PDT for later-stage PDAC is warranted [17] given the potency of abscopal effects [209,210]. Accordingly, PDAC PDX models could facilitate the development of more personalised PDT modalities and, if indeed successful, augment the rate of clinical translation of preclinical research findings as well as promote and expand the use of PDT for a greater number of PDAC patients.

3.3. In Vitro PDAC Models Used in PDT Research

3.3.1. Cell Culture Monolayers (2-D)

Two-dimensional cell cultures are well suited for the investigation of novel PSs, light sources, dosages, and molecular mechanisms as they offer a standardised, reproducible system into which virtually all molecular and cell biology techniques can be plugged. These models often serve as a validatory preface to follow-up in vivo studies. For example, a recent study employed four PDAC cell lines (Capan-1, Capan-2, MIA PaCa-2, and PANC-1) to evaluate the targeting and therapeutic effectiveness of a novel folate-conjugated PS to its cognate receptor folate receptor 1 (FOLR1) [211]. FOLR1 expression was confirmed using qRT-PCR and cells were analysed for PS uptake and localisation, dark toxicity and phototoxicity, and post-PDT immune signalling (cytokine secretion and peripheral blood mononuclear cell activation). The positive in vitro data were subsequently replicated in a humanised SCID mouse model of human PDAC in terms of short-term tumour destruction (complete removal within 9 days after PDT), validating the utility of the in vitro data.

Moreover, genetic modifications through transduction, transfection, or editing (e.g., CRISPR/Cas) has enabled studies on targeting, ligand binding, endocytic mechanisms, and signal transduction pathways using overexpressed or specifically expressed proteins and site-directed pathway modifications (mutagenesis) [212]. For instance, genetically modified cell lines have been utilised to identify proteins involved in the resistance of PDAC to PDT. This is relevant in light of the fact that PDAC signalling pathways have been linked to therapeutic recalcitrance [199,200]. In specific instances, 2-D cell cultures are sufficient in representing the effects of PDT on individual aspects of the PDAC stroma. For example, a 2023 study investigated fibroblast activation protein (FAP)-targeted PDT using 2-D layers of NIH-3T3 cells (mouse embryonic fibroblasts) transfected with FAP [213]. The model was able to demonstrate the in vitro binding and cytotoxicity of the treatment.

Despite the above-referenced benefits, 2-D models are associated with several shortcomings that curtail their utility. Most importantly, the models cannot mimic the native TME and do not account for the crosstalk and intercellular interactions observed in PDAC [214]. This may lead to non-translatable results, particularly in cases where PDT is used as a means to disrupt the TME [215].

3.3.2. Heterotypic Spheroid Cultures

The preclinical investigation of PDT for PDAC has been accelerated by the use of 3-D models that are considered to have greater physiological proximity and predictive value in regard to therapeutic responses. As alluded to previously, a surrounding ECM is required to steer structural and intercellular interactions observed in the PDAC TME [216]. Desmoplasia and interstitial fibrosis in PDACs hamper the delivery of PSs and chemotherapeutics to the tumour parenchyma, resulting in reduced sensitivity to treatment in an immunofriendly environment. Albeit complex outside of an in vivo environment, these factors

should ideally be accounted for in the available in vitro models, especially in light of the increasingly pervasive RRR (reduce, reuse, and recycle) principle in animal research [217].

PDT investigations are commonly performed on PDAC spheroids that are co-cultured with CAFs. Accordingly, Saad et al. generated 3-D MIA PaCa-2 spheroids co-cultured with a varying percentage of PDAC-derived CAFs [218]. The model was employed to study the distribution of a PS-loaded, cancer cell-targeted photoimmunoconjugate (PIC) using fluorescent proteins as reporters. A key finding was that PICs could penetrate spheroids despite high levels of desmoplasia. Another study utilised spheroids composed of MIA PaCa-2, ASPC-1, or Capan-2 cells in combination with pCAFs to investigate the effect of low-dose PDT plus radiation therapy [219]. The spheroids treated by the combinatorial modality exhibited reduced growth and cell–cell adhesion and more profound necrosis and loss of integrity compared to the individual treatments.

Apart from the potentially negative implications on PSs delivery, fibroblasts have also been reported to secrete hepatocyte growth factor (HGF) to activate the HGF–MET signalling axis in a paracrine manner in ASPC-1 and MIA PaCa-2 spheroids [220]. Furthermore, c-MET controls cancer cell proliferation, survival, motility and invasion that, when dysregulated by anomalous c-MET activation, can lead to tumour growth and metastatic progression of cancer cells. When ASPC-1 and MIA PaCa-2 PDAC spheroids were co-cultured with human embryonic lung fibroblasts (MRC-5), the spheroids exhibited less susceptibility to benzoporphyrin derivative (BPD)-PDT compared to fibroblast-lacking spheroids. Although MET expression in ASPC-1 cells is inherently higher than MIA PaCa-2, the combination treatment of PDT and MET inhibition was equally effective in both spheroid test systems, especially at low radiant exposures (0.5–10 J/cm^2).

3.3.3. Hydrogel Scaffold-Supported Spheroids

Instead of using cellular 'production factories' (i.e., fibroblasts) for TME reconstruction, spheroids can be cultured in hydrogel scaffolds to imitate the PDAC TME. The robustness of the spheroid model increases when co-cultured with CAFs. Inasmuch as most PDT research is performed on heterotypic spheroid cultures, the hydrogel materials used for scaffolding of heterotypic spheroids are addressed next.

Matrigel

Matrigel is the commercial name for growth factor-replete, solubilised basement membrane matrix secreted by Engelbreth–Holm–Swarm mouse sarcoma cells that compositionally resembles the extracellular environment found in many tissues and is commonly used to culture cells (2-D and 3-D) [221,222]. It is the most widely used scaffold material in PDT studies that employ spheroids.

An example of seminal research obtained with PDAC/CAF co-cultures supported by a Matrigel scaffold was a study by the Hasan group [200]. As backdrop, therapeutic recalcitrance arising from fibroblast activity in the ECM has traditionally been ascribed to increased ECM formation, metabolic reprogramming, and heterotypic cell–cell interactions [223]. However, Broekgaarden et al. [200] furnished a redox-based explanation that encompasses multiple cellular components in spheroids. Cancer cells typically have inherently higher levels of ROS production due to aberrant cell growth-driven metabolic demand [224]. Elevated intracellular pro-oxidant states in cancer cells have been linked to resistance to therapy [225], but cancer cells do not seem to be solely responsible for the therapeutic recalcitrance in spheroids. The authors demonstrated that CAFs and, to a lesser extent, healthy dermal fibroblasts (HDF1) in Matrigel-supported MIA PaCa-2 spheroids increased redox states, as evidenced by increased cyclooxygenase-2 (COX-2, upregulated via nuclear factor kappa-light-chain-enhancer of activated B cells (NF-κB) in response to

ROS [226]) and heme oxygenase 1 (HO-1, oxidative stress response protein [227]) protein expression. These phenomena, which were reproducible in vivo, concurred with resistance to BPD-PDT as well as oxaliplatin chemotherapy, and were dependent on the cell line combinations used. Less pronounced resistance to PDT and chemotherapy was observed for MIA PaCa-2 spheroids cocultured with HDF1 and especially CAF6 cells and was absent in ASPC-1/CAF6 spheroids. Additional factors that influenced treatment resistance were fibroblast activation status, spheroid size, and therapeutic dosage. It was further shown that metformin, a mitochondrial complex I inhibitor that blocks the passage of electrons along the electron transport chain during aerobic respiration [228], reduced oxidative stress in MIA PaCa-2/CAF microtumours without affecting cell viability. Since redox stress increased in CAF-lacking spheroids, metabolic rerouting for tumour sustenance was clearly mediated by CAFs through as yet unidentified mechanisms. Perturbation of CAF-mediated metabolic rerouting by metformin moreover was associated with increased therapeutic efficacy in MIA PaCa-2/CAF6 microtumours, although this result was again dependent on the PDAC and fibroblast cell lines used. Corroborative results in terms of redox states and their effect on PDAC metabolism and therapeutic susceptibility were obtained with rotenone, another mitochondrial complex I inhibitor [229], in PDT-subjected heterotypic organoid cocultures as well as MIA PaCa-2 xenografts [230]. Taken together, the study demonstrated that these hybrid PDAC microtumours were able to recapitulate some of the essential elements of the PDAC TME, including cell–cell interactions, redox states, metabolic plasticity, and resistance to treatment, which allowed for more representative investigations of potential mechanisms of treatment escape and pharmacological interventions.

Although an excellent substrate for cell development and growth per se, there is lot-to-lot variability of numerous constituents in Matrigel. This variability has been shown to affect PDT and oxaliplatin therapeutic responses and incidentally exacerbate inter-spheroid size variability [200,231]. Moreover, batch differences may also affect spheroid survival before treatment [200]. The exact cause of the heterogeneity is currently unclear.

Collagen

As a more consistent alternative to Matrigel, collagen has proven to be useful scaffold material [78]. PANC-1 spheroids utilising collagen scaffolds exhibited greater invasiveness than when cultured in Matrigel. BPD-PDT treatment exerted more profound photocytotoxicity in an ECM-invading PANC-1 subpopulation of cells, especially in the leading cells that extended beyond a 200-µm radial distance from the spheroid's edge but failed to restrict primary spheroid growth. This was in contrast to the notable cytostatic effect by oxaliplatin on the primary spheroid [232]. The study also used riboflavin-mediated photocrosslinked collagen hydrogels to investigate the growth and invasiveness of primary spheroids as a function of crosslink density [233], which is analogous to ECM density. This model allows control of hydrogel stiffness by regulating the degree of crosslinks through light dose. The invading velocity of the organoid-derived cells monotonically declined with increasing crosslink density. Furthermore, the cells were more sensitive to PDT than to oxaliplatin at lower crosslink densities. Unfortunately, the study did not clarify whether there is a relation between crosslinking degree and PDT response. This would have added valuable information in the sense that increased ECM stiffness (i.e., higher crosslink density) is expected to be inversely proportional to ease of PS penetration into the spheroid.

Alginate and Gelatin

Other materials for creating hydrogel matrices are alginate and gelatin, which are inexpensive and similar alternatives to the commercial ECM hydrogels used for spheroid culture. These hydrogels are compositionally versatile in that hydrogel stiffness can be

regulated by adjusting the ratio of alginate or gelatin to water [231]. It is noteworthy that the purity of alginate should be maximal, as impurities increase the risk of residual endotoxins activating undesirable signalling (via e.g., CD14) that in turn may result in inter-batch spheroid response heterogeneity [234].

With respect to research results with alginate or gelatin-scaffolded spheroids, which at present are relatively scarce in the context of PDT, cationic liposomes encapsulating BPD were more avidly taken up by PANC-1 spheroids generated in alginate than anionic liposomes. The uptake levels were positively correlated with spheroid size [231]. In human breast cancer (MCF-7) 3-D bioprinted hydrogel-based spheroids treated with Ce6-PDT, apoptosis occurred at the top and bottom regions of single spheroids regardless of the vertical axis orientation of the light source and spheroid size [235]. In a co-culture of Matrigel-based PDAC spheroids and MRC-5 fibroblasts, a significant increase in IL-1α/α-SMA ratio was observed in the PANC-1/MRC-5 spheroids compared to PANC-1 spheroids co-cultured with PSCs [16,204]. Increased α-SMA-positive myCAFs subpopulations are normally considered to suppress tumour progression, while increased IL-1α expression can activate the generation of iCAFs and promote tumour behaviour [236]. Also, higher oxaliplatin resistance and BPD-PDT sensitivity occurred in the PDAC/MRC-5 spheroids compared to homotypic PDAC spheroids, regardless of which type of fibroblasts was used [204].

Taken together, these superimposed effects generated by the introduction of CAFs and the inherent differences of PDAC cell lines are particularly important for the assessment of PDT response [200,220,230].

Table 2. Non-exhaustive summary of human PDAC cell line-based models used in PDT research.

Cell Line	Disease	Source	Models	Methods	Tested in PDT	Ref.
A818-1	PDAC	Metastatic	Spheroids	plates coated with agarose in non-supplemented medium at a ratio of 1:3	No	[237]
A818-4	PDAC	Metastatic	Spheroids	nonadherent round-bottom plates with medium containing 20% methyl cellulose	No	[238]
A818-6	PDAC	Metastatic	Spheroids	plates coated with agarose or cultured in rotating culture vessels	No	[239]
ASPC-1	PDAC	Metastatic	Spheroids	ultra-low attachment round-bottom plates; ***PDT regimen***: BPD, 690 nm, 150 mW/cm^2, 0–80 J/cm^2	**Yes**	[219,220]
			Co-cultured spheroids	MRC-5, patient-derived CAFs; ***PDT regimen***: BPD, 690 nm, 150 mW/cm^2, 0–80 J/cm^2	**Yes**	[219,220]
			Microfluidic spheroids	spheroids were generated by liquid overlay method and then transferred to a microfluidic chip	No	[240]
			Hydrogel-based spheroids	PEG hydrogel	No	[241]
			Organoids †	Matrigel; Cultrex Reduced Growth Factor BME, low attachment plates	No	[242,243]
			Cell line-derived xenografts	male nude mice (16 wk), subcutaneous; ***PDT regimen***: zinc phthalocyanine-loaded mesoporous silica nanoparticles, 685 nm, 50 mW/cm^2, 100 J/cm^2, 1980 s	**Yes**	[244]
			Cell line-derived xenografts	male SCID nude mice (6 wk), orthotopic; ***PDT regimen*****:** verteporfin, 690 nm, 74 mW/cm^2, 10–40 J/cm^2, 135–540 s	**Yes**	[245]
BXPC-3	PDAC	Primary	Spheroids	medium containing 0.24% methylcellulose	No	[40]
			Co-cultured spheroids	MRC-5, suspended in polyacrylamide hydrogel coated with collagen type I	No	[246]
			Microfluidic spheroids	HepaChip device	No	[117]
			Hydrogel-based spheroids	Matrigel, collagen I; ***PDT regimen***: BPD, 690 nm, 100 mW/cm^2, 0.5–25 J/cm^2	**Yes**	[232]
			Organoids †	Matrigel, collagen I, tumour-associated PSCs and M2 macrophages in suspension	No	[247]
			Cell line-derived xenografts	female athymic NCR-Nu-F nude mice (5–8 wk), subcutaneous	No	[248]

Table 2. *Cont.*

Cell Line	Disease	Source	Models	Methods	Tested in PDT	Ref.
			Cell line-derived xenografts	BALB/c nude mice (6 wk), orthotopic; ***PDT regimen***: Ce6, 660 nm, 200 mW/cm^2, 200 J/cm^2, 1000 s	**Yes**	[249]
Capan-1	PDAC	Metastatic	Spheroids	medium containing 0.24% methylcellulose	No	[40]
			Co-cultured spheroids	PSCs	No	[250]
			Hydrogel-based spheroids	Matrigel and medium mixture (1:2)	No	[250]
			Cell line-derived xenografts	female BALB/c nude mice (6 wk), subcutaneous; ***PDT regimen***: rBC2-IR700, NIR light 670–710 nm, 100 J/cm^2	**Yes**	[251]
			Cell line-derived xenografts	female BALB/c nude mice (6 wk), orthotopic; ***PDT regimen***: rBC2-IR700, NIR light 670–710 nm, 100 J/cm^2	**Yes**	[251]
Capan-2	PDAC	Primary	Spheroids	ultra-low attachment round-bottom plates; ***PDT regimen***: BPD, 690 nm, 150 mW/cm^2, 0.5–40 J/cm^2	**Yes**	[219,252]
			Co-cultured spheroids	patient-derived CAFs; ***PDT regimen***: BPD, 690 nm, 150 mW/cm^2, 0.5–40 J/cm^2	**Yes**	[219]
			Cell line-derived xenografts	athymic nude mice, subcutaneous; ***PDT regimen***: temoporfin, 980 nm, 500 mW/cm^2, 90 J/cm^2, 180 s	**Yes**	[253]
CFPAC-1	PDAC	Metastatic	Spheroids	cancer stem cell medium	No	[254]
			Co-cultured spheroids	MRC-5 or PSCs; ***PDT regimen***: BPD, 690 nm, 100 mW/cm^2, 0.5–25 J/cm^2	**Yes**	[204]
			Organoids [†]	collagen I, CFPAC-1 cells expressing GRHL2	No	[255]
			Cell line-derived xenografts	athymic CD1 nude mice (6–8 wk), subcutaneous	No	[256]
			Cell line-derived xenografts	female BALB/c nude mice (5 wk), orthotopic	No	[257]
COLO 357	PASC	Metastatic	Spheroids	nonadherent round-bottom plates with medium containing 20% methyl cellulose	No	[238]
			Co-cultured spheroids	patient-derived CAFs	No	[258]
			Hydrogel-based spheroids	gelatin-norbornene (GelNB)-based hydrogels	No	[258]
			Cell line-derived xenografts	female SCID/bg mice (4 wk), subcutaneous	No	[259]
			Cell line-derived xenografts	female SCID/bg mice (4 wk), orthotopic	No	[259]
DAN-G	PAC	Primary	Spheroids	polystyrene-coated ultra-low attachment plates	No	[260]
			Co-cultured spheroids	fibroblast-conditioned medium	No	[260]
			Cell line-derived xenografts	male NMRI nude mice (4–6 wk), subcutaneous	No	[261]
HPAC	PAC	Primary	Spheroids	round-bottom plates pretreated with 0.5% polyHEMA, plates coated with 1% agarose in DMEM; ***PDT regimen***: Ru-bqp-ester, 470 nm, 2.4 ± 0.2 mW/cm^2, 4.3 ± 0.4 J/cm^2, 1800 s	**Yes**	[262,263]
			Cell line-derived xenografts	female athymic BALB/c nude mice (7 wk), subcutaneous	No	[264]
			Cell line-derived xenografts	female SCID nude mice (5 wk), orthotopic	No	[265]
HPAF-II	PDAC	Metastatic	Spheroids	plates coated with 1% agarose in DMEM	No	[263]
			Co-cultured spheroids	fibroblast (DF-1) cells	No	[266]
			Cell line-derived xenografts	female athymic NCR-Nu-F nude mice (5–8 wk), subcutaneous	No	[248]
			Cell line-derived xenografts	female NOD/SCID nude mice (8 wk), orthotopic	No	[267]
Hs 766T	PAC	Metastatic	Hydrogel-based spheroids	Matrigel	No	[268]
			Cell line-derived xenografts	female athymic nude mice (6 wk), subcutaneous	No	[268]
JoPaCa-1	PDAC	Primary	Cell line-derived xenografts	NOD.Cg-Prkdcscid Il2rgtm1Wjl (NOD/SCID/c or NSG) mice, orthotopic	No	[269]
KCI-MOH1	PAC	Primary	Cell line-derived xenografts	female SCID mice (4 wk), subcutaneous	No	[270]
KLM-1	PDAC	Metastatic	Spheroids	NanoCulture plates	No	[271]
			Hydrogel-based spheroids	2-methoxyethyl methacrylate and 2-(diethylamino)ethyl methacrylate heteropolymer	No	[272]
			Cell line-derived xenografts	female athymic nude mice (5 wk), subcutaneous	No	[273]
			Cell line-derived xenografts	female NGS mice (5–6 wk), orthotopic	No	[274]
KP-1N	PASC	Metastatic	Cell line-derived xenografts	nude mice (6–8 wk), subcutaneous	No	[275]
KP-2	PA	Primary	Cell line-derived xenografts	nude mice (6–8 wk), subcutaneous	No	[275]
KP-3	PDAC	Metastatic	Cell line-derived xenografts	nude mice (6–8 wk), subcutaneous	No	[275]
KP-4	PA	Metastatic	Spheroids	ultra-low attachment round-bottom plates	No	[276]

Table 2. *Cont.*

Cell Line	Disease	Source	Models	Methods	Tested in PDT	Ref.
			Cell line-derived xenografts	BALB/c nude mice (6–12 wk), subcutaneous	No	[277]
MIA PaCa-2	PDAC	Primary	Spheroids	ultra-low attachment round-bottom plates; ***PDT regimen***: BPD (including antibody-targeted BPD and liposomal BPD), 690 nm, 150 mW/cm^2, 0–80 J/cm^2	**Yes**	[200,218–220]
			Co-cultured spheroids	MRC-5, patient-derived CAFs; ***PDT regimen***: BPD (including antibody-targeted BPD and liposomal BPD), 690 nm, 150 mW/cm^2, 0–80 J/cm^2	**Yes**	[218–220]
			Microfluidic spheroids	HepaChip device	No	[117]
			Hydrogel-based spheroids	Matrigel; ***PDT regimen***: BPD, 690 nm, 150 mW/cm^2, 1–50 J/cm^2	**Yes**	[200,230]
			Organoids †	Matrigel, collagen I, tumour-associated PSCs and M2 macrophages in suspension		[247]
			Cell line-derived xenografts	female nude mice (6 wk), subcutaneous; ***PDT regimen***: LC-Dox-PoP, 665 nm, 150 mW/cm^2, 50 J/cm^2	**Yes**	[278]
			Cell line-derived xenografts	male Swiss nude mice (4 wk), orthotopic; male Swiss nude mice (4–6 wk) co-implanted with pCAFs, orthotopic; ***PDT regimen***: BPD, 690 nm, 100 mW/cm^2, 50 J/cm^2; verteporfin or liposomal irinotecan, 690 nm, 100 mW/cm^2, 75 J/cm^2	**Yes**	[199,230]
MZ-PC-1	PDAC	Metastatic	Cell line-derived xenografts	NMRI nude mice (4–6 wk), subcutaneous	No	[279]
PaCa-44	PDAC	Primary	Cell line-derived xenografts	C.B-17/IcrHsd-Prkcdscid Lystbg mice (8–10 wk), subcutaneous	No	[280]
			Cell line-derived xenografts	C.B-17/IcrHsd-Prkcdscid Lystbg mice (8–10 wk), orthotopic	No	[280]
PaCa 5061	PDAC	Primary	Cell line-derived xenografts	male and female C57BL/6 mice (14–16 wk), subcutaneous	No	[281]
Pan2M	PDAC	Metastatic	Cell line-derived xenografts	female BALB/c nude mice (4 wk), orthotopic	No	[282]
PANC03.27	PAC	Primary	Cell line-derived xenografts	athymic C57BL/6 nude mice, subcutaneous	No	[283]
PANC04.03	PDAC	Primary	Co-cultured spheroids	PSCs	No	[284]
			Hydrogel-based spheroids	Matrigel and collagen I mixture (3:1)	No	[284]
PANC 04.14	PAC	Unknown	Cell line-derived xenografts	nude mice, orthotopic	No	[285]
PANC 10.05	PDAC	Primary	Cell line-derived xenografts	male nude mice (8 wk), subcutaneous	No	[286]
PANC-1	PDAC	Primary	Spheroids	Nunclon Sphera plates, NanoCulture plates; ***PDT regimen***: 6-amine-2,5-bromophenalenone (OE19), 525 nm, 18.6 mW/cm^2, 16.6 J/cm^2, 900 s	**Yes**	[271,287]
			Co-cultured spheroids	MRC-5, PSCs; ***PDT regimen***: BPD, 690 nm, 100 mW/cm^2, 0.5–25 J/cm^2	**Yes**	[204]
			Microfluidic spheroids	HepaChip device	No	[117]
			Hydrogel-based spheroids	Matrigel, collagen I, riboflavin-mediated collagen photocrosslinking hydrogel, alginate-gelatin hydrogel; ***PDT regimen***: BPD, 690 nm, 100 mW/cm^2, 0.5–25 J/cm^2; BPD, 690 nm, 150 mW/cm^2	**Yes**	[204,231–233]
			Organoids †	Matrigel, collagen I, tumour-associated PSCs and M2-like differentiated macrophages in suspension	No	[247]
			Cell line-derived xenografts	female BALB/c nude mice (6 wk), subcutaneous; female athymic CD1 mice (4 wk), subcutaneous (both 2D and spheroids-based); ***PDT regimen***: YLG-1, 650 nm, 100 J/cm^2	**Yes**	[254,288]
			Cell line-derived xenografts	male SCID nude mice (6 wk), orthotopic; ***PDT regimen***: verteporfin, 690 nm, 74 mW/cm^2, 10–40 J/cm^2, 135–540 s	**Yes**	[245]
PancTU-I	PDAC	Unknown	Spheroids	nonadherent U-form plates with medium containing 20% methyl cellulose	No	[238]
			Cell line-derived xenografts	male or female SCID mice (13–20 wk), subcutaneous	No	[289]
			Cell line-derived xenografts	male or female SCID mice (13–20 wk), orthotopic	No	[289]
PaTu 8902	PAC	Primary	Spheroids	ultra-low attachment round-bottom plates	No	[252]
			Co-cultured spheroids	undifferentiated monocyte-like (THP-1) cells or THP-1 conditioned medium	No	[252]
			Cell line-derived xenografts	athymic nude mice, subcutaneous	No	[290]
PaTu 8988	PAC	Metastatic	Cell line-derived xenografts	male BALB/c nude mice (5–6 wk), subcutaneous	No	[291]
			Cell line-derived xenografts	BALB/c nude mice (5 wk), orthotopic	No	[291]

Table 2. *Cont.*

Cell Line	Disease	Source	Models	Methods	Tested in PDT	Ref.
PC-1	PDAC	Metastatic	Cell line-derived xenografts	male or female NIH athymic nude mice (4–6 wk), subcutaneous	No	[292]
PC-2	PDAC	Metastatic	Spheroids	serum-free medium DMEM/F12 supplemented with bFGF, EGF, insulin, transferrin, sodium selenite, and bovine serum albumin	No	[293]
			Cell line-derived xenografts	male or female NIH athymic nude mice (4–6 wk), subcutaneous	No	[292]
PC-3	PDAC	Unknown	Cell line-derived xenografts	male BALB/c athymic nude mice (5 wk), subcutaneous	No	[294]
PC-7	PDAC	Unknown	Cell line-derived xenografts	female specific pathogen-free athymic nude mice (4 wk), subcutaneous	No	[295]
			Cell line-derived xenografts	BALB/c nude mice (5 wk), orthotopic	No	[291]
PCI-24	PAC	Primary	Cell line-derived xenografts	female BALB/c nude mice (4–6 wk), subcutaneous	No	[296]
PCI-35	PDAC	Primary	Cell line-derived xenografts	KSN Slc nude mice, subcutaneous	No	[297]
PCI-43	PAC	Primary	Cell line-derived xenografts	female BALB/c nude mice (4–6 wk), subcutaneous	No	[296]
PDXPC1	PDAC	Primary	Spheroids	serum-free medium DMEM/F12 supplemented with basic bFGF, EGF, and insulin	No	[298]
			Cell line-derived xenografts	female BALB/c nude mice (4–6 wk), subcutaneous	No	[298]
PK-1	PDAC	Metastatic	Cell line-derived xenografts	male BALB/c nude mice (5 wk), subcutaneous	No	[299]
PK-45P	PA	Unknown	Spheroids	ultra-low attachment round-bottom plates	No	[276]
PK-8	PDAC	Metastatic	Spheroids	ultra-low attachment plates	No	[300]
			Cell line-derived xenografts	SCID mice, subcutaneous	No	[301]
PL45	PAC	Primary	Spheroids	plates coated with 1% agarose in DMEM	No	[263]
			Cell line-derived xenografts	NOD/SCID nude mice (7–9 wk), subcutaneous	No	[302]
			Cell line-derived xenografts	athymic nude mice, orthotopic	No	[303]
PSN1	PAC	Primary	Spheroids	cancer stem cell medium	No	[254]
			Cell line-derived xenografts	male BALB/c nude mice (12–14 wk), subcutaneous	No	[304]
PT45	PDAC	Primary	Spheroids	gelatin porous microbeads	No	[305]
			Co-cultured spheroids	human normal fibroblasts or CAF	No	[305]
			Cell line-derived xenografts	C57BL athymic ICRF nude mice, subcutaneous	No	[306]
PT45-P1	PDAC	Primary	Spheroids	nonadherent round-bottom plates with medium containing 20% methyl cellulose	No	[238]
S2-007	PDAC	Metastatic	Spheroids	not listed	No	[307]
			Hydrogel-based spheroids	polypeptide network hydrogel	No	[308]
			Cell line-derived xenografts	BALB/c nude mice (8–16 wk), subcutaneous	No	[309]
			Cell line-derived xenografts	male athymic nude mice (5 wk), orthotopic	No	[307]
S2-013	PDAC	Metastatic	Co-cultured spheroids	HUVECs and human MSCs	No	[135]
			Organoids †	HUVECs and MSCs	No	[135]
			Cell line-derived xenografts	female athymic BALB/cSlc-*nu*/*nu* mice (7 wk), subcutaneous	No	[135]
			Cell line-derived xenografts	female athymic nude mice (6–8 wk), orthotopic	No	[310]
			Organoid-based xenografts	S2-013 organoids, female athymic BALB/cSlc-*nu*/*nu* (7 wk), subcutaneous	No	[135]
S2-020	PDAC	Metastatic	Cell line-derived xenografts	BALB/c nude mice (8–16 wk), subcutaneous	No	[309]
S2-028	PDAC	Metastatic	Microfluidic spheroids	three-lane OrganoPlate channels	No	[311]
			Cell line-derived xenografts	BALB/c nude mice (8–16 wk), subcutaneous	No	[309]
			Cell line-derived xenografts	athymic mice, intrasplenic injection	No	[312]
S2-CP8	PDAC	Metastatic	Cell line-derived xenografts	male BALB/cAJcl nude mice (6 wk), orthotopic	No	[313]
SK-PC-1	PDAC	Unknown	Cell line-derived xenografts	female athymic BALB/c nude mice (5 wk), subcutaneous	No	[314]
SU8686	PAC	Metastatic	Cell line-derived xenografts	male BALB/cAJcl nude mice (6–8 wk), orthotopic	No	[315]
Sui66-Sui70, Sui72-Sui74	PDAC	Primary	Cell line-derived xenografts	female C.B.17/Icr Jcl-scid SCID mice (6–8 wk), subcutaneous	No	[316]
Sui65, Sui71	PDAC	Metastatic	Cell line-derived xenografts	female C.B.17/Icr Jcl-scid SCID mice (6–8 wk), subcutaneous	No	[316]
SUIT-2	PDAC	Metastatic	Co-cultured spheroids	PSCs	No	[284]

Table 2. *Cont.*

Cell Line	Disease	Source	Models	Methods	Tested in PDT	Ref.
			Hydrogel-based spheroids	Matrigel and collagen I mixture (3:1)	No	[284]
			Cell line-derived xenografts	female BALB/c nude mice (6 wk), subcutaneous; ***PDT regimen***: rBC2-IR700, NIR light 670–710 nm, 100 J/cm^2	**Yes**	[251]
			Cell line-derived xenografts	female nude mice (6 wk), co-implanted with PSCs, orthotopic	No	[317]
SUIT-4	PDAC	Metastatic	Cell line-derived xenografts	BALB/c athymic nude mice (6 wk), subcutaneous	No	[318]
SUIT-58	PDAC	Metastatic	Hydrogel-based spheroids	Collagen I and cell culture insert	No	[319]
SW1990	PAC	Primary	Spheroids	serum-free sphere medium DMEM/F12 supplemented with B27, bFGF, and EGF	No	[320]
			Cell line-derived xenografts	female BALB/c nude mice (5 wk), subcutaneous; ***PDT regimen***: quantum dots conjugated with integrin antagonist arginine-glycine-aspartic acid peptides, 630 nm, 100 mW/cm^2, 1200 s	**Yes**	[321]
			Cell line-derived xenografts	male and female athymic N:NIH (S) nude mice (5–6 wk), orthotopic	No	[322]
T3M-4	PDAC	Primary	Spheroids	ultra-low attachment round-bottom plates	No	[276]
			Cell line-derived xenografts	BALB/c athymic nude mice (7 wk), subcutaneous	No	[323]
			Cell line-derived xenografts	female BALB/c athymic nude mice (6–8 wk), orthotopic	No	[324]
TCC-Pan2	PDAC	Metastatic	Cell line-derived xenografts	female BALB/c nude mice (4 wk), orthotopic	No	[282]
YAPC	PA	Metastatic	Spheroids	hanging drop method	No	[325]
			Cell line-derived xenografts	male NMRI mice (4–6 wk), subcutaneous	No	[326]

Abbreviations (alphabetical): bFGF, basic fibroblast growth factor; BPD, benzoporphyrin derivative; BME, basement membrane extract; CAF, cancer-associated fibroblasts; Ce6, chlorin e6; DMEM, Dulbecco's modified Eagle's medium; EGF, epidermal growth factor; GRHL2, grainyhead like transcription factor 2; HUVECs, human umbilical vein endothelial cells; MSCs, mesenchymal stem cells; NIR, near-infrared; PA, pancreatic carcinoma; PAC, pancreatic adenocarcinoma; PASC: pancreatic adenosquamous carcinoma; PDAC, pancreatic ductal adenocarcinoma; PDT, photodynamic therapy; PEG, polyethylene glycol; PSCs, pancreatic stellate cells; wk, weeks. † Organoid classification ambiguous because the models did not conform to the full definition of organoids. Cell information was retrieved from DepMap and Cellosaurus.

3.4. Challenges and Caveats of Biomimetic PDAC Models in the Context of PDT

A generally applicable rule of thumb in preclinical research is that the more remote a model is from the actual human condition, the less representative the model outcomes will be relative to that human condition [327]. It is therefore important to appreciate that models will never provide full representation of how in situ tumours behave in patients with respect to locoregional biology, biochemistry, physiology, and pharmacodynamic responsiveness. On the spectrum of available models covered in this paper, using cell monolayers (2-D cultures) is associated with the highest probability of achieving results with least translational potential, whereas working with PDXs in a quasi-native milieu (e.g., transplanted into an animal, preferably orthotopically) will probabilistically furnish the highest level of representation. This phenomenon was recently illustrated by Gioeli et al. [328], where RNAseq and subsequent protein–protein interaction networks analysis of cells in 2-D cultures and PDX were compared against patients' tumour biopsies. With tumour biopsies as the transcriptomic baseline, the analyses revealed that 2-D cultures (Figure 8A) exhibited the highest number of differentially expressed transcripts versus PDX (Figure 8B) and 3-D cell co-culture (Figure 8C). These protein–protein interaction networks featured processes that are relevant to PDAC (patho)biology, including oxidative stress, immune function, cell cycle, and ECM interaction. Accordingly, and with respect to biomimetic models, maximal emulation of numerous facets of human tumours in their natural environment is warranted, which necessitates the veering away from simple systems when robust data are a priority.

The complexity involved in the creation of a near-native biomimetic in vitro PDAC model is exemplified in the work by Gioeli et al. [328]. The authors used a dual compart-

ment, porous polycarbonate transwell membrane culture system where human primary PSCs and PDAC-derived cancer cells were plated in spheroid format on the bottom end of the membrane and primary human microvascular endothelial cells were plated in monolayer format on the upper end of the membrane. The top surface of the membrane was coated with gelatin and the bottom surface with collagen, and cells were plated in sequential order and cultured under artificial flow conditions to emulate hemodynamics [331] in the 'vascular' compartment and interstitial flow dynamics [332,333] in the 'parenchymal' compartment. This culture system, which is more complex than the biomimetic models described above, not only resembles PDXs on a transcriptional level [328], but most accurately mimics the in situ tumour transcriptome (Figure 8C) surprisingly more so than PDXs (Figure 8B). The system is suitable to test drug delivery, pharmacodyamics, toxicity, and resistance mechanisms. A system of this calibre is not available to most researchers, which is a caveat in and of itself. Another drawback of in vitro models is that human PDAC is characterised by hyperdense stroma that is hypovascular in the juxta-tumoural and pan-stromal areas, i.e., tissues directly adjacent to the tumour [334], which is a feature that is commonly not emulated in PDAC models and mostly affects drug delivery parameters. Normally, systemically administered (photo)drugs and nanomedicines have to extravasate into the hypervascular normal adjacent pancreatic tissue and transverse a relatively large distance to reach PDAC cells. These drug migration obstacles are commonly discounted in the in vitro and ex vivo models described in this review.

On top of the challenge of technical availability and accessibility, in vitro and in vivo biomimetic models are associated with additional caveats when employed for PDT research. Both models (in cases where human PDAC cell lines are used) lack a complete immune system that is instrumental in ECM shaping, immunotolerance, cell–cell interactions, and anti-tumour immune responses after PDT [335–337]. This not only has a bearing on PS/drug delivery to the tumour cells, which is expected to be easier in especially the in vitro models due to the absence of phagocytic cells, but also skews therapeutic responses. Subsets of innate immune cells such as neutrophils, monocytes, and macrophages typically constitute the first wave of resident and migratory cells to clean up oxidatively afflicted cells and debris [338–341], whereas subsets of the adaptive immune system (e.g., dendritic cells and T cells) are required for long-term tumour control [338,342–345]. Post-PDT immune signals in the form of chemokines, cytokines, and other classes of immunomodulatory mediators [346] emitted by resident and chemoattracted immune cells [338] as well as PDT-treated tumour cells [347] therefore do not materialise at all in in vitro and ex vivo models that completely lack immunological constituents, or materialise partially yet insufficiently in nude mice [342–344] that lack T lymphocytes but do produce innate immune cells [348]. Effectuation of immune system signalling networks and PDT-pertinent immunobiology could be achieved in syngeneic tumour models employed in combination with orthotopic cell transplantation (Table 3), granted that thus obtained tumours sustain a high level of biomimetic integrity relative to their in situ human counterparts.

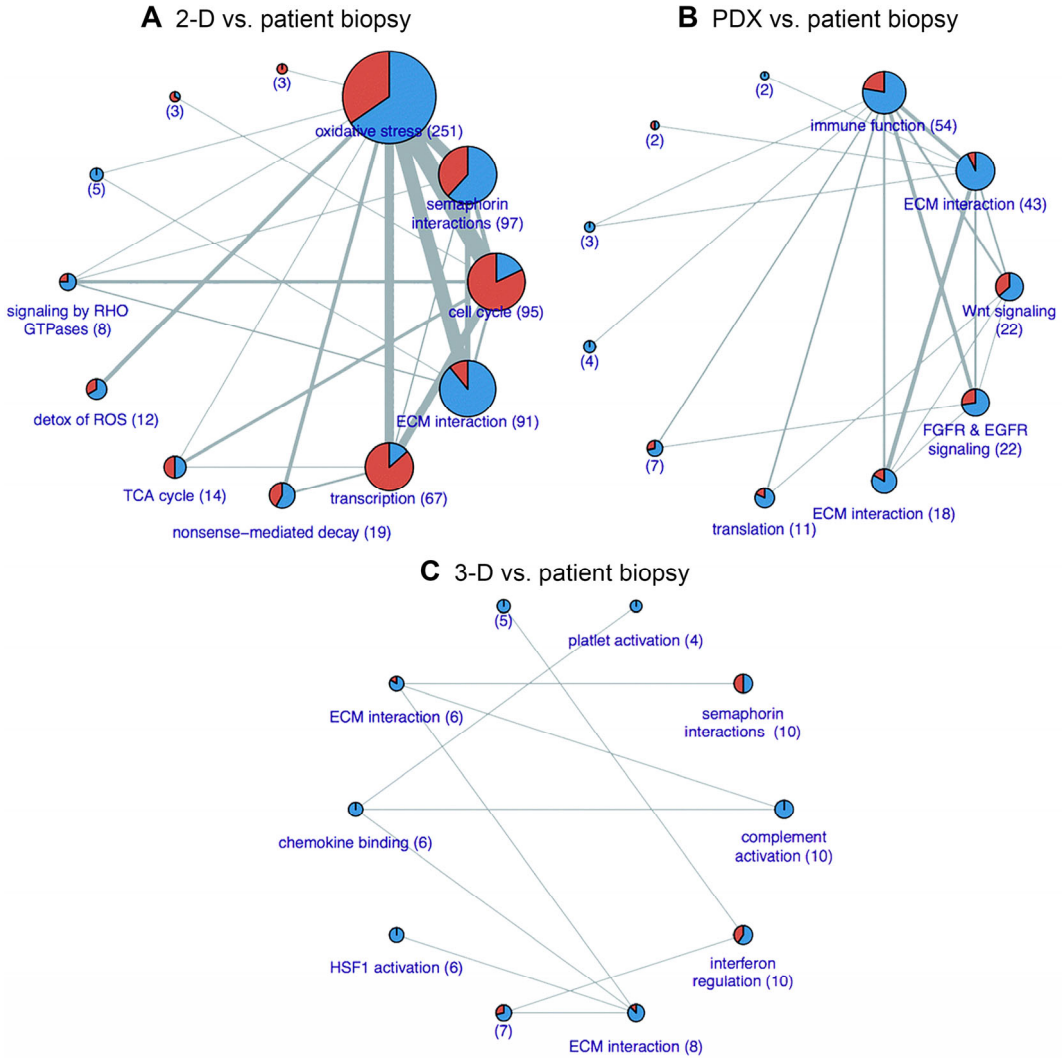

Figure 8. Molecular representability of biomimetic pancreatic ductal adenocarcinoma (PDAC) models. PDAC tissue biopsies were obtained perioperatively from a surgical patient and subjected to RNA sequencing (RNAseq). RNAseq was also performed on cell culture monolayers [329], orthotopic patient-derived xenografts (PDXs) in immunocompromised (athymic) mice [330], and 3-D cell co-cultures [328], all created with cells from the same tumour biopsy (referred to as PDAC cell line 449). The technical aspects of the 3-D culture are explained in the text of this section. Differential expression of genes was analysed and expressed against the patient biopsy transcriptome. Data were plugged into protein–protein interaction networks derived from the STRING database and further processed by partitioning into communities (set of proteins in nodes (spheres) with upregulated (red) and downregulated (blue) genes). The larger communities are specified and the size of each node is scaled to the number of transcriptionally dysregulated proteins in that community. Communities are connected by gray lines to reflect their relationship, while line thickness indicates the degree to which the internode relationship is affected at the transcriptional level. Presented are the differential expression profiles of 2-D cell culture: ((**A**), 665 differentially regulated proteins), PDX; ((**B**), 188 differentially regulated proteins), and the 3-D cell co-culture ((**C**), 72 differentially regulated proteins) relative to the respective clinical biopsy transcript levels. This figure was reproduced from [328] in accordance with creative commons attribution-noncommercial 3.0 unported licence and following written permission from the corresponding author.

Table 3. Non-exhaustive summary of non-human PDAC cell line-based models used in PDT research.

Cell Line	Disease	Source	Models	Methods	Tested in PDT	Ref.
Mouse						
6606PDA	PDAC	Primary	Cell line-derived xenografts	male C57BL/6 mice (6–8 wk), orthotopic	No	[349]
K8484	PDAC	Primary	Cell line-derived xenografts	KPC mice, subcutaneous	No	[350]
KPC3	PN	Primary	Cell line-derived xenografts	male C57BL/6 mice (8–10 wk), subcutaneous	No	[351]
Panc02	PDAC	Primary	Co-culture spheroids	Matrigel, co-culture with $CD8^+$ cytotoxic T cells	No	[352]
			Hydrogel-based spheroids	Matrigel and complete DMEM mixture; Matrigel and collagen type I mixture	No	[352,353]
			Cell line-derived xenografts	female C57BL/6 mice (6–8 wk), subcutaneous; C57BL/6 mice (6–8 wk), orthotopic; ***PDT regimen***: IR700-conjugated anti-CD44 monoclonal antibody, 690 nm, 150 mW/cm^2, 50 J/cm^2; PTT regimen: 980 nm, 850 mW/cm^2, 50 J/cm^2, 600 s	**Yes**	[354,355]
			Cell line-derived xenografts	C57BL/6 mice (6–8 wk), orthotopic; PTT regimen: 980 nm, 850 mW/cm^2, 50 J/cm^2, 600 s	PTT	[355]
UN-KC-6141	PDAC	Primary	Cell line-derived xenografts	C57BL/6 mice, orthotopic	No	[356]
UN-KPC-960	PDAC	Primary	Cell line-derived xenografts	B6.129 mice, orthotopic	No	[356]
UN-KPC-961	PDAC	Primary	Cell line-derived xenografts	B6.129 mice, subcutaneous and orthotopic	No	[356]
Hamster						
HaP-T1	PDAC	Primary	Cell line-derived xenografts	male Syrian golden hamsters (5 wk), orthotopic	No	[322]
PC-1.0	PDAC	Primary	Cell line-derived xenografts	male Syrian golden hamsters (5 wk), orthotopic	No	[357]
PC-1.2	PDAC	Primary	Cell line-derived xenografts	Syrian golden hamsters (8 wk), orthotopic	No	[358]
WD PaCa	PDAC	Primary			No	[359]

Abbreviations (alphabetical): DMEM, Dulbecco's modified Eagle's medium; PDAC, pancreatic ductal adenocarcinoma; PDT, photodynamic therapy; PTT, photothermal therapy; wk, weeks.

Another caveat in the PDAC models when used in PDT research is atmospheric composition, which should change to mirror post-PDT conditions, and the ramifications on PDAC (patho)biology. The in vitro and ex vivo models typically do not account for the switch from normoxia to conditions of low partial pressure of oxygen (pO_2) after PDT. PDT causes a conversion of molecular oxygen to superoxide anion or singlet oxygen [360] (Figure 7), which coincides with a rapid reduction in pO_2 and reduced tumour oxygenation [361]. On top of that, a fraction of the PS molecules is taken up by endothelial cells following injection. Upon PDT, photosensitised endothelial cells are damaged and become

thrombogenic [362–364] owing to photochemical disruption of cell integrity, endothelial cell activation, and exposure of the basement membrane. The corollary vascular shutdown in turn produces prolonged hypoxia or anoxia in tumour cells, metabolic catastrophe [169], and cell death as well as activation of cell survival pathways [158,197]. Moreover, PDT-treated tumours become more acidic as a result of the hypoxia as lactic acid production and build-up increase due to lacking substrate for aerobic respiration (i.e., O_2). As explained in Section 2, acidic conditions select PDAC cells with a more aggressive phenotype geared towards invasion and metastasis [37]. In contrast, although intracellular pO_2 drops during PDT in in vitro and ex vivo models, the cells and tissues are normally maintained in an atmosphere composed of 95% air (containing 20% molecular oxygen) and 5% carbon dioxide (incubator) or 100% air (outside of an incubator), accounting for virtually immediate reoxygenation upon cessation of light exposure. Consequently, the above-referenced features should be incorporated into PDT studies using PDAC models to properly contextualise the research and improve the biomimetic character of the models. This can be achieved by using specialised culture chambers with tunable atmospheric conditions [182,195,196].

The more advanced models where PDACs are grown volumetrically, such as spheroids and organoids, may suffer from drug distribution heterogeneity. Many anti-cancer drugs, including first- and second-generation PSs [167], are lipophilic and hence preferentially localise to cell and organelle membranes [170,365]. Photosensitisation of these PDAC cell clusters occurs by adding the PS to the culture medium and allowing the PS molecules to disperse throughout the cell cluster. However, as shown for spheroids in Figure 9, lipophilic PSs tend to have a predominantly peripheral accumulation pattern in which the core of the cell cluster becomes less photosensitised. Inasmuch as ROS are generated only at loci where PS molecules and oxygen coincide, the core of the spheroid would exhibit less therapeutic effect following PDT. In terms of distribution, the same applies to nanoformulated (liposome-encapsulated) lipophilic PSs (Figure 9) as well as amphipathic compounds such as Hoechst 33342 (Figure 9) but not highly hydrophilic PS derivatives, which tend to penetrate spheroids homogenously (unpublished results). One could argue that a similar distribution pattern will manifest in vivo, where PS molecules or their delivery vehicles are fed to the PDAC through remote extravasation points as explained above.

Finally, tumours grown in vivo are exposed to a partial or full arsenal of immune cells following initial damage that will remove dead and dying cells from the tumour volume and, in case of syngeneic models, facilitate abscopal immunological cell death in residually viable remnants of the PDAC [210,366,367]. These key phenomena are not captured in the in vitro and ex vivo models described here, which could skew experiment results obtained with biomimetic PDAC models.

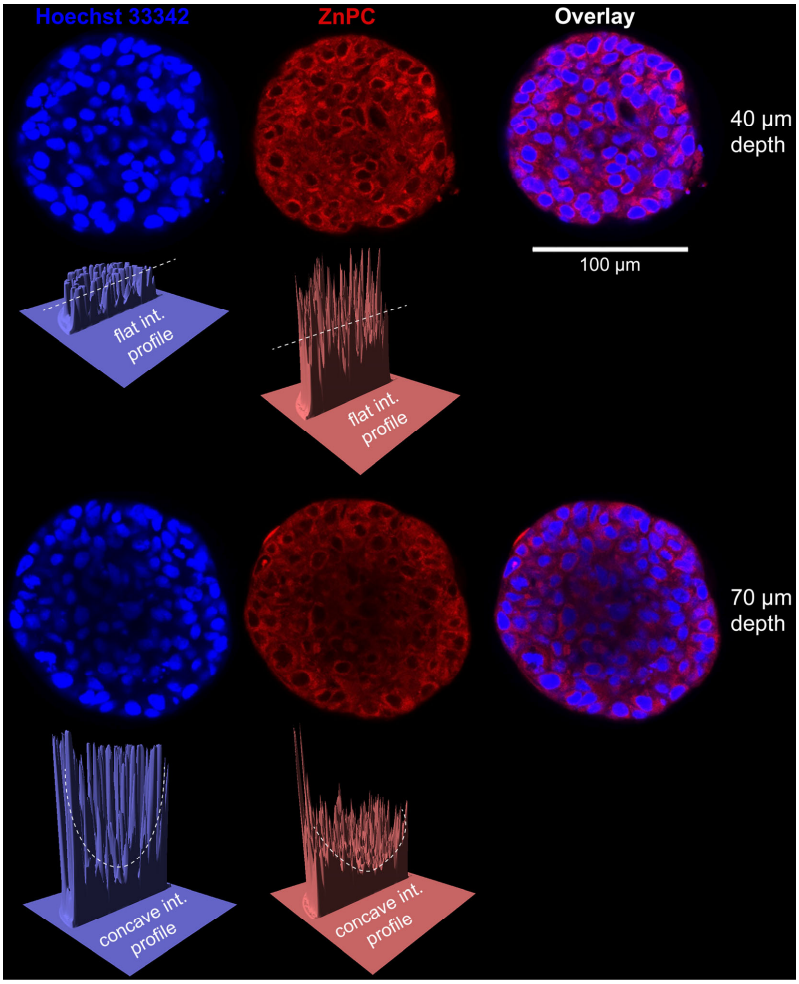

Figure 9. Heterogeneous distribution pattern of Hoechst 33342 and liposomal zinc phthalocyanine (ZnPC) in human extrahepatic cholangiocarcinoma (TFK-1) spheroids. Confocal microscopy-generated planar fluorescence profiles are shown that were acquired at a depth of 40 µm (top row) and 70 µm (bottom row) from the top surface of the spheroid. The fluorescence intensity patterns demonstrate relatively equal distribution of Hoechst 33342 (blue) and liposomal ZnPC (red) across the spheroid in the top plane and tapered penetration towards the spheroid core in the deeper situated plane, as indicated by the dashed lines. The images were quantitatively processed with custom-built image analysis software (CanAlysis version 1, Applive, Amsterdam, The Netherlands), where pixel intensity maps were created for the blue and red hues. Spheroid planes were cross-sectioned at the longest diameter and one half of the plane was tilted to reveal the red or blue intensity landscape (*z*-axis; 0–255-pixel intensity range) across the spheroid plane (x- and y-axes). Whereas the tissue plane at 40 µm depth had a rather flat intensity profile, the intensity profile of the 70 µm tissue plane was concave. The latter indicates lower fluorescence intensities in the centre of the spheroid (i.e., farthest diffusion distance from the outer spheroid surface) and hence limited penetration of lipophilic and amphipathic molecules into the spheroid. TFK-1 spheroids were prepared by liquid overlay in a Nunc Lab-Tek II Chamber Slide System (8-well format). A thin layer of 100% Matrigel was added to each well and incubated at 37 °C for 30 min under standard culture conditions. Subsequently, 4×10^5 TFK-1 cells in 2% Matrigel were added and incubated for 4 d. Medium was refreshed every 2 d. On day 4, spheroids were incubated with ZnPC-loaded PEGylated lecithin liposomes (0.003 ZnPC:phospholipid molar ratio [170,365], 5 µM final ZnPC concentration) for 24 h. Then, spheroids were washed with PBS and fixed with 2% paraformaldehyde/1% glutaraldehyde in PBS for 30 min. Spheroids were washed 3 × with PBS, followed by quenching of background fluorescence with 0.1% $NaBH_4$ for 10 min. Nuclei were stained with Hoechst 33342 (32 µM final concentration; log P = 4.6, PubChem CID 1464) for 2 h and slides were mounted with SlowFade Gold. Imaging was performed with a Leica TCS SP8 system using a 25 × water immersion objective. ZnPC (log P = 8.5 [167]) was imaged owing to its weak autofluorescence [163].

3.5. Future Directions

The challenges described in the previous section regarding biomimetic pancreatic cancer models for a large part shape the future directions. Accordingly, the usually powerful KISS principle (keep it simple, stupid!) does not apply to biomimetic PDAC models. Instead, increasing model complexity is warranted, especially in regard to improving the models' physiologic and biochemical accuracy and relevance to human disease. The first key direction is the formation of more complex TMEs with precise control over cell types and matrix composition, which can be achieved by e.g., 3-D bioprinting [368–370]. Secondly, this approach must be combined with steps to better emulate the interactions between cancer cells, stromal cells, and immunological constituents, which can be realised through the use of co-culture systems. It should be noted that the first two points only apply to spheroids and organoids since PDXs and other forms of ex vivo models with tumour tissue do not allow for such engineering. Thirdly, the cellular components that make up the PDAC and TME require adequate provision of nutrients and exposure to mechanical stress that can be provided by tumour-on-a-chip models [371–373] or bespoke 3-D spheroid systems that incorporate the abovementioned factors (Figure 8) [328] as well as those that can control atmospheric composition [374,375], given that hypoxic conditions are instrumental in both tumour biology [376] and post-PDT responses [158,377]. Finally, PDACs are generally heterogeneous at the genetic-, cellular-, and histological level [378,379], not only intertumourally but also intratumourally [378], which significantly augments treatment difficulty [380]. This aspect has also been reported for other types of hepatopancreaticobiliary tumours such as cholangiocarcinoma [381], equally accounting for its tenacious therapeutic recalcitrance [382,383]. Consequently, tailoring models based on patient-specific tumour data for more effective drug screening and individualised therapies cannot be dismissed and is of particular importance in oncological settings that are centred on personalised medicine.

As to future directions of PDT in the context of biomimetic PDAC models, the following points are noteworthy. Most importantly, several variables, such as circulation, systemic chemotactic gradients, and recruitment of innate and adaptive immune cells to the PDT-treated tumour are absent in all models except for syngeneic tumour models in immunocompetent animals. As alluded to previously, these variables play a quintessential role in therapeutic efficacy and long-term tumour control. In cases where therapeutic efficacy assessment constitutes the main objective of a study, it is recommended that models are used that encapsulate these variables to generate maximally representative results. Guidance on such models is provided in Table 3. Secondly, PDT data produced using in vitro and ex vivo models should ideally be validated in proper animal models of cancer. As an example, complete PS distribution across the tumour volume is critical inasmuch as therapeutic and (patho)biological responses are reliant on the degree of intratumoural photosensitisation [158,384]. Lack of sufficient mimicry could cause a divergence in outcomes and conclusions between in vitro/ex vivo models and in vivo models that are characterised by tumour eradication (complete tumour photosensitisation) in the former versus tumour survival (inadequate or heterogeneous photosensitisation) in the latter. Naturally, this potential issue does not apply to 2-D PDAC cultures, which in our opinion harness little translational utility and should only be employed for the most rudimentary tests. For 3-D tumours it is possible, even likely, that the waning degree of photosensitisation with depth (e.g., Figure 9) also prevails in PDXs, ex vivo models, and in vivo (xenografts). Tumour photosensitisation in vivo is dependent on a plethora of factors, including intratumoural vascularisation, PS or nanoparticulate PS pharmacokinetics and disposition, interstitial fluid flow, and desmoplasia. The first three factors are not recreated in in vitro and ex vivo PDAC models per se, which may lead to an overestimation of the degree of photosensi-

tisation in these models and bias the data in favour of tumour eradication. Furthermore, intratumoural distribution varies with the type of PS or PS delivery system employed. A particular PS therefore does not serve as a template for other PSs, with nano-encapsulation in and of itself being able to fundamentally alter pharmacokinetics, pharmacodynamics, biodistribution, intracellular localisation, and disposition of the PS [385–387]. Also, mapping PS distribution profiles in models should preferably be verified using orthotopic tumour xenografts (Tables 2 and 3). Subcutaneous xenografts may differ from tumours cultivated in their native environment and conditions in terms of, e.g., microvascularisation and angiogenesis [388–390], which comprise the conduit networks that facilitate PS delivery into tumours and hence partially dictate photosensitisation.

Lastly, future directions should be geared towards optimisation of technical aspects of test models. PDT is a modality devised to eradicate cancer cells; measuring cell viability is therefore the primary outcome parameter in many studies whilst functional molecular probes are also used for other purposes such as qualifying and/or quantifying the events that culminate in tumour cell death. As discussed above and shown in Figure 9, the penetration of amphipathic and lipophilic molecules is hampered in 3-D models, which includes reporter dyes such as Hoechst 33342 (nuclear stain) and likely extends to other classes of commonly used molecular reporters such as cell viability probes (e.g., MTT [391], PubChem CID 16218671, logP = 5.9), organelle-specific probes for localisation studies (e.g., MitoTracker Red [196], PubChem CID 22613925, logP = 1.2, fluorescent probe for mitochondria; LysoTracker Red [392], PubChem CID 15410449, logP = 2.1, fluorescent probe for lysosomes [393]), cell and organelle membrane stains (e.g., DiOC6(3) [394], PubChem CID 9894321, logP = 5.5–6.5), mitochondrial membrane depolarisation probes (e.g., JC-1 [395], PubChem CID 5492929, logP range = 3–5), and fluorogenic redox probes to measure ROS (e.g., $DCFH_2$(-DA) [162,229,396], PubChem CID 77718, logP = 4.4–4.6). As a result of the incomplete penetration of molecular probes, the readouts may underestimate effect size or paint a partial picture. These factors should be accounted for in experimental design and measures should be taken to remediate technical hurdles, such as using water-soluble alternatives (e.g., WST-1 instead of MTT to determine cell viability), and protocols should ideally be standardised for the complex models. Secondly, PDT with certain PSs is associated with vascular shutdown [249,397,398] that leads to intratumoural hypoxia/anoxia, which activates survival pathways that in turn affect therapeutic outcome [158,169,182,197]. Accordingly, these treatment-induced pathophysiological conditions should be accounted for in experimental design by equipping the test systems with atmospheric control [195,196,377]. Thirdly, factors that are not representative of the clinical situation yet deleterious to PDT outcomes should be avoided in experimental designs. For example, we have found that mycoplasma infection substantially distorts the molecular biological responses to PDT in tumour cells as well as the temperature at which PDT is performed, which should be body temperature instead of the frequently used room temperature. We are preparing manuscripts that address both issues and provide guidelines for proper experimental design.

4. Conclusions

Although the use of 2-D cell lines has been instrumental for basic in vitro PDAC research, improved 3-D models offer several inherent advantages that move the models towards an in situ biomimetic character. Primarily, the PDAC TME can be represented more faithfully, which facilitates a more accurate investigation of PDAC biology and novel treatment strategies that affect the TME. Ultimately, using representative models under clinically representative conditions is expected to increase the rate of clinical translation and more effectively address the need to improve PDAC treatment outcomes. Evolving technologies may push the representability of biomimetic PDAC models closer to in situ

tumours in humans, while standardisation of the models will allow for intra- and interstudy comparisons.

These predicates are particularly relevant for PDT, an emerging minimally invasive treatment modality that kills photosensitised tumour cells directly through hyperoxidative stress and indirectly through treatment-induced immunological cell death. PDT has the capacity to destroy the TME–a feature of PDAC that has been attributed to therapeutic recalcitrance–and resolve non-treated tumours (e.g., metastases of the same phenotype as the treated tumours) via abscopal effects. Consequently, PDT is a potentially useful treatment strategy for PDAC.

Unfortunately, the majority of PDAC research that focuses on PDT has been performed in 2-D models, which we have deemed to have the lowest level of translational value. In this review we therefore addressed more appropriate biomimetic research models for PDT, including xenografts, PDX, and spheroids and elaborated on the advantages and disadvantages of these models. The most important challenges and caveats of biomimetic PDAC models include the necessity to reconstruct a pleiotropic TME that accounts for photosensitisation and probe gradients as well as differential pO_2 levels across the 3-D models. PDT leads to hypoxia, which in itself is associated with a particular gamut of signalling cascades that add to the post-therapeutic molecular hyperoxidative stress-affected landscape and have the capacity to alter treatment outcomes. In case of xenografts, orthotopic syngeneic PDAC models are favourable due to the presence of a native pancreas milieu and functional immune system, which is mandatory for long-term tumour control. Finally, the finetuning of methodological approaches and standardization of experimental protocols is warranted to ensure interstudy comparisons.

Author Contributions: Conceptualisation, M.H., D.G.J. and Y.S.K.; methodology, O.M.S., N.L., B.M.M., S.O. and J.T.; software, M.H.; validation, O.M.S., N.L. and M.H.; formal analysis, O.M.S., N.L., J.T., B.M.M. and M.H.; investigation, O.M.S., N.L., J.T., B.M.M. and M.H.; resources, A.M.S., D.G.J. and Y.S.K.; data curation, O.M.S., N.L., J.T., B.M.M. and M.H.; writing—original draft preparation, O.M.S., N.L., J.T., M.H. and Y.S.K.; writing—review and editing, all authors; visualisation, O.M.S. and M.H.; supervision, V.V., J.P., A.M.S., M.H., D.G.J. and Y.S.K.; project administration, D.G.J. and Y.S.K.; funding acquisition, Y.S.K. All authors have read and agreed to the published version of the manuscript.

Funding: This research was funded by the Academy of Medical Sciences (grant number SGL027/1011) awarded to Y.S.K. and the project National Institute for Cancer Research (Programme EXCELES, ID Project No. LX22NPO5102) – funded by the European Union – Next Generation EU to V.V.

Institutional Review Board Statement: Not applicable.

Informed Consent Statement: Not applicable.

Data Availability Statement: No new data eligible for sharing were created or analysed in this study. Data sharing is not applicable to this article.

Conflicts of Interest: The authors declare no conflicts of interest.

References

1. Peng, J.; Sun, B.F.; Chen, C.Y.; Zhou, J.Y.; Chen, Y.S.; Chen, H.; Liu, L.; Huang, D.; Jiang, J.; Cui, G.S.; et al. Single-cell RNA-seq highlights intra-tumoral heterogeneity and malignant progression in pancreatic ductal adenocarcinoma. *Cell Res.* **2019**, *29*, 725–738. [CrossRef] [PubMed]
2. Buscail, L.; Bournet, B.; Cordelier, P. Role of oncogenic KRAS in the diagnosis, prognosis and treatment of pancreatic cancer. *Nat. Rev. Gastroenterol. Hepatol.* **2020**, *17*, 153–168. [CrossRef]
3. Conroy, T.; Hammel, P.; Hebbar, M.; Ben Abdelghani, M.; Wei, A.C.; Raoul, J.L.; Chone, L.; Francois, E.; Artru, P.; Biagi, J.J.; et al. FOLFIRINOX or Gemcitabine as Adjuvant Therapy for Pancreatic Cancer. *N. Engl. J. Med.* **2018**, *379*, 2395–2406. [CrossRef]

4. Strobel, O.; Neoptolemos, J.; Jager, D.; Buchler, M.W. Optimizing the outcomes of pancreatic cancer surgery. *Nat. Rev. Clin. Oncol.* **2019**, *16*, 11–26. [CrossRef]
5. Oettle, H.; Neuhaus, P.; Hochhaus, A.; Hartmann, J.T.; Gellert, K.; Ridwelski, K.; Niedergethmann, M.; Zulke, C.; Fahlke, J.; Arning, M.B.; et al. Adjuvant chemotherapy with gemcitabine and long-term outcomes among patients with resected pancreatic cancer: The CONKO-001 randomized trial. *JAMA* **2013**, *310*, 1473–1481. [CrossRef] [PubMed]
6. Strobel, O.; Hank, T.; Hinz, U.; Bergmann, F.; Schneider, L.; Springfeld, C.; Jager, D.; Schirmacher, P.; Hackert, T.; Buchler, M.W. Pancreatic Cancer Surgery: The New R-status Counts. *Ann. Surg.* **2017**, *265*, 565–573. [CrossRef]
7. Hank, T.; Hinz, U.; Tarantino, I.; Kaiser, J.; Niesen, W.; Bergmann, F.; Hackert, T.; Buchler, M.W.; Strobel, O. Validation of at least 1 mm as cut-off for resection margins for pancreatic adenocarcinoma of the body and tail. *Br. J. Surg.* **2018**, *105*, 1171–1181. [CrossRef] [PubMed]
8. Vitali, F.; Pfeifer, L.; Janson, C.; Goertz, R.S.; Neurath, M.F.; Strobel, D.; Wildner, D. Quantitative perfusion analysis in pancreatic contrast enhanced ultrasound (DCE-US): A promising tool for the differentiation between autoimmune pancreatitis and pancreatic cancer. *Z. Gastroenterol.* **2015**, *53*, 1175–1181. [CrossRef]
9. Liu, X.; Fu, Y.; Chen, Q.; Wu, J.; Gao, W.; Jiang, K.; Miao, Y.; Wei, J. Predictors of distant metastasis on exploration in patients with potentially resectable pancreatic cancer. *BMC Gastroenterol.* **2018**, *18*, 168. [CrossRef]
10. Versteijne, E.; Suker, M.; Groothuis, K.; Akkermans-Vogelaar, J.M.; Besselink, M.G.; Bonsing, B.A.; Buijsen, J.; Busch, O.R.; Creemers, G.M.; van Dam, R.M.; et al. Preoperative Chemoradiotherapy Versus Immediate Surgery for Resectable and Borderline Resectable Pancreatic Cancer: Results of the Dutch Randomized Phase III PREOPANC Trial. *J. Clin. Oncol.* **2020**, *38*, 1763–1773. [CrossRef]
11. Bray, F.; Ferlay, J.; Soerjomataram, I.; Siegel, R.L.; Torre, L.A.; Jemal, A. Global cancer statistics 2018: GLOBOCAN estimates of incidence and mortality worldwide for 36 cancers in 185 countries. *CA Cancer J. Clin.* **2018**, *68*, 394–424. [CrossRef]
12. Dangi-Garimella, S.; Sahai, V.; Ebine, K.; Kumar, K.; Munshi, H.G. Three-dimensional collagen I promotes gemcitabine resistance in vitro in pancreatic cancer cells through HMGA2-dependent histone acetyltransferase expression. *PLoS ONE* **2013**, *8*, e64566. [CrossRef]
13. Zhao, J.; Wang, H.; Hsiao, C.H.; Chow, D.S.; Koay, E.J.; Kang, Y.; Wen, X.; Huang, Q.; Ma, Y.; Bankson, J.A.; et al. Simultaneous inhibition of hedgehog signaling and tumor proliferation remodels stroma and enhances pancreatic cancer therapy. *Biomaterials* **2018**, *159*, 215–228. [CrossRef] [PubMed]
14. Sensi, F.; D'Angelo, E.; Biccari, A.; Marangio, A.; Battisti, G.; Crotti, S.; Fassan, M.; Laterza, C.; Giomo, M.; Elvassore, N.; et al. Establishment of a human 3D pancreatic adenocarcinoma model based on a patient-derived extracellular matrix scaffold. *Transl. Res.* **2023**, *253*, 57–67. [CrossRef] [PubMed]
15. Mu, P.; Zhou, S.; Lv, T.; Xia, F.; Shen, L.; Wan, J.; Wang, Y.; Zhang, H.; Cai, S.; Peng, J.; et al. Newly developed 3D in vitro models to study tumor-immune interaction. *J. Exp. Clin. Cancer Res.* **2023**, *42*, 81. [CrossRef]
16. Karimnia, V.; Stanley, M.E.; Fitzgerald, C.T.; Rizvi, I.; Slack, F.J.; Celli, J.P. Photodynamic Stromal Depletion Enhances Therapeutic Nanoparticle Delivery in 3D Pancreatic Ductal Adenocarcinoma Tumor Models. *Photochem. Photobiol.* **2023**, *99*, 120–131. [CrossRef]
17. Lintern, N.; Smith, A.M.; Jayne, D.G.; Khaled, Y.S. Photodynamic Stromal Depletion in Pancreatic Ductal Adenocarcinoma. *Cancers* **2023**, *15*, 4135. [CrossRef] [PubMed]
18. Mei, L.; Du, W.; Ma, W.W. Targeting stromal microenvironment in pancreatic ductal adenocarcinoma: Controversies and promises. *J. Gastrointest. Oncol.* **2016**, *7*, 487–494. [CrossRef]
19. Schnittert, J.; Bansal, R.; Mardhian, D.F.; van Baarlen, J.; Ostman, A.; Prakash, J. Integrin alpha11 in pancreatic stellate cells regulates tumor stroma interaction in pancreatic cancer. *FASEB J.* **2019**, *33*, 6609–6621. [CrossRef]
20. Schnittert, J.; Bansal, R.; Prakash, J. Targeting Pancreatic Stellate Cells in Cancer. *Trends Cancer* **2019**, *5*, 128–142. [CrossRef]
21. Du, W.; Pasca di Magliano, M.; Zhang, Y. Therapeutic Potential of Targeting Stromal Crosstalk-Mediated Immune Suppression in Pancreatic Cancer. *Front. Oncol.* **2021**, *11*, 682217. [CrossRef] [PubMed]
22. Bauer, C.; Kühnemuth, B.; Duewell, P.; Ormanns, S.; Gress, T.; Schnurr, M. Prevailing over T cell exhaustion: New developments in the immunotherapy of pancreatic cancer. *Cancer Lett.* **2016**, *381*, 259–268. [CrossRef] [PubMed]
23. Raskov, H.; Orhan, A.; Christensen, J.P.; Gögenur, I. Cytotoxic CD8. *Br. J. Cancer* **2021**, *124*, 359–367. [CrossRef]
24. Tormoen, G.W.; Crittenden, M.R.; Gough, M.J. Role of the immunosuppressive microenvironment in immunotherapy. *Adv. Radiat. Oncol.* **2018**, *3*, 520–526. [CrossRef] [PubMed]
25. Longo, V.; Brunetti, O.; Gnoni, A.; Cascinu, S.; Gasparini, G.; Lorusso, V.; Ribatti, D.; Silvestris, N. Angiogenesis in pancreatic ductal adenocarcinoma: A controversial issue. *Oncotarget* **2016**, *7*, 58649–58658. [CrossRef]
26. Le Large, T.Y.; Mantini, G.; Meijer, L.L.; Pham, T.V.; Funel, N.; van Grieken, N.C.; Kok, B.; Knol, J.; van Laarhoven, H.W.; Piersma, S.R.; et al. Microdissected pancreatic cancer proteomes reveal tumor heterogeneity and therapeutic targets. *JCI Insight* **2020**, *5*, e138290. [CrossRef]
27. Pan, Z.; Li, L.; Fang, Q.; Zhang, Y.; Hu, X.; Qian, Y.; Huang, P. Analysis of dynamic molecular networks for pancreatic ductal adenocarcinoma progression. *Cancer Cell Int.* **2018**, *18*, 214. [CrossRef]

28. Shen, Y.; Pu, K.; Zheng, K.; Ma, X.; Qin, J.; Jiang, L.; Li, J. Differentially Expressed microRNAs in MIA PaCa-2 and PANC-1 Pancreas Ductal Adenocarcinoma Cell Lines are Involved in Cancer Stem Cell Regulation. *Int. J. Mol. Sci.* **2019**, *20*, 4473. [CrossRef]
29. Khosravani, F.; Mir, H.; Mirzaei, A.; Kobarfard, F.; Bardania, H.; Hosseini, E. Arsenic trioxide and Erlotinib loaded in RGD-modified nanoliposomes for targeted combination delivery to PC3 and PANC-1 cell lines. *Biotechnol. Appl. Biochem.* **2023**, *70*, 811–823. [CrossRef]
30. Malinda, R.R.; Zeeberg, K.; Sharku, P.C.; Ludwig, M.Q.; Pedersen, L.B.; Christensen, S.T.; Pedersen, S.F. TGFβ Signaling Increases Net Acid Extrusion, Proliferation and Invasion in Panc-1 Pancreatic Cancer Cells: SMAD4 Dependence and Link to Merlin/NF2 Signaling. *Front. Oncol.* **2020**, *10*, 687. [CrossRef]
31. Schnittert, J.; Heinrich, M.A.; Kuninty, P.R.; Storm, G.; Prakash, J. Reprogramming tumor stroma using an endogenous lipid lipoxin A4 to treat pancreatic cancer. *Cancer Lett.* **2018**, *420*, 247–258. [CrossRef] [PubMed]
32. Kuninty, P.R.; Bojmar, L.; Tjomsland, V.; Larsson, M.; Storm, G.; Ostman, A.; Sandstrom, P.; Prakash, J. MicroRNA-199a and -214 as potential therapeutic targets in pancreatic stellate cells in pancreatic tumor. *Oncotarget* **2016**, *7*, 16396–16408. [CrossRef]
33. Gunti, S.; Hoke, A.T.K.; Vu, K.P.; London, N.R. Organoid and Spheroid Tumor Models: Techniques and Applications. *Cancers* **2021**, *13*, 874. [CrossRef] [PubMed]
34. Ding, Y.; Mei, W.; Zheng, Z.; Cao, F.; Liang, K.; Jia, Y.; Wang, Y.; Liu, D.; Li, J.; Li, F. Exosomes secreted from human umbilical cord mesenchymal stem cells promote pancreatic ductal adenocarcinoma growth by transferring miR-100-5p. *Tissue Cell* **2021**, *73*, 101623. [CrossRef] [PubMed]
35. Suri, R.; Zimmerman, J.W.; Burkhart, R.A. Modeling human pancreatic ductal adenocarcinoma for translational research: Current options, challenges, and prospective directions. *Ann. Pancreat. Cancer* **2020**, *3*, 17. [CrossRef]
36. Hwang, C.I.; Boj, S.F.; Clevers, H.; Tuveson, D.A. Preclinical models of pancreatic ductal adenocarcinoma. *J. Pathol.* **2016**, *238*, 197–204. [CrossRef]
37. Audero, M.M.; Carvalho, T.M.A.; Ruffinatti, F.A.; Loeck, T.; Yassine, M.; Chinigo, G.; Folcher, A.; Farfariello, V.; Amadori, S.; Vaghi, C.; et al. Acidic Growth Conditions Promote Epithelial-to-Mesenchymal Transition to Select More Aggressive PDAC Cell Phenotypes In Vitro. *Cancers* **2023**, *15*, 2572. [CrossRef]
38. Rodrigues, J.; Heinrich, M.A.; Teixeira, L.M.; Prakash, J. 3D In Vitro Model (R)evolution: Unveiling Tumor-Stroma Interactions. *Trends Cancer* **2021**, *7*, 249–264. [CrossRef]
39. Prakash, J.; Shaked, Y. The Interplay between Extracellular Matrix Remodeling and Cancer Therapeutics. *Cancer Discov.* **2024**, *14*, 1375–1388. [CrossRef]
40. Longati, P.; Jia, X.; Eimer, J.; Wagman, A.; Witt, M.R.; Rehnmark, S.; Verbeke, C.; Toftgård, R.; Löhr, M.; Heuchel, R.L. 3D pancreatic carcinoma spheroids induce a matrix-rich, chemoresistant phenotype offering a better model for drug testing. *BMC Cancer* **2013**, *13*, 95. [CrossRef]
41. Rescigno, F.; Ceriotti, L.; Meloni, M. Extra Cellular Matrix Deposition and Assembly in Dermis Spheroids. *Clin. Cosmet. Investig. Dermatol.* **2021**, *14*, 935–943. [CrossRef] [PubMed]
42. Ncube, K.N.; Jurgens, T.; Steenkamp, V.; Cromarty, A.D.; van den Bout, I.; Cordier, W. Comparative Evaluation of the Cytotoxicity of Doxorubicin in BT-20 Triple-Negative Breast Carcinoma Monolayer and Spheroid Cultures. *Biomedicines* **2023**, *11*, 1484. [CrossRef]
43. Nkune, N.W.; Simelane, N.W.N.; Montaseri, H.; Abrahamse, H. Photodynamic Therapy-Mediated Immune Responses in Three-Dimensional Tumor Models. *Int. J. Mol. Sci.* **2021**, *22*, 12618. [CrossRef] [PubMed]
44. Roy, M.; Alix, C.; Bouakaz, A.; Serriere, S.; Escoffre, J.M. Tumor Spheroids as Model to Design Acoustically Mediated Drug Therapies: A Review. *Pharmaceutics* **2023**, *15*, 806. [CrossRef] [PubMed]
45. Gilazieva, Z.; Ponomarev, A.; Rutland, C.; Rizvanov, A.; Solovyeva, V. Promising Applications of Tumor Spheroids and Organoids for Personalized Medicine. *Cancers* **2020**, *12*, 2727. [CrossRef]
46. Kuntze, A.; Goetsch, O.; Fels, B.; Najder, K.; Unger, A.; Wilhelmi, M.; Sargin, S.; Schimmelpfennig, S.; Neumann, I.; Schwab, A.; et al. Protonation of Piezo1 Impairs Cell-Matrix Interactions of Pancreatic Stellate Cells. *Front. Physiol.* **2020**, *11*, 89. [CrossRef]
47. Ware, M.J.; Keshishian, V.; Law, J.J.; Ho, J.C.; Favela, C.A.; Rees, P.; Smith, B.; Mohammad, S.; Hwang, R.F.; Rajapakshe, K.; et al. Generation of an in vitro 3D PDAC stroma rich spheroid model. *Biomaterials* **2016**, *108*, 129–142. [CrossRef]
48. Lee, K.-H.; Kim, T.-H. Recent Advances in Multicellular Tumor Spheroid Generation for Drug Screening. *Biosensors* **2021**, *11*, 445. [CrossRef]
49. Dufau, I.; Frongia, C.; Sicard, F.; Dedieu, L.; Cordelier, P.; Ausseil, F.; Ducommun, B.; Valette, A. Multicellular tumor spheroid model to evaluate spatio-temporal dynamics effect of chemotherapeutics: Application to the gemcitabine/CHK1 inhibitor combination in pancreatic cancer. *BMC Cancer* **2012**, *12*, 15. [CrossRef]
50. Maietta, I.; Martínez-Pérez, A.; Álvarez, R.; De Lera, Á.R.; González-Fernández, Á.; Simón-Vázquez, R. Synergistic Antitumoral Effect of Epigenetic Inhibitors and Gemcitabine in Pancreatic Cancer Cells. *Pharmaceuticals* **2022**, *15*, 824. [CrossRef]

51. Wang, Z.; He, R.; Dong, S.; Zhou, W. Pancreatic stellate cells in pancreatic cancer: As potential targets for future therapy. *Front. Oncol.* **2023**, *13*, 1185093. [CrossRef] [PubMed]
52. Ferreira, L.P.; Gaspar, V.M.; Mendes, L.; Duarte, I.F.; Mano, J.F. Organotypic 3D decellularized matrix tumor spheroids for high-throughput drug screening. *Biomaterials* **2021**, *275*, 120983. [CrossRef]
53. Scalise, M.; Marino, F.; Salerno, L.; Cianflone, E.; Molinaro, C.; Salerno, N.; De Angelis, A.; Viglietto, G.; Urbanek, K.; Torella, D. From Spheroids to Organoids: The Next Generation of Model Systems of Human Cardiac Regeneration in a Dish. *Int. J. Mol. Sci.* **2021**, *22*, 13180. [CrossRef]
54. Khursheed, M.; Bashyam, M.D. Apico-basal polarity complex and cancer. *J. Biosci.* **2014**, *39*, 145–155. [CrossRef]
55. Tsai, S.; McOlash, L.; Palen, K.; Johnson, B.; Duris, C.; Yang, Q.; Dwinell, M.B.; Hunt, B.; Evans, D.B.; Gershan, J.; et al. Development of primary human pancreatic cancer organoids, matched stromal and immune cells and 3D tumor microenvironment models. *BMC Cancer* **2018**, *18*, 335. [CrossRef] [PubMed]
56. Neesse, A.; Michl, P.; Frese, K.K.; Feig, C.; Cook, N.; Jacobetz, M.A.; Lolkema, M.P.; Buchholz, M.; Olive, K.P.; Gress, T.M.; et al. Stromal biology and therapy in pancreatic cancer. *Gut* **2011**, *60*, 861–868. [CrossRef] [PubMed]
57. Shinkawa, T.; Ohuchida, K.; Nakamura, M. Heterogeneity of Cancer-Associated Fibroblasts and the Tumor Immune Microenvironment in Pancreatic Cancer. *Cancers* **2022**, *14*, 3994. [CrossRef]
58. Luo, Y.; Li, Z.; Kong, Y.; He, W.; Zheng, H.; An, M.; Lin, Y.; Zhang, D.; Yang, J.; Zhao, Y.; et al. KRAS mutant-driven SUMOylation controls extracellular vesicle transmission to trigger lymphangiogenesis in pancreatic cancer. *J. Clin. Investig.* **2022**, *132*, e157644. [CrossRef]
59. McGuigan, A.J.; Coleman, H.G.; McCain, R.S.; Kelly, P.J.; Johnston, D.I.; Taylor, M.A.; Turkington, R.C. Immune cell infiltrates as prognostic biomarkers in pancreatic ductal adenocarcinoma: A systematic review and meta-analysis. *J. Pathol. Clin. Res.* **2021**, *7*, 99–112. [CrossRef]
60. Liu, X.; Iovanna, J.; Santofimia-Castaño, P. Stroma-targeting strategies in pancreatic cancer: A double-edged sword. *J. Physiol. Biochem.* **2023**, *79*, 213–222. [CrossRef]
61. Stouten, I.; van Montfoort, N.; Hawinkels, L.J.A.C. The Tango between Cancer-Associated Fibroblasts (CAFs) and Immune Cells in Affecting Immunotherapy Efficacy in Pancreatic Cancer. *Int. J. Mol. Sci.* **2023**, *24*, 8707. [CrossRef] [PubMed]
62. Maneshi, P.; Mason, J.; Dongre, M.; Oehlund, D. Targeting Tumor-Stromal Interactions in Pancreatic Cancer: Impact of Collagens and Mechanical Traits. *Front. Cell Dev. Biol.* **2021**, *9*, 787485. [CrossRef]
63. Miyazaki, Y.; Oda, T.; Inagaki, Y.; Kushige, H.; Saito, Y.; Mori, N.; Takayama, Y.; Kumagai, Y.; Mitsuyama, T.; Kida, Y.S. Adipose-derived mesenchymal stem cells differentiate into heterogeneous cancer-associated fibroblasts in a stroma-rich xenograft model. *Sci. Rep.* **2021**, *11*, 4690. [CrossRef]
64. Hwang, H.J.; Oh, M.S.; Lee, D.W.; Kuh, H.J. Multiplex quantitative analysis of stroma-mediated cancer cell invasion, matrix remodeling, and drug response in a 3D co-culture model of pancreatic tumor spheroids and stellate cells. *J. Exp. Clin. Cancer Res.* **2019**, *38*, 258. [CrossRef]
65. Knight, E.; Przyborski, S. Advances in 3D cell culture technologies enabling tissue-like structures to be created in vitro. *J. Anat.* **2015**, *227*, 746–756. [CrossRef] [PubMed]
66. Lee, J.H.; Kim, S.K.; Khawar, I.A.; Jeong, S.Y.; Chung, S.; Kuh, H.J. Microfluidic co-culture of pancreatic tumor spheroids with stellate cells as a novel 3D model for investigation of stroma-mediated cell motility and drug resistance. *J. Exp. Clin. Cancer Res.* **2018**, *37*, 4. [CrossRef]
67. Jang, S.D.; Song, J.; Kim, H.A.; Im, C.N.; Khawar, I.A.; Park, J.K.; Kuh, H.J. Anti-Cancer Activity Profiling of Chemotherapeutic Agents in 3D Co-Cultures of Pancreatic Tumor Spheroids with Cancer-Associated Fibroblasts and Macrophages. *Cancers* **2021**, *13*, 5955. [CrossRef]
68. Kpeglo, D.; Hughes, M.D.G.; Dougan, L.; Haddrick, M.; Knowles, M.A.; Evans, S.D.; Peyman, S.A. Modeling the mechanical stiffness of pancreatic ductal adenocarcinoma. *Matrix Biol. Plus* **2022**, *14*, 100109. [CrossRef] [PubMed]
69. Ding, L.; Zhang, Z.; Shang, D.; Cheng, J.; Yuan, H.; Wu, Y.; Song, X.; Jiang, H. α-Smooth muscle actin-positive myofibroblasts, in association with epithelial-mesenchymal transition and lymphogenesis, is a critical prognostic parameter in patients with oral tongue squamous cell carcinoma. *J. Oral Pathol. Med.* **2014**, *43*, 335–343. [CrossRef]
70. Kaszak, I.; Witkowska-Piłaszewicz, O.; Niewiadomska, Z.; Dworecka-Kaszak, B.; Ngosa Toka, F.; Jurka, P. Role of Cadherins in Cancer-A Review. *Int. J. Mol. Sci.* **2020**, *21*, 7624. [CrossRef]
71. Kim, S.; You, D.; Jeong, Y.; Yu, J.; Kim, S.W.; Nam, S.J.; Lee, J.E. TP53 upregulates α-smooth muscle actin expression in tamoxifen-resistant breast cancer cells. *Oncol. Rep.* **2019**, *41*, 1075–1082. [CrossRef] [PubMed]
72. Öhlund, D.; Handly-Santana, A.; Biffi, G.; Elyada, E.; Almeida, A.S.; Ponz-Sarvise, M.; Corbo, V.; Oni, T.E.; Hearn, S.A.; Lee, E.J.; et al. Distinct populations of inflammatory fibroblasts and myofibroblasts in pancreatic cancer. *J. Exp. Med.* **2017**, *214*, 579–596. [CrossRef]

73. Priwitaningrum, D.L.; Blonde, J.G.; Sridhar, A.; van Baarlen, J.; Hennink, W.E.; Storm, G.; Le Gac, S.; Prakash, J. Tumor stroma-containing 3D spheroid arrays: A tool to study nanoparticle penetration. *J. Control. Release* **2016**, *244*, 257–268. [CrossRef] [PubMed]
74. Kuninty, P.R.; Bansal, R.; De Geus, S.W.L.; Mardhian, D.F.; Schnittert, J.; van Baarlen, J.; Storm, G.; Bijlsma, M.F.; van Laarhoven, H.W.; Metselaar, J.M.; et al. ITGA5 inhibition in pancreatic stellate cells attenuates desmoplasia and potentiates efficacy of chemotherapy in pancreatic cancer. *Sci. Adv.* **2019**, *5*, eaax2770. [CrossRef]
75. Anane-Adjei, A.B.; Fletcher, N.L.; Cavanagh, R.J.; Houston, Z.H.; Crawford, T.; Pearce, A.K.; Taresco, V.; Ritchie, A.A.; Clarke, P.; Grabowska, A.M.; et al. Synthesis, characterisation and evaluation of hyperbranched N-(2-hydroxypropyl) methacrylamides for transport and delivery in pancreatic cell lines in vitro and in vivo. *Biomater. Sci.* **2022**, *10*, 2328–2344. [CrossRef]
76. Saito, K.; Sakaguchi, M.; Maruyama, S.; Iioka, H.; Putranto, E.W.; Sumardika, I.W.; Tomonobu, N.; Kawasaki, T.; Homma, K.; Kondo, E. Stromal mesenchymal stem cells facilitate pancreatic cancer progression by regulating specific secretory molecules through mutual cellular interaction. *J. Cancer* **2018**, *9*, 2916–2929. [CrossRef]
77. Ullah, I.; Subbarao, R.B.; Rho, G.J. Human mesenchymal stem cells—Current trends and future prospective. *Biosci. Rep.* **2015**, *35*, e00191. [CrossRef] [PubMed]
78. Pednekar, K.P.; Heinrich, M.A.; van Baarlen, J.; Prakash, J. Novel 3D microtissues Mimicking the Fibrotic Stroma in Pancreatic Cancer to Study Cellular Interactions and Stroma-Modulating Therapeutics. *Cancers* **2021**, *13*, 5006. [CrossRef]
79. Ammar, N.; Hildebrandt, M.; Geismann, C.; Roder, C.; Gemoll, T.; Sebens, S.; Trauzold, A.; Schafer, H. Monocarboxylate Transporter-1 (MCT1)-Mediated Lactate Uptake Protects Pancreatic Adenocarcinoma Cells from Oxidative Stress during Glutamine Scarcity Thereby Promoting Resistance against Inhibitors of Glutamine Metabolism. *Antioxidants* **2023**, *12*, 1818. [CrossRef]
80. Kitamura, F.; Semba, T.; Yasuda-Yoshihara, N.; Yamada, K.; Nishimura, A.; Yamasaki, J.; Nagano, O.; Yasuda, T.; Yonemura, A.; Tong, Y.; et al. Cancer-associated fibroblasts reuse cancer-derived lactate to maintain a fibrotic and immunosuppressive microenvironment in pancreatic cancer. *JCI Insight* **2023**, *8*, e163022. [CrossRef]
81. Xu, R.; Yang, J.; Ren, B.; Wang, H.; Yang, G.; Chen, Y.; You, L.; Zhao, Y. Reprogramming of Amino Acid Metabolism in Pancreatic Cancer: Recent Advances and Therapeutic Strategies. *Front. Oncol.* **2020**, *10*, 572722. [CrossRef]
82. Jin, M.-Z.; Han, R.-R.; Qiu, G.-Z.; Ju, X.-C.; Lou, G.; Jin, W.-L. Organoids: An intermediate modeling platform in precision oncology. *Cancer Lett.* **2018**, *414*, 174–180. [CrossRef] [PubMed]
83. Ye, L.; Swingen, C.; Zhang, J. Induced pluripotent stem cells and their potential for basic and clinical sciences. *Curr. Cardiol. Rev.* **2013**, *9*, 63–72. [CrossRef]
84. Zhang, Y.; Houchen, C.W.; Li, M. Patient-Derived Organoid Pharmacotyping Guides Precision Medicine for Pancreatic Cancer. *Clin. Cancer Res.* **2022**, *28*, 3176–3178. [CrossRef] [PubMed]
85. Yang, H.; Wang, Y.; Wang, P.; Zhang, N.; Wang, P. Tumor organoids for cancer research and personalized medicine. *Cancer Biol. Med.* **2021**, *18*, 319–332. [CrossRef]
86. Broguiere, N.; Isenmann, L.; Hirt, C.; Ringel, T.; Placzek, S.; Cavalli, E.; Ringnalda, F.; Villiger, L.; Züllig, R.; Lehmann, R.; et al. Growth of Epithelial Organoids in a Defined Hydrogel. *Adv. Mater.* **2018**, *30*, e1801621. [CrossRef]
87. Schuster, B.; Junkin, M.; Kashaf, S.S.; Romero-Calvo, I.; Kirby, K.; Matthews, J.; Weber, C.R.; Rzhetsky, A.; White, K.P.; Tay, S. Automated microfluidic platform for dynamic and combinatorial drug screening of tumor organoids. *Nat. Commun.* **2020**, *11*, 5271. [CrossRef]
88. Aberle, M.R.; Burkhart, R.A.; Tiriac, H.; Damink, S.W.M.O.; Dejong, C.H.C.; Tuveson, D.A.; van Dam, R.M. Patient-derived organoid models help define personalized management of gastrointestinal cancer. *Br. J. Surg.* **2018**, *105*, E48–E60. [CrossRef]
89. Boucherit, N.; Gorvel, L.; Olive, D. 3D Tumor Models and Their Use for the Testing of Immunotherapies. *Front. Immunol.* **2020**, *11*, 603640. [CrossRef]
90. Romero-Calvo, I.; Weber, C.R.; Ray, M.; Brown, M.; Kirby, K.; Nandi, R.K.; Long, T.M.; Sparrow, S.M.; Ugolkov, A.; Qiang, W.; et al. Human Organoids Share Structural and Genetic Features with Primary Pancreatic Adenocarcinoma Tumors. *Mol. Cancer Res.* **2019**, *17*, 70–83. [CrossRef]
91. Driehuis, E.; van Hoeck, A.; Moore, K.; Kolders, S.; Francies, H.E.; Gulersonmez, M.C.; Stigter, E.C.A.; Burgering, B.; Geurts, V.; Gracanin, A.; et al. Pancreatic cancer organoids recapitulate disease and allow personalized drug screening. *Proc. Natl. Acad. Sci. USA* **2019**, *116*, 26580–26590. [CrossRef] [PubMed]
92. Zeöld, A.; Sándor, G.O.; Kiss, A.; Soós, A.Á.; Tölgyes, T.; Bursics, A.; Szűcs, Á.; Harsányi, L.; Kittel, Á.; Gézsi, A.; et al. Shared extracellular vesicle miRNA profiles of matched ductal pancreatic adenocarcinoma organoids and blood plasma samples show the power of organoid technology. *Cell. Mol. Life Sci.* **2021**, *78*, 3005–3020. [CrossRef]
93. Sereti, E.; Papapostolou, I.; Dimas, K. Pancreatic Cancer Organoids: An Emerging Platform for Precision Medicine? *Biomedicines* **2023**, *11*, 890. [CrossRef]
94. Holokai, L.; Chakrabarti, J.; Lundy, J.; Croagh, D.; Adhikary, P.; Richards, S.S.; Woodson, C.; Steele, N.; Kuester, R.; Scott, A.; et al. Murine- and Human-Derived Autologous Organoid/Immune Cell Co-Cultures as Pre-Clinical Models of Pancreatic Ductal Adenocarcinoma. *Cancers* **2020**, *12*, 3816. [CrossRef] [PubMed]

95. Hennig, A.; Baenke, F.; Klimova, A.; Drukewitz, S.; Jahnke, B.; Brückmann, S.; Secci, R.; Winter, C.; Schmäche, T.; Seidlitz, T.; et al. Detecting drug resistance in pancreatic cancer organoids guides optimized chemotherapy treatment. *J. Pathol.* **2022**, *257*, 607–619. [CrossRef]
96. Krieger, T.G.; Le Blanc, S.; Jabs, J.; Ten, F.W.; Ishaque, N.; Jechow, K.; Debnath, O.; Leonhardt, C.-S.; Giri, A.; Eils, R.; et al. Single-cell analysis of patient-derived PDAC organoids reveals cell state heterogeneity and a conserved developmental hierarchy. *Nat. Commun.* **2021**, *12*, 5826. [CrossRef]
97. Lee, S.; Shanti, A. Effect of Exogenous pH on Cell Growth of Breast Cancer Cells. *Int. J. Mol. Sci.* **2021**, *22*, 9910. [CrossRef]
98. Baker, L.A.; Tiriac, H.; Clevers, H.; Tuveson, D.A. Modeling pancreatic cancer with organoids. *Trends Cancer* **2016**, *2*, 176–190. [CrossRef]
99. Givant-Horwitz, V.; Davidson, B.; Reich, R. Laminin-induced signaling in tumor cells: The role of the M(r) 67,000 laminin receptor. *Cancer Res.* **2004**, *64*, 3572–3579. [CrossRef]
100. Aisenbrey, E.A.; Murphy, W.L. Synthetic alternatives to Matrigel. *Nat. Rev. Mater.* **2020**, *5*, 539–551. [CrossRef]
101. Athukorala, S.S.; Tran, T.S.; Balu, R.; Truong, V.K.; Chapman, J.; Dutta, N.K.; Roy Choudhury, N. 3D Printable Electrically Conductive Hydrogel Scaffolds for Biomedical Applications: A Review. *Polymers* **2021**, *13*, 474. [CrossRef] [PubMed]
102. Unnikrishnan, K.; Thomas, L.V.; Ram Kumar, R.M. Advancement of Scaffold-Based 3D Cellular Models in Cancer Tissue Engineering: An Update. *Front. Oncol.* **2021**, *11*, 733652. [CrossRef]
103. Ermis, M.; Falcone, N.; Roberto de Barros, N.; Mecwan, M.; Haghniaz, R.; Choroomi, A.; Monirizad, M.; Lee, Y.; Song, J.; Cho, H.J.; et al. Tunable hybrid hydrogels with multicellular spheroids for modeling desmoplastic pancreatic cancer. *Bioact. Mater.* **2023**, *25*, 360–373. [CrossRef]
104. Ma, B.; Wang, X.; Bove, A.M.; Simone, G. Molecular Bases of VEGFR-2-Mediated Physiological Function and Pathological Role. *Front. Cell Dev. Biol.* **2020**, *8*, 599281. [CrossRef]
105. Yan, M.; Wang, L.; Wu, Y.; Lu, Y. Three-dimensional highly porous hydrogel scaffold for neural circuit dissection and modulation. *Acta Biomater.* **2023**, *157*, 252–262. [CrossRef]
106. Curvello, R.; Kast, V.; Abuwarwar, M.H.; Fletcher, A.L.; Garnier, G.; Loessner, D. 3D Collagen-Nanocellulose Matrices Model the Tumour Microenvironment of Pancreatic Cancer. *Front. Digit. Health* **2021**, *3*, 704584. [CrossRef]
107. Khan, A.H.; Zhou, S.P.; Moe, M.; Ortega Quesada, B.A.; Bajgiran, K.R.; Lassiter, H.R.; Dorman, J.A.; Martin, E.C.; Pojman, J.A.; Melvin, A.T. Generation of 3D Spheroids Using a Thiol–Acrylate Hydrogel Scaffold to Study Endocrine Response in ER^+ Breast Cancer. *ACS Biomater. Sci. Eng.* **2022**, *8*, 3977–3985. [CrossRef]
108. El-Sherbiny, I.M.; Yacoub, M.H. Hydrogel scaffolds for tissue engineering: Progress and challenges. *Glob. Cardiol. Sci. Pract.* **2013**, *2013*, 316–342. [CrossRef]
109. Geckil, H.; Xu, F.; Zhang, X.; Moon, S.; Demirci, U. Engineering hydrogels as extracellular matrix mimics. *Nanomedicine* **2010**, *5*, 469–484. [CrossRef]
110. Kanton, S.; Paşca, S.P. Human assembloids. *Development* **2022**, *149*, dev201120. [CrossRef]
111. Choi, J.I.; Rim, J.H.; Jang, S.I.; Park, J.S.; Park, H.; Cho, J.H.; Lim, J.B. The role of Jagged1 as a dynamic switch of cancer cell plasticity in PDAC assembloids. *Theranostics* **2022**, *12*, 4431–4445. [CrossRef] [PubMed]
112. Mondadori, C.; Crippa, M.; Moretti, M.; Candrian, C.; Lopa, S.; Arrigoni, C. Advanced Microfluidic Models of Cancer and Immune Cell Extravasation: A Systematic Review of the Literature. *Front. Bioeng. Biotechnol.* **2020**, *8*, 907. [CrossRef] [PubMed]
113. Dadgar, N.; Gonzalez-Suarez, A.M.; Fattahi, P.; Hou, X.; Weroha, J.S.; Gaspar-Maia, A.; Stybayeva, G.; Revzin, A. A microfluidic platform for cultivating ovarian cancer spheroids and testing their responses to chemotherapies. *Microsyst. Nanoeng.* **2020**, *6*, 93. [CrossRef]
114. Lim, W.; Park, S. A Microfluidic Spheroid Culture Device with a Concentration Gradient Generator for High-Throughput Screening of Drug Efficacy. *Molecules* **2018**, *23*, 3355. [CrossRef]
115. Bradney, M.J.; Venis, S.M.; Yang, Y.; Konieczny, S.F.; Han, B. A Biomimetic Tumor Model of Heterogeneous Invasion in Pancreatic Ductal Adenocarcinoma. *Small* **2020**, *16*, e1905500. [CrossRef]
116. Sonmez, U.M.; Cheng, Y.-W.; Watkins, S.C.; Roman, B.L.; Davidson, L.A. Endothelial cell polarization and orientation to flow in a novel microfluidic multimodal shear stress generator. *Lab Chip* **2020**, *2*, 4373–4439. [CrossRef]
117. Beer, M.; Kuppalu, N.; Stefanini, M.; Becker, H.; Schulz, I.; Manoli, S.; Schuette, J.; Schmees, C.; Casazza, A.; Stelzle, M.; et al. A novel microfluidic 3D platform for culturing pancreatic ductal adenocarcinoma cells: Comparison with in vitro cultures and in vivo xenografts. *Sci. Rep.* **2017**, *7*, 1325. [CrossRef]
118. Sato, O.; Tsuchikawa, T.; Kato, T.; Amaishi, Y.; Okamoto, S.; Mineno, J.; Takeuchi, Y.; Sasaki, K.; Nakamura, T.; Umemoto, K.; et al. Tumor Growth Suppression of Pancreatic Cancer Orthotopic Xenograft Model by CEA-Targeting CAR-T Cells. *Cancers* **2023**, *15*, 601. [CrossRef]
119. Wu, C.; Hu, B.; Wang, L.; Wu, X.; Gu, H.; Dong, H.; Yan, J.; Qi, Z.; Zhang, Q.; Chen, H.; et al. Assessment of stromal SCD-induced drug resistance of PDAC using 3D-printed zPDX model chips. *iScience* **2023**, *26*, 105723. [CrossRef]

120. Mallya, K.; Gautam, S.K.; Aithal, A.; Batra, S.K.; Jain, M. Modeling pancreatic cancer in mice for experimental therapeutics. *Biochim. Biophys. Acta Rev. Cancer* **2021**, *1876*, 188554. [CrossRef]
121. Zeng, Z.; Wong, C.J.; Yang, L.; Ouardaoui, N.; Li, D.; Zhang, W.; Gu, S.; Zhang, Y.; Liu, Y.; Wang, X.; et al. TISMO: Syngeneic mouse tumor database to model tumor immunity and immunotherapy response. *Nucleic Acids Res.* **2022**, *50*, D1391–D1397. [CrossRef] [PubMed]
122. Rovithi, M.; Avan, A.; Funel, N.; Leon, L.G.; Gomez, V.E.; Wurdinger, T.; Griffioen, A.W.; Verheul, H.M.W.; Giovannetti, E. Development of bioluminescent chick chorioallantoic membrane (CAM) models for primary pancreatic cancer cells: A platform for drug testing. *Sci. Rep.* **2017**, *7*, 44686. [CrossRef]
123. Johnson, J.I.; Decker, S.; Sausville, E.A.; Zaharevitz, D.; Rubinstein, L.V.; Venditti, J.M.; Schepartz, S.; Kalyandrug, S.; Christian, M.; Arbuck, S.; et al. Relationships between drug activity in NCI preclinical in vitro and in vivo models and early clinical trials. *Br. J. Cancer* **2001**, *84*, 1424–1431. [CrossRef]
124. Voskoglou-Nomikos, T.; Pater, J.L.; Seymour, L. Clinical Predictive Value of the in Vitro Cell Line, Human Xenograft, and Mouse Allograft Preclinical Cancer Models. *Clin. Cancer Res.* **2003**, *9*, 4227–4239. [PubMed]
125. Garber, K. From Human to Mouse and Back: "Tumorgraft" Models Surge in Popularity. *JNCI J. Natl. Cancer Inst.* **2009**, *101*, 6–8. [CrossRef]
126. Bruns, C.J.; Harbison, M.T.; Davis, D.W.; Portera, C.A.; Tsan, R.; McConkey, D.J.; Evans, D.B.; Abbruzzese, J.L.; Hicklin, D.J.; Radinsky, R. Epidermal Growth Factor Receptor Blockade with C225 Plus Gemcitabine Results in Regression of Human Pancreatic Carcinoma Growing Orthotopically in Nude Mice by Antiangiogenic Mechanisms. *Clin. Cancer Res.* **2000**, *6*, 1936–1948. [PubMed]
127. Philip, P.A.; Benedetti, J.; Khorana, A.A.; Goldman, B.; Fenoglio-Preiser, C.M.; Abbruzzese, J.L.; Blanke, C.D.; Corless, C.L.; Wong, R.; O'Reilly, E.M.; et al. Phase III Study Comparing Gemcitabine Plus Cetuximab Versus Gemcitabine in Patients with Advanced Pancreatic Adenocarcinoma: Southwest Oncology Group–Directed Intergroup Trial S0205. *J. Clin. Oncol.* **2010**, *28*, 3605–3610. [CrossRef]
128. Koutsounas, I.; Giaginis, C.; Theocharis, S. Histone deacetylase inhibitors and pancreatic cancer: Are there any promising clinical trials? *World J. Gastroenterol.* **2013**, *19*, 1173–1181. [CrossRef]
129. Mak, I.W.; Evaniew, N.; Ghert, M. Lost in translation: Animal models and clinical trials in cancer treatment. *Am. J. Transl. Res.* **2014**, *6*, 114–118.
130. Van Hemelryk, A.; Tomljanovic, I.; Stuurman, D.; de Ridder, C.M.A.; Teubel, W.J.; Erkens-Schulze, S.; van de Werken, H.J.G.; van Royen, M.; Grudniewska, M.; Jenster, G.W.; et al. Patient-derived xenografts and organoids recapitulate castration-resistant prostate cancer with sustained androgen receptor signaling. *Eur. J. Cancer* **2022**, *174*, S43. [CrossRef]
131. Heinrich, M.A.; Uboldi, I.; Kuninty, P.R.; Ankone, M.J.K.; van Baarlen, J.; Zhang, Y.S.; Jain, K.; Prakash, J. Microarchitectural mimicking of stroma-induced vasculature compression in pancreatic tumors using a 3D engineered model. *Bioact. Mater.* **2023**, *22*, 18–33. [CrossRef]
132. Miyabayashi, K.; Baker, L.A.; Deschênes, A.; Traub, B.; Caligiuri, G.; Plenker, D.; Alagesan, B.; Belleau, P.; Li, S.; Kendall, J.; et al. Intraductal Transplantation Models of Human Pancreatic Ductal Adenocarcinoma Reveal Progressive Transition of Molecular Subtypes. *Cancer Discov.* **2020**, *10*, 1566–1589. [CrossRef]
133. Boj, S.F.; Hwang, C.-I.; Baker, L.A.; Chio, I.I.C.; Engle, D.D.; Corbo, V.; Jager, M.; Ponz-Sarvise, M.; Tiriac, H.; Spector, M.S.; et al. Organoid Models of Human and Mouse Ductal Pancreatic Cancer. *Cell* **2015**, *160*, 324–338. [CrossRef] [PubMed]
134. Olive, K.P.; Jacobetz, M.A.; Davidson, C.J.; Gopinathan, A.; McIntyre, D.; Honess, D.; Madhu, B.; Goldgraben, M.A.; Caldwell, M.E.; Allard, D.; et al. Inhibition of Hedgehog Signaling Enhances Delivery of Chemotherapy in a Mouse Model of Pancreatic Cancer. *Science* **2009**, *324*, 1457–1461. [CrossRef] [PubMed]
135. Tanaka, C.; Furihata, K.; Naganuma, S.; Ogasawara, M.; Yoshioka, R.; Taniguchi, H.; Furihata, M.; Taniuchi, K. Establishment of a mouse model of pancreatic cancer using human pancreatic cancer cell line S2-013-derived organoid. *Hum. Cell Off. J. Hum. Cell Res. Soc.* **2022**, *35*, 735–744. [CrossRef]
136. Raimondi, G.; Mato-Berciano, A.; Pascual-Sabater, S.; Rovira-Rigau, M.; Cuatrecasas, M.; Fondevila, C.; Sánchez-Cabús, S.; Begthel, H.; Boj, S.F.; Clevers, H.; et al. Patient-derived pancreatic tumour organoids identify therapeutic responses to oncolytic adenoviruses. *EBioMedicine* **2020**, *56*, 102786. [CrossRef]
137. Le Bras, A. Humanized mouse models of drug metabolism. *Lab Anim.* **2024**, *53*, 87. [CrossRef]
138. Gonzalez, H.; Hagerling, C.; Werb, Z. Roles of the immune system in cancer: From tumor initiation to metastatic progression. *Genes. Dev.* **2018**, *32*, 1267–1284. [CrossRef]
139. Lee, S.H.; Hu, W.; Matulay, J.T.; Silva, M.V.; Owczarek, T.B.; Kim, K.; Chua, C.W.; Barlow, L.J.; Kandoth, C.; Williams, A.B.; et al. Tumor Evolution and Drug Response in Patient-Derived Organoid Models of Bladder Cancer. *Cell* **2018**, *173*, 515–528.e517. [CrossRef]
140. Edgar, R.D.; Perrone, F.; Foster, A.R.; Payne, F.; Lewis, S.; Nayak, K.M.; Kraiczy, J.; Cenier, A.; Torrente, F.; Salvestrini, C.; et al. Culture-Associated DNA Methylation Changes Impact on Cellular Function of Human Intestinal Organoids. *Cell Mol. Gastroenterol. Hepatol.* **2022**, *14*, 1295–1310. [CrossRef]

141. Fang, Z.; Li, P.; Du, F.; Shang, L.; Li, L. The role of organoids in cancer research. *Exp. Hematol. Oncol.* **2023**, *12*, 69. [CrossRef]
142. Peng, Z.; Lv, X.; Sun, H.; Zhao, L.; Huang, S. 3D tumor cultures for drug resistance and screening development in clinical applications. *Mol. Cancer* **2025**, *24*, 93. [CrossRef] [PubMed]
143. Abdolahi, S.; Ghazvinian, Z.; Muhammadnejad, S.; Saleh, M.; Asadzadeh Aghdaei, H.; Baghaei, K. Patient-derived xenograft (PDX) models, applications and challenges in cancer research. *J. Transl. Med.* **2022**, *20*, 206. [CrossRef] [PubMed]
144. Seppälä, T.T.; Zimmerman, J.W.; Sereni, E.; Plenker, D.; Suri, R.; Rozich, N.; Blair, A.; Thomas, D.L.; Teinor, J.; Javed, A.; et al. Patient-derived Organoid Pharmacotyping is a Clinically Tractable Strategy for Precision Medicine in Pancreatic Cancer. *Ann. Surg.* **2020**, *272*, 427–435. [CrossRef]
145. Magouliotis, D.; Dimas, K.; Sakellaridis, N.; Ioannou, M.; Zacharouli, K.; Ntalagiorgos, A.; Fergadi, M.; Zacharoulis, D. Development of an Orthotopic Pancreatic Ductal Adenocarcinoma (PDAC) Patient Derived Xenografts (PDX) Preclinical Model and Characterization of Aquaporin 7 (AQP7) Expression. *HPB* **2022**, *24*, S304. [CrossRef]
146. Wu, L.; Zhang, F.; Chen, X.; Wan, J.; Wang, Y.; Li, T.; Wang, H. Self-Assembled Gemcitabine Prodrug Nanoparticles Show Enhanced Efficacy against Patient-Derived Pancreatic Ductal Adenocarcinoma. *ACS Appl. Mater. Interfaces* **2020**, *12*, 3327–3340. [CrossRef]
147. Garcia, P.L.; Miller, A.L.; Kreitzburg, K.M.; Council, L.N.; Gamblin, T.L.; Christein, J.D.; Heslin, M.J.; Arnoletti, J.P.; Richardson, J.H.; Chen, D.; et al. The BET bromodomain inhibitor JQ1 suppresses growth of pancreatic ductal adenocarcinoma in patient-derived xenograft models. *Oncogene* **2016**, *35*, 833–845. [CrossRef]
148. Zanella, E.R.; Grassi, E.; Trusolino, L. Towards precision oncology with patient-derived xenografts. *Nat. Rev. Clin. Oncol.* **2022**, *19*, 719–732. [CrossRef]
149. Delitto, D.; Pham, K.; Vlada, A.C.; Sarosi, G.A.; Thomas, R.M.; Behrns, K.E.; Liu, C.; Hughes, S.J.; Wallet, S.M.; Trevino, J.G. Patient-Derived Xenograft Models for Pancreatic Adenocarcinoma Demonstrate Retention of Tumor Morphology through Incorporation of Murine Stromal Elements. *Am. J. Pathol.* **2015**, *185*, 1297–1303. [CrossRef]
150. Yoshida, G.J. Applications of patient-derived tumor xenograft models and tumor organoids. *J. Hematol. Oncol.* **2020**, *13*, 4–16. [CrossRef]
151. Liu, X.; Xin, Z.; Wang, K. Patient-derived xenograft model in colorectal cancer basic and translational research. *Anim. Models Exp. Med.* **2023**, *6*, 26–40. [CrossRef] [PubMed]
152. De La Rochere, P.; Guil-Luna, S.; Decaudin, D.; Azar, G.; Sidhu, S.S.; Piaggio, E. Humanized Mice for the Study of Immuno-Oncology. *Trends Immunol.* **2018**, *39*, 748–763. [CrossRef] [PubMed]
153. Tentler, J.J.; Tan, A.C.; Weekes, C.D.; Jimeno, A.; Leong, S.; Pitts, T.M.; Arcaroli, J.J.; Messersmith, W.A.; Eckhardt, S.G. Patient-derived tumour xenografts as models for oncology drug development. *Nat. Rev. Clin. Oncol.* **2012**, *9*, 338–350. [CrossRef]
154. Ekins, S.; Mestres, J.; Testa, B. In silico pharmacology for drug discovery: Methods for virtual ligand screening and profiling. *Br. J. Pharmacol.* **2007**, *152*, 9–20. [CrossRef]
155. Güven, E. Gene Expression Characteristics of Tumor and Adjacent Non-Tumor Tissues of Pancreatic Ductal Adenocarcinoma (PDAC) In-Silico. *Iran. J. Biotechnol.* **2022**, *20*, e3092. [CrossRef]
156. Zaccagnino, A.; Pilarsky, C.; Tawfik, D.; Sebens, S.; Trauzold, A.; Novak, I.; Schwab, A.; Kalthoff, H. In silico analysis of the transportome in human pancreatic ductal adenocarcinoma. *Eur. Biophys. J.* **2016**, *45*, 749–763. [CrossRef] [PubMed]
157. Jain, A.; Bhardwaj, V. Therapeutic resistance in pancreatic ductal adenocarcinoma: Current challenges and future opportunities. *World J. Gastroenterol.* **2021**, *27*, 6527–6550. [CrossRef]
158. Broekgaarden, M.; Weijer, R.; van Gulik, T.M.; Hamblin, M.R.; Heger, M. Tumor cell survival pathways activated by photodynamic therapy: A molecular basis for pharmacological inhibition strategies. *Cancer Metastasis Rev.* **2015**, *34*, 643–690. [CrossRef]
159. Yanovsky, R.L.; Bartenstein, D.W.; Rogers, G.S.; Isakoff, S.J.; Chen, S.T. Photodynamic therapy for solid tumors: A review of the literature. *Photodermatol. Photoimmunol. Photomed.* **2019**, *35*, 295–303. [CrossRef]
160. Schuitmaker, J.J.; Baas, P.; van Leengoed, H.L.; van der Meulen, F.W.; Star, W.M.; van Zandwijk, N. Photodynamic therapy: A promising new modality for the treatment of cancer. *J. Photochem. Photobiol. B* **1996**, *34*, 3–12. [CrossRef]
161. Kim, T.E.; Chang, J.E. Recent Studies in Photodynamic Therapy for Cancer Treatment: From Basic Research to Clinical Trials. *Pharmaceutics* **2023**, *15*, 2257. [CrossRef]
162. Reiniers, M.J.; van Golen, R.F.; Bonnet, S.; Broekgaarden, M.; van Gulik, T.M.; Egmond, M.R.; Heger, M. Preparation and Practical Applications of 2′,7′-Dichlorodihydrofluorescein in Redox Assays. *Anal. Chem.* **2017**, *89*, 3853–3857. [CrossRef] [PubMed]
163. Broekgaarden, M.; de Kroon, A.I.; Gulik, T.M.; Heger, M. Development and in vitro proof-of-concept of interstitially targeted zinc-phthalocyanine liposomes for photodynamic therapy. *Curr. Med. Chem.* **2014**, *21*, 377–391. [CrossRef] [PubMed]
164. Hsieh, Y.J.; Chien, K.Y.; Yang, I.F.; Lee, I.N.; Wu, C.C.; Huang, T.Y.; Yu, J.S. Oxidation of protein-bound methionine in Photofrin-photodynamic therapy-treated human tumor cells explored by methionine-containing peptide enrichment and quantitative proteomics approach. *Sci. Rep.* **2017**, *7*, 1370. [CrossRef]
165. Sakharov, D.V.; Elstak, E.D.; Chernyak, B.; Wirtz, K.W. Prolonged lipid oxidation after photodynamic treatment. Study with oxidation-sensitive probe C11-BODIPY581/591. *FEBS Lett.* **2005**, *579*, 1255–1260. [CrossRef]

166. Kanamori, T.; Kaneko, S.; Hamamoto, K.; Yuasa, H. Mapping the diffusion pattern of (1)O(2) along DNA duplex by guanine photooxidation with an appended biphenyl photosensitizer. *Sci. Rep.* **2023**, *13*, 288. [CrossRef] [PubMed]
167. Weijer, R.; Broekgaarden, M.; Kos, M.; van Vught, R.; Rauws, E.A.; Breukink, E.J.; van Gulik, T.M.; Storm, G.; Heger, M. Enhancing photodynamic therapy of refractory solid cancers: Combining second-generation photosensitizers with multi-targeted liposomal delivery. *J. Photochem. Photobiol. C* **2015**, *23*, 103–131. [CrossRef]
168. Castano, A.P.; Demidova, T.N.; Hamblin, M.R. Mechanisms in photodynamic therapy: Part two-cellular signaling, cell metabolism and modes of cell death. *Photodiagnosis Photodyn. Ther.* **2005**, *2*, 1–23. [CrossRef]
169. Weijer, R.; Clavier, S.; Zaal, E.A.; Pijls, M.M.; van Kooten, R.T.; Vermaas, K.; Leen, R.; Jongejan, A.; Moerland, P.D.; van Kampen, A.H.; et al. Multi-OMIC profiling of survival and metabolic signaling networks in cells subjected to photodynamic therapy. *Cell Mol. Life Sci.* **2017**, *74*, 1133–1151. [CrossRef]
170. Dias, L.M.; Sharifi, F.; de Keijzer, M.J.; Mesquita, B.; Desclos, E.; Kochan, J.A.; de Klerk, D.J.; Ernst, D.; de Haan, L.R.; Franchi, L.P.; et al. Attritional evaluation of lipophilic and hydrophilic metallated phthalocyanines for oncological photodynamic therapy. *J. Photochem. Photobiol. B* **2021**, *216*, 112146. [CrossRef]
171. Mishchenko, T.; Balalaeva, I.; Gorokhova, A.; Vedunova, M.; Krysko, D.V. Which cell death modality wins the contest for photodynamic therapy of cancer? *Cell Death Dis.* **2022**, *13*, 455. [CrossRef] [PubMed]
172. Alzeibak, R.; Mishchenko, T.A.; Shilyagina, N.Y.; Balalaeva, I.V.; Vedunova, M.V.; Krysko, D.V. Targeting immunogenic cancer cell death by photodynamic therapy: Past, present and future. *J. Immunother. Cancer* **2021**, *9*, e001926. [CrossRef]
173. Behrend, L.; Henderson, G.; Zwacka, R.M. Reactive oxygen species in oncogenic transformation. *Biochem. Soc. Trans.* **2003**, *31*, 1441–1444. [CrossRef] [PubMed]
174. Hu, Y.; Rosen, D.G.; Zhou, Y.; Feng, L.; Yang, G.; Liu, J.; Huang, P. Mitochondrial manganese-superoxide dismutase expression in ovarian cancer: Role in cell proliferation and response to oxidative stress. *J. Biol. Chem.* **2005**, *280*, 39485–39492. [CrossRef] [PubMed]
175. Trachootham, D.; Lu, W.; Ogasawara, M.A.; Nilsa, R.D.; Huang, P. Redox regulation of cell survival. *Antioxid. Redox Signal.* **2008**, *10*, 1343–1374. [CrossRef]
176. Ushio-Fukai, M.; Nakamura, Y. Reactive oxygen species and angiogenesis: NADPH oxidase as target for cancer therapy. *Cancer Lett.* **2008**, *266*, 37–52. [CrossRef]
177. Wu, W.S. The signaling mechanism of ROS in tumor progression. *Cancer Metastasis Rev.* **2006**, *25*, 695–705. [CrossRef]
178. Nishikawa, M. Reactive oxygen species in tumor metastasis. *Cancer Lett.* **2008**, *266*, 53–59. [CrossRef]
179. Arfin, S.; Jha, N.K.; Jha, S.K.; Kesari, K.K.; Ruokolainen, J.; Roychoudhury, S.; Rathi, B.; Kumar, D. Oxidative Stress in Cancer Cell Metabolism. *Antioxidants* **2021**, *10*, 642. [CrossRef]
180. Trachootham, D.; Alexandre, J.; Huang, P. Targeting cancer cells by ROS-mediated mechanisms: A radical therapeutic approach? *Nat. Rev. Drug Discov.* **2009**, *8*, 579–591. [CrossRef]
181. Zhou, Z.; Song, J.; Nie, L.; Chen, X. Reactive oxygen species generating systems meeting challenges of photodynamic cancer therapy. *Chem. Soc. Rev.* **2016**, *45*, 6597–6626. [CrossRef] [PubMed]
182. Weijer, R.; Broekgaarden, M.; van Golen, R.F.; Bulle, E.; Nieuwenhuis, E.; Jongejan, A.; Moerland, P.D.; van Kampen, A.H.; van Gulik, T.M.; Heger, M. Low-power photodynamic therapy induces survival signaling in perihilar cholangiocarcinoma cells. *BMC Cancer* **2015**, *15*, 1014. [CrossRef]
183. De Silva, P.; Bano, S.; Pogue, B.W.; Wang, K.K.; Maytin, E.V.; Hasan, T. Photodynamic priming with triple-receptor targeted nanoconjugates that trigger T cell-mediated immune responses in a 3D in vitro heterocellular model of pancreatic cancer. *Nanophotonics* **2021**, *10*, 3199–3214. [CrossRef]
184. Seshadri, M.; Spernyak, J.A.; Mazurchuk, R.; Camacho, S.H.; Oseroff, A.R.; Cheney, R.T.; Bellnier, D.A. Tumor vascular response to photodynamic therapy and the antivascular agent 5,6-dimethylxanthenone-4-acetic acid: Implications for combination therapy. *Clin. Cancer Res.* **2005**, *11*, 4241–4250. [CrossRef]
185. Wang, W.; Moriyama, L.T.; Bagnato, V.S. Photodynamic therapy induced vascular damage: An overview of experimental PDT. *Laser Phys. Lett.* **2013**, *10*, 023001. [CrossRef]
186. Bano, S.; Alburquerque, J.Q.; Roberts, H.J.; Pang, S.; Huang, H.C.; Hasan, T. Minocycline and photodynamic priming significantly improve chemotherapy efficacy in heterotypic spheroids of pancreatic ductal adenocarcinoma. *J. Photochem. Photobiol. B* **2024**, *255*, 112910. [CrossRef]
187. Kleinovink, J.W.; van Driel, P.B.; Snoeks, T.J.; Prokopi, N.; Fransen, M.F.; Cruz, L.J.; Mezzanotte, L.; Chan, A.; Lowik, C.W.; Ossendorp, F. Combination of Photodynamic Therapy and Specific Immunotherapy Efficiently Eradicates Established Tumors. *Clin. Cancer Res.* **2016**, *22*, 1459–1468. [CrossRef] [PubMed]
188. Schroder, T.; Chen, I.W.; Sperling, M.; Bell, R.H., Jr.; Brackett, K.; Joffe, S.N. Hematoporphyrin derivative uptake and photodynamic therapy in pancreatic carcinoma. *J. Surg. Oncol.* **1988**, *38*, 4–9. [CrossRef] [PubMed]
189. Chatlani, P.T.; Nuutinen, P.J.; Toda, N.; Barr, H.; MacRobert, A.J.; Bedwell, J.; Bown, S.G. Selective necrosis in hamster pancreatic tumours using photodynamic therapy with phthalocyanine photosensitization. *Br. J. Surg.* **1992**, *79*, 786–790. [CrossRef]

190. Mikvy, P.; Messman, H.; MacRobert, A.J.; Pauer, M.; Sams, V.R.; Davies, C.L.; Stewart, J.C.; Bown, S.G. Photodynamic therapy of a transplanted pancreatic cancer model using meta-tetrahydroxyphenylchlorin (mTHPC). *Br. J. Cancer* **1997**, *76*, 713–718. [CrossRef]
191. Hajri, A.; Coffy, S.; Vallat, F.; Evrard, S.; Marescaux, J.; Aprahamian, M. Human pancreatic carcinoma cells are sensitive to photodynamic therapy in vitro and in vivo. *Br. J. Surg.* **1999**, *86*, 899–906. [CrossRef] [PubMed]
192. Sun, F.; Zhu, Q.; Li, T.; Saeed, M.; Xu, Z.; Zhong, F.; Song, R.; Huai, M.; Zheng, M.; Xie, C.; et al. Regulating Glucose Metabolism with Prodrug Nanoparticles for Promoting Photoimmunotherapy of Pancreatic Cancer. *Adv. Sci.* **2021**, *8*, 2002746. [CrossRef]
193. De Silva, P.; Saad, M.A.; Camargo, A.P.; Swain, J.; Palanasami, A.; Obaid, G.; Shetty, S.; Hasan, T. Abstract A17: Enhanced immune infiltration and antitumor immune reactivity in response to optical priming in pancreatic cancer. *Cancer Immunol. Res.* **2020**, *8*, A17. [CrossRef]
194. Huang, H.C.; Rizvi, I.; Liu, J.; Anbil, S.; Kalra, A.; Lee, H.; Baglo, Y.; Paz, N.; Hayden, D.; Pereira, S.; et al. Photodynamic Priming Mitigates Chemotherapeutic Selection Pressures and Improves Drug Delivery. *Cancer Res.* **2018**, *78*, 558–571. [CrossRef] [PubMed]
195. Weijer, R.; Broekgaarden, M.; Krekorian, M.; Alles, L.K.; van Wijk, A.C.; Mackaaij, C.; Verheij, J.; van der Wal, A.C.; van Gulik, T.M.; Storm, G.; et al. Inhibition of hypoxia inducible factor 1 and topoisomerase with acriflavine sensitizes perihilar cholangiocarcinomas to photodynamic therapy. *Oncotarget* **2016**, *7*, 3341–3356. [CrossRef]
196. Broekgaarden, M.; Weijer, R.; Krekorian, M.; van den Ijssel, B.; Kos, M.; Alles, L.K.; van Wijk, A.C.; Bikadi, Z.; Hazai, E.; van Gulik, T.M.; et al. Inhibition of hypoxia-inducible factor 1 with acriflavine sensitizes hypoxic tumor cells to photodynamic therapy with zinc phthalocyanine-encapsulating cationic liposomes. *Nano Res.* **2016**, *9*, 1639–1662. [CrossRef]
197. de Keijzer, M.J.; de Klerk, D.J.; de Haan, L.R.; van Kooten, R.T.; Franchi, L.P.; Dias, L.M.; Kleijn, T.G.; van Doorn, D.J.; Heger, M.; on behalf of the Photodynamic Therapy Study Group. Inhibition of the HIF-1 Survival Pathway as a Strategy to Augment Photodynamic Therapy Efficacy. *Methods Mol. Biol.* **2022**, *2451*, 285–403. [CrossRef]
198. Conte, M.; Cauda, V. Multimodal Therapies against Pancreatic Ductal Adenocarcinoma: A Review on Synergistic Approaches toward Ultimate Nanomedicine Treatments. *Adv. Ther.* **2022**, *5*, 2200079. [CrossRef]
199. Anbil, S.; Pigula, M.; Huang, H.C.; Mallidi, S.; Broekgaarden, M.; Baglo, Y.; De Silva, P.; Simeone, D.M.; Mino-Kenudson, M.; Maytin, E.V.; et al. Vitamin D Receptor Activation and Photodynamic Priming Enables Durable Low-dose Chemotherapy. *Mol. Cancer Ther.* **2020**, *19*, 1308–1319. [CrossRef]
200. Obaid, G.; Bano, S.; Mallidi, S.; Broekgaarden, M.; Kuriakose, J.; Silber, Z.; Bulin, A.L.; Wang, Y.; Mai, Z.; Jin, W.; et al. Impacting Pancreatic Cancer Therapy in Heterotypic in Vitro Organoids and in Vivo Tumors with Specificity-Tuned, NIR-Activable Photoimmunonanoconjugates: Towards Conquering Desmoplasia? *Nano Lett.* **2019**, *19*, 7573–7587. [CrossRef]
201. Obaid, G.; Bano, S.; Thomsen, H.; Callaghan, S.; Shah, N.; Swain, J.W.R.; Jin, W.; Ding, X.; Cameron, C.G.; McFarland, S.A.; et al. Remediating Desmoplasia with EGFR-Targeted Photoactivable Multi-Inhibitor Liposomes Doubles Overall Survival in Pancreatic Cancer. *Adv. Sci.* **2022**, *9*, e2104594. [CrossRef]
202. Grunwald, B.T.; Devisme, A.; Andrieux, G.; Vyas, F.; Aliar, K.; McCloskey, C.W.; Macklin, A.; Jang, G.H.; Denroche, R.; Romero, J.M.; et al. Spatially confined sub-tumor microenvironments in pancreatic cancer. *Cell* **2021**, *184*, 5577–5592.e18. [CrossRef] [PubMed]
203. Bailey, P.; Zhou, X.; An, J.; Peccerella, T.; Hu, K.; Springfeld, C.; Buchler, M.; Neoptolemos, J.P. Refining the Treatment of Pancreatic Cancer From Big Data to Improved Individual Survival. *Function* **2023**, *4*, zqad011. [CrossRef]
204. Karimnia, V.; Rizvi, I.; Slack, F.J.; Celli, J.P. Photodestruction of Stromal Fibroblasts Enhances Tumor Response to PDT in 3D Pancreatic Cancer Coculture Models. *Photochem. Photobiol.* **2021**, *97*, 416–426. [CrossRef] [PubMed]
205. Tan, P.; Cai, H.; Wei, Q.; Tang, X.; Zhang, Q.; Kopytynski, M.; Yang, J.; Yi, Y.; Zhang, H.; Gong, Q.; et al. Enhanced chemo-photodynamic therapy of an enzyme-responsive prodrug in bladder cancer patient-derived xenograft models. *Biomaterials* **2021**, *277*, 121061. [CrossRef]
206. Murayama, T.; Gotoh, N. Patient-Derived Xenograft Models of Breast Cancer and Their Application. *Cells* **2019**, *8*, 621. [CrossRef]
207. Chitrangi, S.; Vaity, P.; Jamdar, A.; Bhatt, S. Patient-derived organoids for precision oncology: A platform to facilitate clinical decision making. *BMC Cancer* **2023**, *23*, 689. [CrossRef] [PubMed]
208. Bubin, R.; Uljanovs, R.; Strumfa, I. Cancer Stem Cells in Pancreatic Ductal Adenocarcinoma. *Int. J. Mol. Sci.* **2023**, *24*, 7030. [CrossRef]
209. Gurung, P.; Lim, J.; Shrestha, R.; Kim, Y.W. Chlorin e6-associated photodynamic therapy enhances abscopal antitumor effects via inhibition of PD-1/PD-L1 immune checkpoint. *Sci. Rep.* **2023**, *13*, 4647. [CrossRef]
210. Lou, J.; Aragaki, M.; Bernards, N.; Chee, T.; Gregor, A.; Hiraishi, Y.; Ishiwata, T.; Leung, C.; Ding, L.; Kitazawa, S.; et al. Repeated photodynamic therapy mediates the abscopal effect through multiple innate and adaptive immune responses with and without immune checkpoint therapy. *Biomaterials* **2023**, *292*, 121918. [CrossRef]
211. Quilbe, A.; Morales, O.; Baydoun, M.; Kumar, A.; Mustapha, R.; Murakami, T.; Leroux, B.; de Schutter, C.; Thecua, E.; Ziane, L.; et al. An Efficient Photodynamic Therapy Treatment for Human Pancreatic Adenocarcinoma. *J. Clin. Med.* **2020**, *9*, 192. [CrossRef] [PubMed]

212. Wang, Y.; Wang, H.; Zhou, L.; Lu, J.; Jiang, B.; Liu, C.; Guo, J. Photodynamic therapy of pancreatic cancer: Where have we come from and where are we going? *Photodiagnosis Photodyn. Ther.* **2020**, *31*, 101876. [CrossRef]
213. Dorst, D.N.; Smeets, E.M.M.; Klein, C.; Frielink, C.; Geijs, D.; Trajkovic-Arsic, M.; Cheung, P.F.Y.; Stommel, M.W.J.; Gotthardt, M.; Siveke, J.T.; et al. Fibroblast Activation Protein-Targeted Photodynamic Therapy of Cancer-Associated Fibroblasts in Murine Models for Pancreatic Ductal Adenocarcinoma. *Mol. Pharm.* **2023**, *20*, 4319–4330. [CrossRef]
214. Tomas-Bort, E.; Kieler, M.; Sharma, S.; Candido, J.B.; Loessner, D. 3D approaches to model the tumor microenvironment of pancreatic cancer. *Theranostics* **2020**, *10*, 5074–5089. [CrossRef] [PubMed]
215. Foglizzo, V.; Cocco, E.; Marchio, S. Advanced Cellular Models for Preclinical Drug Testing: From 2D Cultures to Organ-on-a-Chip Technology. *Cancers* **2022**, *14*, 3692. [CrossRef]
216. Pinto, B.; Henriques, A.C.; Silva, P.M.A.; Bousbaa, H. Three-Dimensional Spheroids as In Vitro Preclinical Models for Cancer Research. *Pharmaceutics* **2020**, *12*, 1186. [CrossRef]
217. Hubrecht, R.C.; Carter, E. The 3Rs and Humane Experimental Technique: Implementing Change. *Animals* **2019**, *9*, 754. [CrossRef]
218. Saad, M.A.; Zhung, W.; Stanley, M.E.; Formica, S.; Grimaldo-Garcia, S.; Obaid, G.; Hasan, T. Photoimmunotherapy Retains Its Anti-Tumor Efficacy with Increasing Stromal Content in Heterotypic Pancreatic Cancer Spheroids. *Mol. Pharm.* **2022**, *19*, 2549–2563. [CrossRef] [PubMed]
219. Bulin, A.L.; Broekgaarden, M.; Simeone, D.; Hasan, T. Low dose photodynamic therapy harmonizes with radiation therapy to induce beneficial effects on pancreatic heterocellular spheroids. *Oncotarget* **2019**, *10*, 2625–2643. [CrossRef]
220. Broekgaarden, M.; Alkhateeb, A.; Bano, S.; Bulin, A.L.; Obaid, G.; Rizvi, I.; Hasan, T. Cabozantinib Inhibits Photodynamic Therapy-Induced Auto- and Paracrine MET Signaling in Heterotypic Pancreatic Microtumors. *Cancers* **2020**, *12*, 1401. [CrossRef]
221. Hughes, C.S.; Postovit, L.M.; Lajoie, G.A. Matrigel: A complex protein mixture required for optimal growth of cell culture. *Proteomics* **2010**, *10*, 1886–1890. [CrossRef]
222. Benton, G.; George, J.; Kleinman, H.K.; Arnaoutova, I.P. Advancing science and technology via 3D culture on basement membrane matrix. *J. Cell Physiol.* **2009**, *221*, 18–25. [CrossRef]
223. Kalluri, R. The biology and function of fibroblasts in cancer. *Nat. Rev. Cancer* **2016**, *16*, 582–598. [CrossRef] [PubMed]
224. Hayes, J.D.; Dinkova-Kostova, A.T.; Tew, K.D. Oxidative Stress in Cancer. *Cancer Cell* **2020**, *38*, 167–197. [CrossRef] [PubMed]
225. Pervaiz, S.; Clement, M.V. Tumor intracellular redox status and drug resistance--serendipity or a causal relationship? *Curr. Pharm. Des.* **2004**, *10*, 1969–1977. [CrossRef]
226. Onodera, Y.; Teramura, T.; Takehara, T.; Shigi, K.; Fukuda, K. Reactive oxygen species induce Cox-2 expression via TAK1 activation in synovial fibroblast cells. *FEBS Open Bio* **2015**, *5*, 492–501. [CrossRef] [PubMed]
227. Chiang, S.K.; Chen, S.E.; Chang, L.C. The Role of HO-1 and Its Crosstalk with Oxidative Stress in Cancer Cell Survival. *Cells* **2021**, *10*, 2401. [CrossRef]
228. Fontaine, E. Metformin-Induced Mitochondrial Complex I Inhibition: Facts, Uncertainties, and Consequences. *Front. Endocrinol.* **2018**, *9*, 753. [CrossRef]
229. de Haan, L.R.; Reiniers, M.J.; Reeskamp, L.F.; Belkouz, A.; Ao, L.; Cheng, S.; Ding, B.; van Golen, R.F.; Heger, M. Experimental Conditions That Influence the Utility of 2′7′-Dichlorodihydrofluorescein Diacetate (DCFH(2)-DA) as a Fluorogenic Biosensor for Mitochondrial Redox Status. *Antioxidants* **2022**, *11*, 1424. [CrossRef]
230. Broekgaarden, M.; Bulin, A.L.; Frederick, J.; Mai, Z.; Hasan, T. Tracking Photodynamic- and Chemotherapy-Induced Redox-State Perturbations in 3D Culture Models of Pancreatic Cancer: A Tool for Identifying Therapy-Induced Metabolic Changes. *J. Clin. Med.* **2019**, *8*, 1399. [CrossRef]
231. Carigga Gutierrez, N.M.; Le Clainche, T.; Coll, J.L.; Sancey, L.; Broekgaarden, M. Generating Large Numbers of Pancreatic Microtumors on Alginate-Gelatin Hydrogels for Quantitative Imaging of Tumor Growth and Photodynamic Therapy Optimization. *Methods Mol. Biol.* **2022**, *2451*, 91–105. [CrossRef]
232. Cramer, G.M.; Jones, D.P.; El-Hamidi, H.; Celli, J.P. ECM Composition and Rheology Regulate Growth, Motility, and Response to Photodynamic Therapy in 3D Models of Pancreatic Ductal Adenocarcinoma. *Mol. Cancer Res.* **2017**, *15*, 15–25. [CrossRef] [PubMed]
233. Jafari, R.; Cramer, G.M.; Celli, J.P. Modulation of Extracellular Matrix Rigidity Via Riboflavin-mediated Photocrosslinking Regulates Invasive Motility and Treatment Response in a 3D Pancreatic Tumor Model. *Photochem. Photobiol.* **2020**, *96*, 365–372. [CrossRef] [PubMed]
234. Andersen, T.; Auk-Emblem, P.; Dornish, M. 3D Cell Culture in Alginate Hydrogels. *Microarrays* **2015**, *4*, 133–161. [CrossRef]
235. Abdelrahim, A.A.; Hong, S.; Song, J.M. Integrative In Situ Photodynamic Therapy-Induced Cell Death Measurement of 3D-Bioprinted MCF-7 Tumor Spheroids. *Anal. Chem.* **2022**, *94*, 13936–13943. [CrossRef] [PubMed]
236. Biffi, G.; Oni, T.E.; Spielman, B.; Hao, Y.; Elyada, E.; Park, Y.; Preall, J.; Tuveson, D.A. IL1-Induced JAK/STAT Signaling Is Antagonized by TGFbeta to Shape CAF Heterogeneity in Pancreatic Ductal Adenocarcinoma. *Cancer Discov.* **2019**, *9*, 282–301. [CrossRef]

237. Lehnert, L.; Trost, H.; Schmiegel, W.; Roder, C.; Kalthoff, H. Hollow-spheres: A new model for analyses of differentiation of pancreatic duct epithelial cells. *Ann. N. Y. Acad. Sci.* **1999**, *880*, 83–93. [CrossRef]
238. Sipos, B.; Moser, S.; Kalthoff, H.; Torok, V.; Lohr, M.; Kloppel, G. A comprehensive characterization of pancreatic ductal carcinoma cell lines: Towards the establishment of an in vitro research platform. *Virchows Arch.* **2003**, *442*, 444–452. [CrossRef]
239. Winterhoff, B.J.; Arlt, A.; Duttmann, A.; Ungefroren, H.; Schafer, H.; Kalthoff, H.; Kruse, M.L. Characterisation of FAP-1 expression and CD95 mediated apoptosis in the A818-6 pancreatic adenocarcinoma differentiation system. *Differentiation* **2012**, *83*, 148–157. [CrossRef]
240. Algarni, A.; Greenman, J.; Madden, L.A. PO-48—Assessment of the procoagulant potential state of tumour-MP in cancer patients. *Thromb. Res.* **2016**, *140* (Suppl. 1), S194. [CrossRef]
241. Lee, W.T.; Lee, J.; Kim, H.; Nguyen, N.T.; Lee, E.S.; Oh, K.T.; Choi, H.G.; Youn, Y.S. Photoreactive-proton-generating hyaluronidase/albumin nanoparticles-loaded PEG-hydrogel enhances antitumor efficacy and disruption of the hyaluronic acid extracellular matrix in AsPC-1 tumors. *Mater. Today Bio* **2021**, *12*, 100164. [CrossRef]
242. Yang, J.; Zhang, Z.; Zhang, Y.; Ni, X.; Zhang, G.; Cui, X.; Liu, M.; Xu, C.; Zhang, Q.; Zhu, H.; et al. ZIP4 Promotes Muscle Wasting and Cachexia in Mice with Orthotopic Pancreatic Tumors by Stimulating RAB27B-Regulated Release of Extracellular Vesicles From Cancer Cells. *Gastroenterology* **2019**, *156*, 722–734.e726. [CrossRef] [PubMed]
243. Hye Jeong, J.; Park, S.; Lee, S.; Kim, Y.; Kyong Shim, I.; Jeong, S.Y.; Kyung Choi, E.; Kim, J.; Jun, E. Orthotopic model of pancreatic cancer using CD34^{+} humanized mice and generation of tumor organoids from humanized tumors. *Int. Immunopharmacol.* **2023**, *121*, 110451. [CrossRef] [PubMed]
244. Er, O.; Tuncel, A.; Ocakoglu, K.; Ince, M.; Kolatan, E.H.; Yilmaz, O.; Aktas, S.; Yurt, F. Radiolabeling, In Vitro Cell Uptake, and In Vivo Photodynamic Therapy Potential of Targeted Mesoporous Silica Nanoparticles Containing Zinc Phthalocyanine. *Mol. Pharm.* **2020**, *17*, 2648–2659. [CrossRef]
245. Samkoe, K.S.; Chen, A.; Rizvi, I.; O'Hara, J.A.; Hoopes, P.J.; Pereira, S.P.; Hasan, T.; Pogue, B.W. Imaging tumor variation in response to photodynamic therapy in pancreatic cancer xenograft models. *Int. J. Radiat. Oncol. Biol. Phys.* **2010**, *76*, 251–259. [CrossRef]
246. Yu, L.S.; Jhunjhunwala, M.; Hong, S.Y.; Yu, L.Y.; Lin, W.R.; Chen, C.S. Tissue Architecture Influences the Biological Effectiveness of Boron Neutron Capture Therapy in In Vitro/In Silico Three-Dimensional Self-Assembly Cell Models of Pancreatic Cancers. *Cancers* **2021**, *13*, 4058. [CrossRef]
247. Karnevi, E.; Rosendahl, A.H.; Hilmersson, K.S.; Saleem, M.A.; Andersson, R. Impact by pancreatic stellate cells on epithelial-mesenchymal transition and pancreatic cancer cell invasion: Adding a third dimension in vitro. *Exp. Cell Res.* **2016**, *346*, 206–215. [CrossRef] [PubMed]
248. Jhaveri, A.V.; Zhou, L.; Ralff, M.D.; Lee, Y.S.; Navaraj, A.; Carneiro, B.A.; Safran, H.; Prabhu, V.V.; Ross, E.A.; Lee, S.; et al. Combination of ONC201 and TLY012 induces selective, synergistic apoptosis in vitro and significantly delays PDAC xenograft growth in vivo. *Cancer Biol. Ther.* **2021**, *22*, 607–618. [CrossRef]
249. Lee, J.; Han, S.; Thapa Magar, T.B.; Gurung, P.; Lee, J.; Seong, D.; Park, S.; Kim, Y.W.; Jeon, M.; Kim, J. Efficient Assessment of Tumor Vascular Shutdown by Photodynamic Therapy on Orthotopic Pancreatic Cancer Using High-Speed Wide-Field Waterproof Galvanometer Scanner Photoacoustic Microscopy. *Int. J. Mol. Sci.* **2024**, *25*, 3457. [CrossRef]
250. Froeling, F.E.; Feig, C.; Chelala, C.; Dobson, R.; Mein, C.E.; Tuveson, D.A.; Clevers, H.; Hart, I.R.; Kocher, H.M. Retinoic acid-induced pancreatic stellate cell quiescence reduces paracrine Wnt-beta-catenin signaling to slow tumor progression. *Gastroenterology* **2011**, *141*, 1486–1497.e14. [CrossRef]
251. Kuroda, Y.; Oda, T.; Shimomura, O.; Hashimoto, S.; Akashi, Y.; Miyazaki, Y.; Furuya, K.; Furuta, T.; Nakahashi, H.; Louphrasitthiphol, P.; et al. Lectin-based phototherapy targeting cell surface glycans for pancreatic cancer. *Int. J. Cancer* **2023**, *152*, 1425–1437. [CrossRef] [PubMed]
252. Benzing, C.; Lam, H.; Tsang, C.M.; Rimmer, A.; Arroyo-Berdugo, Y.; Calle, Y.; Wells, C.M. TIMP-2 secreted by monocyte-like cells is a potent suppressor of invadopodia formation in pancreatic cancer cells. *BMC Cancer* **2019**, *19*, 1214. [CrossRef] [PubMed]
253. Shapoval, O.; Vetvicka, D.; Patsula, V.; Engstova, H.; Kockova, O.; Konefal, M.; Kabesova, M.; Horak, D. Temoporfin-Conjugated Upconversion Nanoparticles for NIR-Induced Photodynamic Therapy: Studies with Pancreatic Adenocarcinoma Cells In Vitro and In Vivo. *Pharmaceutics* **2023**, *15*, 2694. [CrossRef]
254. Gaviraghi, M.; Tunici, P.; Valensin, S.; Rossi, M.; Giordano, C.; Magnoni, L.; Dandrea, M.; Montagna, L.; Ritelli, R.; Scarpa, A.; et al. Pancreatic cancer spheres are more than just aggregates of stem marker-positive cells. *Biosci. Rep.* **2011**, *31*, 45–55. [CrossRef]
255. Nishino, H.; Takano, S.; Yoshitomi, H.; Suzuki, K.; Kagawa, S.; Shimazaki, R.; Shimizu, H.; Furukawa, K.; Miyazaki, M.; Ohtsuka, M. Grainyhead-like 2 (GRHL2) regulates epithelial plasticity in pancreatic cancer progression. *Cancer Med.* **2017**, *6*, 2686–2696. [CrossRef]
256. Anthiya, S.; Ozturk, S.C.; Yanik, H.; Tavukcuoglu, E.; Sahin, A.; Datta, D.; Charisse, K.; Alvarez, D.M.; Loza, M.I.; Calvo, A.; et al. Targeted siRNA lipid nanoparticles for the treatment of KRAS-mutant tumors. *J. Control. Release* **2023**, *357*, 67–83. [CrossRef] [PubMed]

257. Xu, D.; Yuan, H.; Meng, Z.; Yang, C.; Li, Z.; Li, M.; Zhang, Z.; Gan, Y.; Tu, H. Cadherin 13 Inhibits Pancreatic Cancer Progression and Epithelial-mesenchymal Transition by Wnt/beta-Catenin Signaling. *J. Cancer* **2020**, *11*, 2101–2112. [CrossRef] [PubMed]
258. Nguyen, H.D.; Lin, C.C. Viscoelastic stiffening of gelatin hydrogels for dynamic culture of pancreatic cancer spheroids. *Acta Biomater.* **2024**, *177*, 203–215. [CrossRef]
259. Kettler, B.; Trauzold, A.; Roder, C.; Egberts, J.H.; Kalthoff, H. Topology impacts TRAIL therapy: Differences in primary cancer growth and liver metastasis between orthotopic and subcutaneous xenotransplants of pancreatic ductal adenocarcinoma cells. *Hepatobiliary Pancreat. Dis. Int.* **2021**, *20*, 279–284. [CrossRef]
260. Feng, H.; Ou, B.C.; Zhao, J.K.; Yin, S.; Lu, A.G.; Oechsle, E.; Thasler, W.E. Homogeneous pancreatic cancer spheroids mimic growth pattern of circulating tumor cell clusters and macrometastases: Displaying heterogeneity and crater-like structure on inner layer. *J. Cancer Res. Clin. Oncol.* **2017**, *143*, 1771–1786. [CrossRef]
261. Fiore, P.F.; Di Pace, A.L.; Conti, L.A.; Tumino, N.; Besi, F.; Scaglione, S.; Munari, E.; Moretta, L.; Vacca, P. Different effects of NK cells and NK-derived soluble factors on cell lines derived from primary or metastatic pancreatic cancers. *Cancer Immunol. Immunother.* **2023**, *72*, 1417–1428. [CrossRef]
262. Curley, R.C.; Burke, C.S.; Gkika, K.S.; Noorani, S.; Walsh, N.; Keyes, T.E. Phototoxicity of Tridentate Ru(II) Polypyridyl Complex with Expanded Bite Angles toward Mammalian Cells and Multicellular Tumor Spheroids. *Inorg. Chem.* **2023**, *62*, 13089–13102. [CrossRef]
263. Gagliano, N.; Celesti, G.; Tacchini, L.; Pluchino, S.; Sforza, C.; Rasile, M.; Valerio, V.; Laghi, L.; Conte, V.; Procacci, P. Epithelial-to-mesenchymal transition in pancreatic ductal adenocarcinoma: Characterization in a 3D-cell culture model. *World J. Gastroenterol.* **2016**, *22*, 4466–4483. [CrossRef] [PubMed]
264. Gang, J.; Park, S.B.; Hyung, W.; Choi, E.H.; Wen, J.; Kim, H.S.; Shul, Y.G.; Haam, S.; Song, S.Y. Magnetic poly epsilon-caprolactone nanoparticles containing Fe3O4 and gemcitabine enhance anti-tumor effect in pancreatic cancer xenograft mouse model. *J. Drug Target.* **2007**, *15*, 445–453. [CrossRef]
265. Mohammad, R.M.; Al-Katib, A.; Pettit, G.R.; Vaitkevicius, V.K.; Joshi, U.; Adsay, V.; Majumdar, A.P.; Sarkar, F.H. An orthotopic model of human pancreatic cancer in severe combined immunodeficient mice: Potential application for preclinical studies. *Clin. Cancer Res.* **1998**, *4*, 887–894.
266. Usha, L.; Klapko, O.; Edassery, S. Xenogeneic fibroblasts inhibit the growth of the breast and ovarian cancer cell lines in co-culture. *Neoplasma* **2021**, *68*, 1265–1271. [CrossRef]
267. Chen, S.T.; Kuo, T.C.; Liao, Y.Y.; Lin, M.C.; Tien, Y.W.; Huang, M.C. Silencing of MUC20 suppresses the malignant character of pancreatic ductal adenocarcinoma cells through inhibition of the HGF/MET pathway. *Oncogene* **2018**, *37*, 6041–6053. [CrossRef] [PubMed]
268. Lal, S.; Cheung, E.C.; Zarei, M.; Preet, R.; Chand, S.N.; Mambelli-Lisboa, N.C.; Romeo, C.; Stout, M.C.; Londin, E.; Goetz, A.; et al. CRISPR Knockout of the HuR Gene Causes a Xenograft Lethal Phenotype. *Mol. Cancer Res.* **2017**, *15*, 696–707. [CrossRef] [PubMed]
269. Fredebohm, J.; Boettcher, M.; Eisen, C.; Gaida, M.M.; Heller, A.; Keleg, S.; Tost, J.; Greulich-Bode, K.M.; Hotz-Wagenblatt, A.; Lathrop, M.; et al. Establishment and characterization of a highly tumourigenic and cancer stem cell enriched pancreatic cancer cell line as a well defined model system. *PLoS ONE* **2012**, *7*, e48503. [CrossRef]
270. Mohammad, R.M.; Dugan, M.C.; Mohamed, A.N.; Almatchy, V.P.; Flake, T.M.; Dergham, S.T.; Shields, A.F.; Al-Katib, A.A.; Vaitkevicius, V.K.; Sarkar, F.H. Establishment of a human pancreatic tumor xenograft model: Potential application for preclinical evaluation of novel therapeutic agents. *Pancreas* **1998**, *16*, 19–25. [CrossRef]
271. Matsuda, Y.; Ishiwata, T.; Kawamoto, Y.; Kawahara, K.; Peng, W.X.; Yamamoto, T.; Naito, Z. Morphological and cytoskeletal changes of pancreatic cancer cells in three-dimensional spheroidal culture. *Med. Mol. Morphol.* **2010**, *43*, 211–217. [CrossRef] [PubMed]
272. Murota, Y.; Nagane, M.; Wu, M.; Santra, M.; Venkateswaran, S.; Tanaka, S.; Bradley, M.; Taga, T.; Tabu, K. A niche-mimicking polymer hydrogel-based approach to identify molecular targets for tackling human pancreatic cancer stem cells. *Inflamm. Regen.* **2023**, *43*, 46. [CrossRef]
273. Hollevoet, K.; Mason-Osann, E.; Liu, X.F.; Imhof-Jung, S.; Niederfellner, G.; Pastan, I. In vitro and in vivo activity of the low-immunogenic antimesothelin immunotoxin RG7787 in pancreatic cancer. *Mol. Cancer Ther.* **2014**, *13*, 2040–2049. [CrossRef] [PubMed]
274. Tomar, S.; Zhang, J.; Khanal, M.; Hong, J.; Venugopalan, A.; Jiang, Q.; Sengupta, M.; Miettinen, M.; Li, N.; Pastan, I.; et al. Development of Highly Effective Anti-Mesothelin hYP218 Chimeric Antigen Receptor T Cells with Increased Tumor Infiltration and Persistence for Treating Solid Tumors. *Mol. Cancer Ther.* **2022**, *21*, 1195–1206. [CrossRef] [PubMed]
275. Ikeda, Y.; Ezaki, M.; Hayashi, I.; Yasuda, D.; Nakayama, K.; Kono, A. Establishment and characterization of human pancreatic cancer cell lines in tissue culture and in nude mice. *Jpn. J. Cancer Res.* **1990**, *81*, 987–993. [CrossRef]

276. Shichi, Y.; Gomi, F.; Hasegawa, Y.; Nonaka, K.; Shinji, S.; Takahashi, K.; Ishiwata, T. Artificial intelligence-based analysis of time-lapse images of sphere formation and process of plate adhesion and spread of pancreatic cancer cells. *Front. Cell Dev. Biol.* **2023**, *11*, 1290753. [CrossRef]
277. Xiong, W.; Friese-Hamim, M.; Johne, A.; Stroh, C.; Klevesath, M.; Falchook, G.S.; Hong, D.S.; Girard, P.; El Bawab, S. Translational pharmacokinetic-pharmacodynamic modeling of preclinical and clinical data of the oral MET inhibitor tepotinib to determine the recommended phase II dose. *CPT Pharmacomet. Syst. Pharmacol.* **2021**, *10*, 428–440. [CrossRef]
278. Ghosh, S.; Lovell, J.F. Two Laser Treatments Can Improve Tumor Ablation Efficiency of Chemophototherapy. *Pharmaceutics* **2021**, *13*, 2183. [CrossRef]
279. Heike, M.; Rohrig, O.; Gabbert, H.E.; Moll, R.; Meyer zum Buschenfelde, K.H.; Dippold, W.G.; Knuth, A. New cell lines of gastric and pancreatic cancer: Distinct morphology, growth characteristics, expression of epithelial and immunoregulatory antigens. *Virchows Arch.* **1995**, *426*, 375–384. [CrossRef]
280. Hlavaty, J.; Petznek, H.; Holzmuller, H.; Url, A.; Jandl, G.; Berger, A.; Salmons, B.; Gunzburg, W.H.; Renner, M. Evaluation of a gene-directed enzyme-product therapy (GDEPT) in human pancreatic tumor cells and their use as in vivo models for pancreatic cancer. *PLoS ONE* **2012**, *7*, e40611. [CrossRef]
281. Kalinina, T.; Gungor, C.; Thieltges, S.; Moller-Krull, M.; Penas, E.M.; Wicklein, D.; Streichert, T.; Schumacher, U.; Kalinin, V.; Simon, R.; et al. Establishment and characterization of a new human pancreatic adenocarcinoma cell line with high metastatic potential to the lung. *BMC Cancer* **2010**, *10*, 295. [CrossRef] [PubMed]
282. Yanagihara, K.; Kubo, T.; Mihara, K.; Kuwata, T.; Ochiai, A.; Seyama, T.; Yokozaki, H. Development and Biological Analysis of a Novel Orthotopic Peritoneal Dissemination Mouse Model Generated Using a Pancreatic Ductal Adenocarcinoma Cell Line. *Pancreas* **2019**, *48*, 315–322. [CrossRef] [PubMed]
283. Blackham, A.U.; Northrup, S.A.; Willingham, M.; Sirintrapun, J.; Russell, G.B.; Lyles, D.S.; Stewart, J.H. Molecular determinants of susceptibility to oncolytic vesicular stomatitis virus in pancreatic adenocarcinoma. *J. Surg. Res.* **2014**, *187*, 412–426. [CrossRef] [PubMed]
284. Man, Y.K.S.; Davies, J.A.; Coughlan, L.; Pantelidou, C.; Blazquez-Moreno, A.; Marshall, J.F.; Parker, A.L.; Hallden, G. The Novel Oncolytic Adenoviral Mutant Ad5-3Delta-A20T Retargeted to alphavbeta6 Integrins Efficiently Eliminates Pancreatic Cancer Cells. *Mol. Cancer Ther.* **2018**, *17*, 575–587. [CrossRef]
285. Xu, Y.; Fu, J.; Henderson, M.; Lee, F.; Jurcak, N.; Henn, A.; Wahl, J.; Shao, Y.; Wang, J.; Lyman, M.; et al. CLDN18.2 BiTE Engages Effector and Regulatory T Cells for Antitumor Immune Response in Preclinical Models of Pancreatic Cancer. *Gastroenterology* **2023**, *165*, 1219–1232. [CrossRef]
286. Salem, A.F.; Bonuccelli, G.; Bevilacqua, G.; Arafat, H.; Pestell, R.G.; Sotgia, F.; Lisanti, M.P. Caveolin-1 promotes pancreatic cancer cell differentiation and restores membranous E-cadherin via suppression of the epithelial-mesenchymal transition. *Cell Cycle* **2011**, *10*, 3692–3700. [CrossRef]
287. Kaye, E.G.; Kailass, K.; Sadovski, O.; Beharry, A.A. A Green-Absorbing, Red-Fluorescent Phenalenone-Based Photosensitizer as a Theranostic Agent for Photodynamic Therapy. *ACS Med. Chem. Lett.* **2021**, *12*, 1295–1301. [CrossRef]
288. Shen, Y.J.; Cao, J.; Sun, F.; Cai, X.L.; Li, M.M.; Zheng, N.N.; Qu, C.Y.; Zhang, Y.; Shen, F.; Zhou, M.; et al. Effect of photodynamic therapy with (17R,18R)-2-(1-hexyloxyethyl)-2-devinyl chlorine E6 trisodium salt on pancreatic cancer cells in vitro and in vivo. *World J. Gastroenterol.* **2018**, *24*, 5246–5258. [CrossRef]
289. Alves, F.; Contag, S.; Missbach, M.; Kaspareit, J.; Nebendahl, K.; Borchers, U.; Heidrich, B.; Streich, R.; Hiddemann, W. An orthotopic model of ductal adenocarcinoma of the pancreas in severe combined immunodeficient mice representing all steps of the metastatic cascade. *Pancreas* **2001**, *23*, 227–235. [CrossRef]
290. Vankova, K.; Markova, I.; Jasprova, J.; Dvorak, A.; Subhanova, I.; Zelenka, J.; Novosadova, I.; Rasl, J.; Vomastek, T.; Sobotka, R.; et al. Chlorophyll-Mediated Changes in the Redox Status of Pancreatic Cancer Cells Are Associated with Its Anticancer Effects. *Oxid. Med. Cell. Longev.* **2018**, *2018*, 4069167. [CrossRef]
291. Zhao, X.; Li, D.C.; Zhu, X.G.; Gan, W.J.; Li, Z.; Xiong, F.; Zhang, Z.X.; Zhang, G.B.; Zhang, X.G.; Zhao, H. B7-H3 overexpression in pancreatic cancer promotes tumor progression. *Int. J. Mol. Med.* **2013**, *31*, 283–291. [CrossRef]
292. Chen, J.; Liu, T.H.; Guo, X.Y.; Ye, S.F. Two new human exocrine pancreatic adenocarcinoma cell lines in vitro and in vivo. *Chin. Med. J.* **1990**, *103*, 369–375. [PubMed]
293. Wei, H.J.; Yin, T.; Zhu, Z.; Shi, P.F.; Tian, Y.; Wang, C.Y. Expression of CD44, CD24 and ESA in pancreatic adenocarcinoma cell lines varies with local microenvironment. *Hepatobiliary Pancreat. Dis. Int.* **2011**, *10*, 428–434. [CrossRef]
294. Kumar, M.; Liu, Z.R.; Thapa, L.; Wang, D.Y.; Tian, R.; Qin, R.Y. Mechanisms of inhibition of growth of human pancreatic carcinoma implanted in nude mice by somatostatin receptor subtype 2. *Pancreas* **2004**, *29*, 141–151. [CrossRef] [PubMed]
295. Zhu, H.; Liang, Z.Y.; Ren, X.Y.; Liu, T.H. Small interfering RNAs targeting mutant K-ras inhibit human pancreatic carcinoma cells growth in vitro and in vivo. *Cancer Biol. Ther.* **2006**, *5*, 1693–1698. [CrossRef] [PubMed]

296. Yano, T.; Ishikura, H.; Kato, H.; Ogawa, Y.; Kondo, S.; Kato, H.; Yoshiki, T. Vaccination effect of interleukin-6-producing pancreatic cancer cells in nude mice: A model of tumor prevention and treatment in immune-compromised patients. *Jpn. J. Cancer Res.* **2001**, *92*, 83–87. [CrossRef]
297. Shichinohe, T.; Senmaru, N.; Furuuchi, K.; Ogiso, Y.; Ishikura, H.; Yoshiki, T.; Takahashi, T.; Kato, H.; Kuzumaki, N. Suppression of pancreatic cancer by the dominant negative ras mutant, N116Y. *J. Surg. Res.* **1996**, *66*, 125–130. [CrossRef]
298. Du, X.; He, K.; Huang, Y.; Xu, Z.; Kong, M.; Zhang, J.; Cao, J.; Teng, L. Establishment of a novel human cell line retaining the characteristics of the original pancreatic adenocarcinoma, and evaluation of MEK as a therapeutic target. *Int. J. Oncol.* **2020**, *56*, 761–771. [CrossRef]
299. Rahman, A.; Matsuyama, M.; Ebihara, A.; Shibayama, Y.; Hasan, A.U.; Nakagami, H.; Suzuki, F.; Sun, J.; Kobayashi, T.; Hayashi, H.; et al. Antiproliferative Effects of Monoclonal Antibodies against (Pro)Renin Receptor in Pancreatic Ductal Adenocarcinoma. *Mol. Cancer Ther.* **2020**, *19*, 1844–1855. [CrossRef]
300. Shichi, Y.; Gomi, F.; Ueda, Y.; Nonaka, K.; Hasegawa, F.; Hasegawa, Y.; Hinata, N.; Yoshimura, H.; Yamamoto, M.; Takahashi, K.; et al. Multiple cystic sphere formation from PK-8 cells in three-dimensional culture. *Biochem. Biophys. Rep.* **2022**, *32*, 101339. [CrossRef]
301. Hoshida, T.; Sunamura, M.; Duda, D.G.; Egawa, S.; Miyazaki, S.; Shineha, R.; Hamada, H.; Ohtani, H.; Satomi, S.; Matsuno, S. Gene therapy for pancreatic cancer using an adenovirus vector encoding soluble flt-1 vascular endothelial growth factor receptor. *Pancreas* **2002**, *25*, 111–121. [CrossRef] [PubMed]
302. Suemizu, H.; Monnai, M.; Ohnishi, Y.; Ito, M.; Tamaoki, N.; Nakamura, M. Identification of a key molecular regulator of liver metastasis in human pancreatic carcinoma using a novel quantitative model of metastasis in NOD/SCID/gammacnull (NOG) mice. *Int. J. Oncol.* **2007**, *31*, 741–751. [CrossRef] [PubMed]
303. Hafeez, B.B.; Mustafa, A.; Fischer, J.W.; Singh, A.; Zhong, W.; Shekhani, M.O.; Meske, L.; Havighurst, T.; Kim, K.; Verma, A.K. alpha-Mangostin: A dietary antioxidant derived from the pericarp of Garcinia mangostana L. inhibits pancreatic tumor growth in xenograft mouse model. *Antioxid. Redox Signal.* **2014**, *21*, 682–699. [CrossRef] [PubMed]
304. Cykowiak, M.; Kleszcz, R.; Kucinska, M.; Paluszczak, J.; Szaefer, H.; Plewinski, A.; Piotrowska-Kempisty, H.; Murias, M.; Krajka-Kuzniak, V. Attenuation of Pancreatic Cancer In Vitro and In Vivo via Modulation of Nrf2 and NF-kappaB Signaling Pathways by Natural Compounds. *Cells* **2021**, *10*, 3556. [CrossRef]
305. Brancato, V.; Comunanza, V.; Imparato, G.; Cora, D.; Urciuolo, F.; Noghero, A.; Bussolino, F.; Netti, P.A. Bioengineered tumoral microtissues recapitulate desmoplastic reaction of pancreatic cancer. *Acta Biomater.* **2017**, *49*, 152–166. [CrossRef]
306. Cherubini, G.; Kallin, C.; Mozetic, A.; Hammaren-Busch, K.; Muller, H.; Lemoine, N.R.; Hallden, G. The oncolytic adenovirus AdDeltaDelta enhances selective cancer cell killing in combination with DNA-damaging drugs in pancreatic cancer models. *Gene Ther.* **2011**, *18*, 1157–1165. [CrossRef]
307. Dandawate, P.; Ghosh, C.; Palaniyandi, K.; Paul, S.; Rawal, S.; Pradhan, R.; Sayed, A.A.A.; Choudhury, S.; Standing, D.; Subramaniam, D.; et al. The Histone Demethylase KDM3A, Increased in Human Pancreatic Tumors, Regulates Expression of DCLK1 and Promotes Tumorigenesis in Mice. *Gastroenterology* **2019**, *157*, 1646–1659.e1611. [CrossRef]
308. Lachowski, D.; Matellan, C.; Cortes, E.; Saiani, A.; Miller, A.F.; Del Rio Hernandez, A.E. Self-Assembling Polypeptide Hydrogels as a Platform to Recapitulate the Tumor Microenvironment. *Cancers* **2021**, *13*, 3286. [CrossRef]
309. Taniguchi, S.; Iwamura, T.; Katsuki, T. Correlation between spontaneous metastatic potential and type I collagenolytic activity in a human pancreatic cancer cell line (SUIT-2) and sublines. *Clin. Exp. Metastasis* **1992**, *10*, 259–266. [CrossRef]
310. Hennig, R.; Ventura, J.; Segersvard, R.; Ward, E.; Ding, X.Z.; Rao, S.M.; Jovanovic, B.D.; Iwamura, T.; Talamonti, M.S.; Bell, R.H., Jr.; et al. LY293111 improves efficacy of gemcitabine therapy on pancreatic cancer in a fluorescent orthotopic model in athymic mice. *Neoplasia* **2005**, *7*, 417–425. [CrossRef]
311. Kramer, B.; Haan, L.; Vermeer, M.; Olivier, T.; Hankemeier, T.; Vulto, P.; Joore, J.; Lanz, H.L. Interstitial Flow Recapitulates Gemcitabine Chemoresistance in A 3D Microfluidic Pancreatic Ductal Adenocarcinoma Model by Induction of Multidrug Resistance Proteins. *Int. J. Mol. Sci.* **2019**, *20*, 4647. [CrossRef] [PubMed]
312. Kurahara, H.; Bohl, C.; Natsugoe, S.; Nishizono, Y.; Harihar, S.; Sharma, R.; Iwakuma, T.; Welch, D.R. Suppression of pancreatic cancer growth and metastasis by HMP19 identified through genome-wide shRNA screen. *Int. J. Cancer* **2016**, *139*, 628–638. [CrossRef] [PubMed]
313. Ye, J.; Kawaguchi, M.; Haruyama, Y.; Kanemaru, A.; Fukushima, T.; Yamamoto, K.; Lin, C.Y.; Kataoka, H. Loss of hepatocyte growth factor activator inhibitor type 1 participates in metastatic spreading of human pancreatic cancer cells in a mouse orthotopic transplantation model. *Cancer Sci.* **2014**, *105*, 44–51. [CrossRef]
314. Diaz, V.M.; Planaguma, J.; Thomson, T.M.; Reventos, J.; Paciucci, R. Tissue plasminogen activator is required for the growth, invasion, and angiogenesis of pancreatic tumor cells. *Gastroenterology* **2002**, *122*, 806–819. [CrossRef]
315. Liu, C.; Deng, S.; Jin, K.; Gong, Y.; Cheng, H.; Fan, Z.; Qian, Y.; Huang, Q.; Ni, Q.; Luo, G.; et al. Lewis antigen-negative pancreatic cancer: An aggressive subgroup. *Int. J. Oncol.* **2020**, *56*, 900–908. [CrossRef]

316. Yanagihara, K.; Takigahira, M.; Tanaka, H.; Arao, T.; Aoyagi, Y.; Oda, T.; Ochiai, A.; Nishio, K. Establishment and molecular profiling of a novel human pancreatic cancer panel for 5-FU. *Cancer Sci.* **2008**, *99*, 1859–1864. [CrossRef] [PubMed]
317. Kozono, S.; Ohuchida, K.; Eguchi, D.; Ikenaga, N.; Fujiwara, K.; Cui, L.; Mizumoto, K.; Tanaka, M. Pirfenidone inhibits pancreatic cancer desmoplasia by regulating stellate cells. *Cancer Res.* **2013**, *73*, 2345–2356. [CrossRef]
318. Kawano, K.; Iwamura, T.; Yamanari, H.; Seo, Y.; Suganuma, T.; Chijiiwa, K. Establishment and characterization of a novel human pancreatic cancer cell line (SUIT-4) metastasizing to lymph nodes and lungs in nude mice. *Oncology* **2004**, *66*, 458–467. [CrossRef]
319. Takahashi, N.; Aoyama, F.; Sawaguchi, A. Three-dimensional culture of a pancreatic cancer cell line, SUIT-58, with air exposure can reflect the intrinsic features of the original tumor through electron microscopy. *Microscopy* **2021**, *70*, 192–200. [CrossRef]
320. Sang, M.; Nakamura, M.; Ogata, T.; Sun, D.; Shimozato, O.; Nikaido, T.; Ozaki, T. Impact of RUNX2 gene silencing on the gemcitabine sensitivity of p53-mutated pancreatic cancer MiaPaCa-2 spheres. *Oncol. Rep.* **2018**, *39*, 2749–2758. [CrossRef]
321. Li, M.M.; Cao, J.; Yang, J.C.; Shen, Y.J.; Cai, X.L.; Chen, Y.W.; Qu, C.Y.; Zhang, Y.; Shen, F.; Xu, L.M. Effects of arginine-glycine-aspartic acid peptide-conjugated quantum dots-induced photodynamic therapy on pancreatic carcinoma in vivo. *Int. J. Nanomed.* **2017**, *12*, 2769–2779. [CrossRef]
322. Weber, H.L.; Gidekel, M.; Werbajh, S.; Salvatierra, E.; Rotondaro, C.; Sganga, L.; Haab, G.A.; Curiel, D.T.; Cafferata, E.G.; Podhajcer, O.L. A Novel CDC25B Promoter-Based Oncolytic Adenovirus Inhibited Growth of Orthotopic Human Pancreatic Tumors in Different Preclinical Models. *Clin. Cancer Res.* **2015**, *21*, 1665–1674. [CrossRef] [PubMed]
323. Okabe, T.; Yamaguchi, N.; Ohsawa, N. Establishment and characterization of a carcinoembryonic antigen (CEA)-producing cell line from a human carcinoma of the exocrine pancreas. *Cancer* **1983**, *51*, 662–668. [CrossRef]
324. Saxena, S.; Purohit, A.; Varney, M.L.; Hayashi, Y.; Singh, R.K. Semaphorin-5A maintains epithelial phenotype of malignant pancreatic cancer cells. *BMC Cancer* **2018**, *18*, 1283. [CrossRef]
325. Stefano, E.; Cossa, L.G.; De Castro, F.; De Luca, E.; Vergaro, V.; My, G.; Rovito, G.; Migoni, D.; Muscella, A.; Marsigliante, S.; et al. Evaluation of the Antitumor Effects of Platinum-Based $[Pt(\eta^1\text{-}C_2H_4\text{-}OR)(DMSO)(phen)]^+$ (R = Me, Et) Cationic Organometallic Complexes on Chemoresistant Pancreatic Cancer Cell Lines. *Bioinorg. Chem. Appl.* **2023**, *2023*, 5564624. [CrossRef]
326. Neureiter, D.; Zopf, S.; Dimmler, A.; Stintzing, S.; Hahn, E.G.; Kirchner, T.; Herold, C.; Ocker, M. Different capabilities of morphological pattern formation and its association with the expression of differentiation markers in a xenograft model of human pancreatic cancer cell lines. *Pancreatology* **2005**, *5*, 387–397. [CrossRef]
327. Heger, M. Editor's inaugural issue foreword: Perspectives on translational and clinical research. *J. Clin. Transl. Res.* **2015**, *1*, 1–5. [CrossRef] [PubMed]
328. Gioeli, D.; Snow, C.J.; Simmers, M.B.; Hoang, S.A.; Figler, R.A.; Allende, J.A.; Roller, D.G.; Parsons, J.T.; Wulfkuhle, J.D.; Petricoin, E.F.; et al. Development of a multicellular pancreatic tumor microenvironment system using patient-derived tumor cells. *Lab Chip* **2019**, *19*, 1193–1204. [CrossRef] [PubMed]
329. Stokes, J.B.; Adair, S.J.; Slack-Davis, J.K.; Walters, D.M.; Tilghman, R.W.; Hershey, E.D.; Lowrey, B.; Thomas, K.S.; Bouton, A.H.; Hwang, R.F.; et al. Inhibition of focal adhesion kinase by PF-562,271 inhibits the growth and metastasis of pancreatic cancer concomitant with altering the tumor microenvironment. *Mol. Cancer Ther.* **2011**, *10*, 2135–2145. [CrossRef]
330. Walters, D.M.; Stokes, J.B.; Adair, S.J.; Stelow, E.B.; Borgman, C.A.; Lowrey, B.T.; Xin, W.; Blais, E.M.; Lee, J.K.; Papin, J.A.; et al. Clinical, molecular and genetic validation of a murine orthotopic xenograft model of pancreatic adenocarcinoma using fresh human specimens. *PLoS ONE* **2013**, *8*, e77065. [CrossRef]
331. Gorg, C.; Seifart, U.; Gorg, K.; Zugmaier, G. Color Doppler sonographic mapping of pulmonary lesions: Evidence of dual arterial supply by spectral analysis. *J. Ultrasound Med.* **2003**, *22*, 1033–1039. [CrossRef] [PubMed]
332. Baronzio, G.; Schwartz, L.; Kiselevsky, M.; Guais, A.; Sanders, E.; Milanesi, G.; Baronzio, M.; Freitas, I. Tumor interstitial fluid as modulator of cancer inflammation, thrombosis, immunity and angiogenesis. *Anticancer Res.* **2012**, *32*, 405–414.
333. Majumder, S.; Islam, M.T.; Righetti, R. Non-invasive imaging of interstitial fluid transport parameters in solid tumors in vivo. *Sci. Rep.* **2023**, *13*, 7132. [CrossRef]
334. Di Maggio, F.; Arumugam, P.; Delvecchio, F.R.; Batista, S.; Lechertier, T.; Hodivala-Dilke, K.; Kocher, H.M. Pancreatic stellate cells regulate blood vessel density in the stroma of pancreatic ductal adenocarcinoma. *Pancreatology* **2016**, *16*, 995–1004. [CrossRef]
335. Korbelik, M. Induction of tumor immunity by photodynamic therapy. *J. Clin. Laser Med. Surg.* **1996**, *14*, 329–334. [CrossRef]
336. van Duijnhoven, F.H.; Aalbers, R.I.; Rovers, J.P.; Terpstra, O.T.; Kuppen, P.J. The immunological consequences of photodynamic treatment of cancer, a literature review. *Immunobiology* **2003**, *207*, 105–113. [CrossRef]
337. Canti, G.; De Simone, A.; Korbelik, M. Photodynamic therapy and the immune system in experimental oncology. *Photochem. Photobiol. Sci.* **2002**, *1*, 79–80. [CrossRef] [PubMed]
338. Castano, A.P.; Mroz, P.; Hamblin, M.R. Photodynamic therapy and anti-tumour immunity. *Nat. Rev. Cancer* **2006**, *6*, 535–545. [CrossRef] [PubMed]
339. Kousis, P.C.; Henderson, B.W.; Maier, P.G.; Gollnick, S.O. Photodynamic therapy enhancement of antitumor immunity is regulated by neutrophils. *Cancer Res.* **2007**, *67*, 10501–10510. [CrossRef]

340. Gollnick, S.O.; Evans, S.S.; Baumann, H.; Owczarczak, B.; Maier, P.; Vaughan, L.; Wang, W.C.; Unger, E.; Henderson, B.W. Role of cytokines in photodynamic therapy-induced local and systemic inflammation. *Br. J. Cancer* **2003**, *88*, 1772–1779. [CrossRef]
341. Hwang, H.S.; Shin, H.; Han, J.; Na, K. Combination of photodynamic therapy (PDT) and anti-tumor immunity in cancer therapy. *J. Pharm. Investig.* **2018**, *48*, 143–151. [CrossRef]
342. Korbelik, M.; Krosl, G.; Krosl, J.; Dougherty, G.J. The role of host lymphoid populations in the response of mouse EMT6 tumor to photodynamic therapy. *Cancer Res.* **1996**, *56*, 5647–5652. [PubMed]
343. Korbelik, M.; Dougherty, G.J. Photodynamic therapy-mediated immune response against subcutaneous mouse tumors. *Cancer Res.* **1999**, *59*, 1941–1946.
344. Hendrzak-Henion, J.A.; Knisely, T.L.; Cincotta, L.; Cincotta, E.; Cincotta, A.H. Role of the immune system in mediating the antitumor effect of benzophenothiazine photodynamic therapy. *Photochem. Photobiol.* **1999**, *69*, 575–581. [CrossRef]
345. Castano, A.P.; Liu, Q.; Hamblin, M.R. A green fluorescent protein-expressing murine tumour but not its wild-type counterpart is cured by photodynamic therapy. *Br. J. Cancer* **2006**, *94*, 391–397. [CrossRef] [PubMed]
346. Uenaka, A.; Nakayama, E. Murine leukemia RL male 1 and sarcoma Meth A antigens recognized by cytotoxic T lymphocytes (CTL). *Cancer Sci.* **2003**, *94*, 931–936. [CrossRef] [PubMed]
347. Broekgaarden, M.; Kos, M.; Jurg, F.A.; van Beek, A.A.; van Gulik, T.M.; Heger, M. Inhibition of NF-kappaB in Tumor Cells Exacerbates Immune Cell Activation Following Photodynamic Therapy. *Int. J. Mol. Sci.* **2015**, *16*, 19960–19977. [CrossRef]
348. Chen, J.; Liao, S.; Xiao, Z.; Pan, Q.; Wang, X.; Shen, K.; Wang, S.; Yang, L.; Guo, F.; Liu, H.F.; et al. The development and improvement of immunodeficient mice and humanized immune system mouse models. *Front. Immunol.* **2022**, *13*, 1007579. [CrossRef]
349. Partecke, I.L.; Kaeding, A.; Sendler, M.; Albers, N.; Kuhn, J.P.; Speerforck, S.; Roese, S.; Seubert, F.; Diedrich, S.; Kuehn, S.; et al. In vivo imaging of pancreatic tumours and liver metastases using 7 Tesla MRI in a murine orthotopic pancreatic cancer model and a liver metastases model. *BMC Cancer* **2011**, *11*, 40. [CrossRef]
350. Courtin, A.; Richards, F.M.; Bapiro, T.E.; Bramhall, J.L.; Neesse, A.; Cook, N.; Krippendorff, B.F.; Tuveson, D.A.; Jodrell, D.I. Anti-tumour efficacy of capecitabine in a genetically engineered mouse model of pancreatic cancer. *PLoS ONE* **2013**, *8*, e67330. [CrossRef]
351. Blaauboer, A.; Van Koetsveld, P.M.; Mustafa, D.A.M.; Dumas, J.; Dogan, F.; Van Zwienen, S.; Van Eijck, C.H.J.; Hofland, L.J. Immunomodulatory antitumor effect of interferon-beta combined with gemcitabine in pancreatic cancer. *Int. J. Oncol.* **2022**, *61*, 97. [CrossRef] [PubMed]
352. Nasiri, E.; Student, M.; Roth, K.; Siti Utami, N.; Huber, M.; Buchholz, M.; Gress, T.M.; Bauer, C. IL18 Receptor Signaling Inhibits Intratumoral CD8$^+$ T-Cell Migration in a Murine Pancreatic Cancer Model. *Cells* **2023**, *12*, 456. [CrossRef]
353. Czaplinska, D.; Ialchina, R.; Andersen, H.B.; Yao, J.; Stigliani, A.; Dannesboe, J.; Flinck, M.; Chen, X.; Mitrega, J.; Gnosa, S.P.; et al. Crosstalk between tumor acidosis, p53 and extracellular matrix regulates pancreatic cancer aggressiveness. *Int. J. Cancer* **2023**, *152*, 1210–1225. [CrossRef]
354. Fukushima, H.; Furusawa, A.; Kato, T.; Wakiyama, H.; Takao, S.; Okuyama, S.; Choyke, P.L.; Kobayashi, H. Intratumoral IL15 Improves Efficacy of Near-Infrared Photoimmunotherapy. *Mol. Cancer Ther.* **2023**, *22*, 1215–1227. [CrossRef] [PubMed]
355. Zhou, F.; Yang, J.; Zhang, Y.; Liu, M.; Lang, M.L.; Li, M.; Chen, W.R. Local Phototherapy Synergizes with Immunoadjuvant for Treatment of Pancreatic Cancer through Induced Immunogenic Tumor Vaccine. *Clin. Cancer Res.* **2018**, *24*, 5335–5346. [CrossRef] [PubMed]
356. Torres, M.P.; Rachagani, S.; Souchek, J.J.; Mallya, K.; Johansson, S.L.; Batra, S.K. Novel pancreatic cancer cell lines derived from genetically engineered mouse models of spontaneous pancreatic adenocarcinoma: Applications in diagnosis and therapy. *PLoS ONE* **2013**, *8*, e80580. [CrossRef]
357. Benali, N.; Cordelier, P.; Calise, D.; Pages, P.; Rochaix, P.; Nagy, A.; Esteve, J.P.; Pour, P.M.; Schally, A.V.; Vaysse, N.; et al. Inhibition of growth and metastatic progression of pancreatic carcinoma in hamster after somatostatin receptor subtype 2 (sst2) gene expression and administration of cytotoxic somatostatin analog AN-238. *Proc. Natl. Acad. Sci. USA* **2000**, *97*, 9180–9185. [CrossRef]
358. Hirota, M.; Egami, H.; Mogaki, M.; Kazakoff, K.; Chaney, W.G.; Pour, P.M. Relationship between blood group-A antigen expression and malignant potential in hamster pancreatic cancers. *Teratog. Carcinog. Mutagen.* **1993**, *13*, 217–224. [CrossRef]
359. Chang, B.K.; Gutman, R. Chemotherapy of pancreatic adenocarcinoma: Initial report on two transplantable models in the Syrian hamster. *Cancer Res.* **1982**, *42*, 2666–2670.
360. Baptista, M.S.; Cadet, J.; Di Mascio, P.; Ghogare, A.A.; Greer, A.; Hamblin, M.R.; Lorente, C.; Nunez, S.C.; Ribeiro, M.S.; Thomas, A.H.; et al. Type I and Type II Photosensitized Oxidation Reactions: Guidelines and Mechanistic Pathways. *Photochem. Photobiol.* **2017**, *93*, 912–919. [CrossRef]
361. Sitnik, T.M.; Hampton, J.A.; Henderson, B.W. Reduction of tumour oxygenation during and after photodynamic therapy in vivo: Effects of fluence rate. *Br. J. Cancer* **1998**, *77*, 1386–1394. [CrossRef]

362. Debefve, E.; Pegaz, B.; van den Bergh, H.; Wagnieres, G.; Lange, N.; Ballini, J.P. Video monitoring of neovessel occlusion induced by photodynamic therapy with verteporfin (Visudyne), in the CAM model. *Angiogenesis* **2008**, *11*, 235–243. [CrossRef] [PubMed]
363. Castano, A.P.; Demidova, T.N.; Hamblin, M.R. Mechanisms in photodynamic therapy: Part three-Photosensitizer pharmacokinetics, biodistribution, tumor localization and modes of tumor destruction. *Photodiagnosis Photodyn. Ther.* **2005**, *2*, 91–106. [CrossRef]
364. Kwiatkowski, S.; Knap, B.; Przystupski, D.; Saczko, J.; Kedzierska, E.; Knap-Czop, K.; Kotlinska, J.; Michel, O.; Kotowski, K.; Kulbacka, J. Photodynamic therapy—Mechanisms, photosensitizers and combinations. *Biomed. Pharmacother.* **2018**, *106*, 1098–1107. [CrossRef] [PubMed]
365. Dias, L.M.; de Keijzer, M.J.; Ernst, D.; Sharifi, F.; de Klerk, D.J.; Kleijn, T.G.; Desclos, E.; Kochan, J.A.; de Haan, L.R.; Franchi, L.P.; et al. Metallated phthalocyanines and their hydrophilic derivatives for multi-targeted oncological photodynamic therapy. *J. Photochem. Photobiol. B* **2022**, *234*, 112500. [CrossRef]
366. Xie, Q.; Li, Z.; Liu, Y.; Zhang, D.; Su, M.; Niitsu, H.; Lu, Y.; Coffey, R.J.; Bai, M. Translocator protein-targeted photodynamic therapy for direct and abscopal immunogenic cell death in colorectal cancer. *Acta Biomater.* **2021**, *134*, 716–729. [CrossRef] [PubMed]
367. Lou, J.; Aragaki, M.; Bernards, N.; Kinoshita, T.; Mo, J.; Motooka, Y.; Ishiwata, T.; Gregor, A.; Chee, T.; Chen, Z.; et al. Repeated porphyrin lipoprotein-based photodynamic therapy controls distant disease in mouse mesothelioma via the abscopal effect. *Nanophotonics* **2021**, *10*, 3279–3294. [CrossRef] [PubMed]
368. Osuna de la Pena, D.; Trabulo, S.M.D.; Collin, E.; Liu, Y.; Sharma, S.; Tatari, M.; Behrens, D.; Erkan, M.; Lawlor, R.T.; Scarpa, A.; et al. Bioengineered 3D models of human pancreatic cancer recapitulate in vivo tumour biology. *Nat. Commun.* **2021**, *12*, 5623. [CrossRef]
369. Godier, C.; Baka, Z.; Lamy, L.; Gribova, V.; Marchal, P.; Lavalle, P.; Gaffet, E.; Bezdetnaya, L.; Alem, H. A 3D Bio-Printed-Based Model for Pancreatic Ductal Adenocarcinoma. *Diseases* **2024**, *12*, 206. [CrossRef]
370. Sun, H.; Wang, Y.; Sun, M.; Ke, X.; Li, C.; Jin, B.; Pang, M.; Wang, Y.; Jiang, S.; Du, L.; et al. Developing Patient-Derived 3D-Bioprinting models of pancreatic cancer. *J. Adv. Res.* **2024**, *in press*. [CrossRef]
371. Haque, M.R.; Wessel, C.R.; Leary, D.D.; Wang, C.; Bhushan, A.; Bishehsari, F. Patient-derived pancreatic cancer-on-a-chip recapitulates the tumor microenvironment. *Microsyst. Nanoeng.* **2022**, *8*, 36. [CrossRef] [PubMed]
372. Sgarminato, V.; Marasso, S.L.; Cocuzza, M.; Scordo, G.; Ballesio, A.; Ciardelli, G.; Tonda-Turo, C. PDAC-on-chip for in vitro modeling of stromal and pancreatic cancer cell crosstalk. *Biomater. Sci.* **2022**, *11*, 208–224. [CrossRef]
373. Goluba, K.; Parfejevs, V.; Rostoka, E.; Jekabsons, K.; Blake, I.; Neimane, A.; Ule, A.A.; Rimsa, R.; Vangravs, R.; Pcolkins, A.; et al. Personalized PDAC chip with functional endothelial barrier for tumour biomarker detection: A platform for precision medicine applications. *Mater. Today Bio* **2024**, *29*, 101262. [CrossRef]
374. Geyer, M.; Schreyer, D.; Gaul, L.M.; Pfeffer, S.; Pilarsky, C.; Queiroz, K. A microfluidic-based PDAC organoid system reveals the impact of hypoxia in response to treatment. *Cell Death Discov.* **2023**, *9*, 20. [CrossRef] [PubMed]
375. Kumano, K.; Nakahashi, H.; Louphrasitthiphol, P.; Kuroda, Y.; Miyazaki, Y.; Shimomura, O.; Hashimoto, S.; Akashi, Y.; Mathis, B.J.; Kim, J.; et al. Hypoxia at 3D organoid establishment selects essential subclones within heterogenous pancreatic cancer. *Front. Cell Dev. Biol.* **2024**, *12*, 1327772. [CrossRef]
376. Abou Khouzam, R.; Lehn, J.M.; Mayr, H.; Clavien, P.A.; Wallace, M.B.; Ducreux, M.; Limani, P.; Chouaib, S. Hypoxia, a Targetable Culprit to Counter Pancreatic Cancer Resistance to Therapy. *Cancers* **2023**, *15*, 1235. [CrossRef]
377. Broekgaarden, M.; Weijer, R.; van Wijk, A.C.; Cox, R.C.; Egmond, M.R.; Hoebe, R.; van Gulik, T.M.; Heger, M. Photodynamic Therapy with Liposomal Zinc Phthalocyanine and Tirapazamine Increases Tumor Cell Death via DNA Damage. *J. Biomed. Nanotechnol.* **2017**, *13*, 204–220. [CrossRef]
378. Cros, J.; Raffenne, J.; Couvelard, A.; Pote, N. Tumor Heterogeneity in Pancreatic Adenocarcinoma. *Pathobiology* **2018**, *85*, 64–71. [CrossRef] [PubMed]
379. Palma, A.M.; Vudatha, V.; Peixoto, M.L.; Madan, E. Tumor heterogeneity: An oncogenic driver of PDAC progression and therapy resistance under stress conditions. *Adv. Cancer Res.* **2023**, *159*, 203–249. [CrossRef]
380. Evan, T.; Wang, V.M.; Behrens, A. The roles of intratumour heterogeneity in the biology and treatment of pancreatic ductal adenocarcinoma. *Oncogene* **2022**, *41*, 4686–4695. [CrossRef]
381. Roos, E.; Soer, E.C.; Klompmaker, S.; Meijer, L.L.; Besselink, M.G.; Giovannetti, E.; Heger, M.; Kazemier, G.; Klumpen, H.J.; Takkenberg, R.B.; et al. Crossing borders: A systematic review with quantitative analysis of genetic mutations of carcinomas of the biliary tract. *Crit. Rev. Oncol. Hematol.* **2019**, *140*, 8–16. [CrossRef] [PubMed]
382. Patel, T. Cholangiocarcinoma—Controversies and challenges. *Nat. Rev. Gastroenterol. Hepatol.* **2011**, *8*, 189–200. [CrossRef]
383. Banales, J.M.; Marin, J.J.G.; Lamarca, A.; Rodrigues, P.M.; Khan, S.A.; Roberts, L.R.; Cardinale, V.; Carpino, G.; Andersen, J.B.; Braconi, C.; et al. Cholangiocarcinoma 2020: The next horizon in mechanisms and management. *Nat. Rev. Gastroenterol. Hepatol.* **2020**, *17*, 557–588. [CrossRef]

384. de Klerk, D.J.; de Keijzer, M.J.; Dias, L.M.; Heemskerk, J.; de Haan, L.R.; Kleijn, T.G.; Franchi, L.P.; Heger, M.; Photodynamic Therapy Study, G. Strategies for Improving Photodynamic Therapy Through Pharmacological Modulation of the Immediate Early Stress Response. *Methods Mol. Biol.* **2022**, *2451*, 405–480. [CrossRef] [PubMed]
385. Moss, D.M.; Siccardi, M. Optimizing nanomedicine pharmacokinetics using physiologically based pharmacokinetics modelling. *Br. J. Pharmacol.* **2014**, *171*, 3963–3979. [CrossRef]
386. Kadam, R.S.; Bourne, D.W.; Kompella, U.B. Nano-advantage in enhanced drug delivery with biodegradable nanoparticles: Contribution of reduced clearance. *Drug Metab. Dispos.* **2012**, *40*, 1380–1388. [CrossRef]
387. Zhang, A.; Meng, K.; Liu, Y.; Pan, Y.; Qu, W.; Chen, D.; Xie, S. Absorption, distribution, metabolism, and excretion of nanocarriers in vivo and their influences. *Adv. Colloid. Interface Sci.* **2020**, *284*, 102261. [CrossRef] [PubMed]
388. Liu, W.; Zhu, Y.; Ye, L.; Zhu, Y.; Wang, Y. Comparison of tumor angiogenesis in subcutaneous and orthotopic LNCaP mouse models using contrast-enhanced ultrasound imaging. *Transl. Cancer Res.* **2021**, *10*, 3268–3277. [CrossRef]
389. Guerin, M.V.; Finisguerra, V.; Van den Eynde, B.J.; Bercovici, N.; Trautmann, A. Preclinical murine tumor models: A structural and functional perspective. *Elife* **2020**, *9*, e50740. [CrossRef]
390. Fung, A.S.; Lee, C.; Yu, M.; Tannock, I.F. The effect of chemotherapeutic agents on tumor vasculature in subcutaneous and orthotopic human tumor xenografts. *BMC Cancer* **2015**, *15*, 112. [CrossRef]
391. Li, M.; Bosman, E.D.C.; Smith, O.M.; Lintern, N.; de Klerk, D.J.; Sun, H.; Cheng, S.; Pan, W.; Storm, G.; Khaled, Y.S.; et al. Comparative analysis of whole cell-derived vesicular delivery systems for photodynamic therapy of extrahepatic cholangiocarcinoma. *J. Photochem. Photobiol. B* **2024**, *254*, 112903. [CrossRef]
392. Price, O.T.; Lau, C.; Zucker, R.M. Quantitative fluorescence of 5-FU-treated fetal rat limbs using confocal laser scanning microscopy and Lysotracker Red. *Cytom. A* **2003**, *53*, 9–21. [CrossRef] [PubMed]
393. Zhitomirsky, B.; Farber, H.; Assaraf, Y.G. LysoTracker and MitoTracker Red are transport substrates of P-glycoprotein: Implications for anticancer drug design evading multidrug resistance. *J. Cell. Mol. Med.* **2018**, *22*, 2131–2141. [CrossRef]
394. Heger, M.; Salles, I.I.; van Vuure, W.; Hamelers, I.H.; de Kroon, A.I.; Deckmyn, H.; Beek, J.F. On the interaction of fluorophore-encapsulating PEGylated lecithin liposomes with hamster and human platelets. *Microvasc. Res.* **2009**, *78*, 57–66. [CrossRef] [PubMed]
395. Barton, B.E.; Karras, J.G.; Murphy, T.F.; Barton, A.; Huang, H.F. Signal transducer and activator of transcription 3 (STAT3) activation in prostate cancer: Direct STAT3 inhibition induces apoptosis in prostate cancer lines. *Mol. Cancer Ther.* **2004**, *3*, 11–20. [CrossRef] [PubMed]
396. Reiniers, M.J.; de Haan, L.R.; Reeskamp, L.F.; Broekgaarden, M.; van Golen, R.F.; Heger, M. Analysis and Optimization of Conditions for the Use of 2′,7′-Dichlorofluorescein Diacetate in Cultured Hepatocytes. *Antioxidants* **2021**, *10*, 674. [CrossRef]
397. Harada, M.; Woodhams, J.; MacRobert, A.J.; Feneley, M.R.; Kato, H.; Bown, S.G. The vascular response to photodynamic therapy with ATX-S10Na(II) in the normal rat colon. *J. Photochem. Photobiol. B* **2005**, *79*, 223–230. [CrossRef]
398. Suzuki, T.; Tanaka, M.; Sasaki, M.; Ichikawa, H.; Nishie, H.; Kataoka, H. Vascular Shutdown by Photodynamic Therapy Using Talaporfin Sodium. *Cancers* **2020**, *12*, 2369. [CrossRef]